THE INTERACTION BETWEEN WEBS AND ROLLERS IN ROLL-TO-ROLL MANUFACTURING PROCESS MACHINES

By

JINXIN SHI

Bachelor of Science in Process Equipment and Control Engineering
Beijing University of Chemical Technology
Beijing, China
2010

Master of Science in Machinery in Chemical Industry Process
Beijing University of Chemical Technology
Beijing, China
2013

Submitted to the Faculty of the
Graduate College of the
Oklahoma State University
in partial fulfillment of
the requirements for
the Degree of
DOCTOR OF PHILOSOPHY
May, 2019

THE INTERACTION BETWEEN WEBS AND

ROLLERS IN ROLL-TO-ROLL MANUFACTURING

PROCESS MACHINES

Dissertation Approved:

Dr. J. K. Good

Dissertation Adviser

Dr. D. A. Lucca

Dr. O. San

Dr. B. W. Russell

.

ACKNOWLEDGEMENTS

First of all, I express sincere thanks and appreciation to my advisor Dr. J. K. Good. His guidance and assistance have always inspired me and led me to the accomplishments presented here. He granted me a comfortable amount of freedom and his measured criticism has always been invaluable in my research endeavors. I have never for a minute doubted my good fortune at having him for my advisor.

Secondly, I would like to thank my dissertation committee for their suggestions and help. I would like to thank each committee member for their time, effort, and patience required to conduct each of the three exams required for this degree.

Thirdly, I would like to extend my special appreciation to Mr. Ron Markum for his help during experimental studies and for his friendship. I also thank my team-mates and colleagues from WHRC for their friendship and for all the great discussions we have had. The support from sponsors of WHRC for their funding and help is greatly appreciated.

Finally, I thank my parents, and my brother for their constant love and support. I am also deeply grateful to my boyfriend, Sheng, for his support and patience of my work during those tough years.

Name: JINXIN SHI

Date of Degree: MAY, 2019

Title of Study: THE INTERACTION BETWEEN WEBS AND ROLLERS IN ROLL-TO-ROLL MANUFACTURING PROCESS MACHINES

Major Field: MECHANICAL AND AEROSPACE ENGINEERING

Abstract: A web can be defined as a continuous flexible strip which is supported, guided and propelled by rollers. The work presented here studies the steady state behavior of the web between rollers and treated the web span as beam with kinematic and kinetic boundary conditions at rollers. Web registration due to machine and web imperfections has been studied and the exact boundary conditions are compared with simulation and experimental results: straight web steering due to a downstream misaligned roller and a tapered roller, and cambered web steering phenomenon in spans. The interaction between webs and rollers treating the web as a plate or shell revealed a web wrapping a roller is a disturbance to a web, and normal entry condition is only valid at web center. A trough failure criterion for the laminated web is developed based upon Timoshenko's shell buckling theory. This failure criterion is employed to predict the misalignment of a roller for trough formation in a laminated web. ABAQUS/Standard finite element analysis will be used to compare the results from the closed form expressions and tests.

TABLE OF CONTENTS

Chapter Page

LIST OF TABLES

Table Page

LIST OF FIGURES

Figure Page

Figure Page

Figure Page

Figure Page

.

NOMENCLATURE

A	Cross sectional area
A_{mn}	Amplitude of the buckled wave
A_i	Sectional area of the web associate with node i
A_s	Shear area of a beam
c_d	Dilatational wave speed
CShear	Contact shear stress between the web and roller
CL	Chord length
d	Distance between the arc of the web and the chord
D	$Et^3/(12(1 - \nu^2))$
D_{ij}	Bending stiffness of the laminate
E	Young's modulus
F	Vertical shear force
G	Shear modulus
h_0	Air film layer due to hydrodynamic lubrication
H	$\int Eytdy$
I	Area moment of inertia, $tW^3/12$
K	(T/EI)^0.5
K_e	(T/EI(1 + n'T/AG))^0.5
K_ε	$TS/(\Omega S - H^2)$
L	Length of the web span
L^e	Characteristic element length
m	Slope in radius over the roller width for a tapered roller
M	Moment
n	Half wave number
n'	stress averaging factor
N	Shear force
N'	Edge load
P	External force vector
Q_{ij}	Stiffness parameter
r_x	Radius of the cylinder

R	Roller radius
R_0	Nominal radius
s	Curvilinear coordinate following the elastic axis of the web
S	$\int Etdy$
t	Thickness
T	Web tension
u	Web displacement along MD
$\ddot{u}$	Acceleration vector
v	Web displacement along CMD
V	Web MD velocity
w	Web displacement in out-of-plane direction
W	Web width
WA	Wrap angle
x	MD direction
y	CMD direction
z	Web out-of-plane direction
α	Expansion coefficient
β	Wrap angle
ε	Strain
ε_i	Frozen – in strain
θ	Angle
κ_j	Web curvature at the downstream roller
λ	Wavelength
μ	Coefficient of friction
ν	Poisson's ratio
ρ	Radius of curvature of a cambered web
$\rho_{density}$	Mass density
σ	Stress
τ	Time constant
ϕ	Shear parameter, $12EI/(L^2GA_s)$
Ω	$\int Ey^2tdy$
Δt	Stable time increment

CHAPTER I

INTRODUCTION

Continuous materials were first made with the invention of the Fourdrinier paper machine in 1799. From then on, processing of continuous materials became pervasive through many industries. In the beginning, most continuous materials were paper or textiles, steel and plastic webs followed later. Nowadays, products with web process in their manufacturing can be found almost everywhere. A web is a strip of continuous flexible material which can be manufactured for coating, laminating, slitting, printing and other processes. The length of a web greatly exceeds its width and its thickness is much less than the width. Typical web materials include papers, textiles, plastic films, non-woven materials, composites, etc.

Webs are needed for products that can be made by continuous manufacturing processes and are always stored as wound rolls for convenience. Typically before the web turns into a final product, it is unwound from a roll and then transits over numerous rollers which define the path of the web while being processed before it is rewound into a roll or enters another process machine. During a process, the web lateral position and longitudinal tension may vary as the web passes over successive rollers, so instability and registration errors may occur which can interrupt the web process or deter product quality. The goal of web handling is to transport a web through a process with maximum productivity and minimum waste.

The coordinates of a web are defined as MD and CMD. The Machine Direction (MD) is the coordinate direction that a web travels through a web line and Cross Machine Direction (CMD)

is defined as the coordinate direction which is perpendicular to the MD. The MD and the CMD both lie in the plane of the web.

Troughs and wrinkles are two forms of instability which appear in different sections of the web. Troughs are web out-of-plane deformations caused when the tensioned and unsupported web travels through a free span between two rollers. Wrinkles are web out-of-plane deformations caused when the web transits over a roller. Both troughs and wrinkles are generated by web compressive CMD stresses. Since the thickness dimension of a web is typically much smaller compared to its length and width dimensions, its in-plane bending stiffness is very small, and small CMD compressive stresses can induce troughs [1]. Wrinkles appear in the sections where the webs are supported by the rollers and they are known to be caused by much larger compressive CMD stresses than troughs. Many web processes cannot be conducted properly when troughs or wrinkles are present. For example, in a printing process, webs will not be printed properly if troughs and wrinkles appear before or during printing. Both situations will bring complaints by customers. Generally, wrinkles are more unacceptable than troughs. Troughs may occur with or without wrinkles and they may or may not be accepted based on whether the process needs the web to be flat. Sometimes troughs may cause little problem and disappear as the web travels downstream. Wrinkles will produce permanent damage to the web and are unacceptable under any circumstances because the web may fold over, crease or even fracture.

Registration error is another common problem in web processing [2][3][4]. Webs are often coated in successive processes. For example, to print a transistor in printed electronics a base is to be printed first followed by the printing of P and N junctions [5]. If the transistor is small, on the order of a few m, the P and N junctions must be printed on the base with sub m precision to produce a functioning device. Let us consider another commonly used example: the printing of color images by the rotogravure method. In this method, a final image is produced by printing an overlap of images of several basic colors. Each basic color image is printed with an impression roller that prints only one

basic color. If each basic color image cannot be congruently superimposed with high accuracy then the final image will look blurred or "out of register". In order to control final print quality, whether a magazine or a transistor is being produced, registration error should be controlled within a specified range. An ideal web state cannot always exist so registration errors appear in practice. The occurrences of registration errors are often due to web strain variations, roller velocity variations or web lateral movement.

Web instability and registration issues have been long time problems in the web handling industry. Today these issues have become more critical with the advent of printed electronics at micro and nano scales. A picture in a magazine with a blur may still convey the information to a reader. A transistor with a P junction not printed on the base is a non-functioning device. Thus the need to present stable webs to processes where only tiny registration errors are acceptable has become more demanding.

The focus of the research reported and proposed herein will be to examine web behaviors that have previously been neglected when web stability and registration errors were not as critical. The vast majority of web instability research has been conducted under assumptions of steady state conditions. Beam and plate theories have been employed for webs to develop the closed form expressions for web lateral deflection and instability behaviors. Webs are driven through web processes through frictional engagement with rollers, some of which are driven and some of which are idlers with non-repeatable bearing drag. Many web processes are run continuously. Unwinding rolls of web expire and new rolls are spliced in while attempting to maintain the web in the process section within bounds of velocity and tension required by the process. Webs undergo cyclic bending strains as they enter and exit rollers in process machines. Thus the web is subject to many non-steady state disturbances where a dynamic response affecting registration or web stability can result.

CHAPTER II

REVIEW OF LITERATURE

2.1 The Analysis of Registration Error and Web Instability due to Lateral Steering

In roll-to-roll (R2R) process machines, the lateral steering of the web is a long time problem. The web tends to move laterally as it passes over a roller due to many reasons. For example, if the straight web contacts with a roller which has a misaligned angle, the web would move laterally on the roller since it should follow the normal entry rule, and the slippage would occur if there is no sufficient friction force between the web and the roller. In addition, the lateral compressive stresses would be induced as the web transits over the misaligned roller which would cause the troughs and wrinkles. There are several papers discussed the criterion that the web would have troughs or wrinkles under steady state condition [1][6][7].

Good [1] discussed the shear wrinkling in a single web span. A single web span is an unsupported zone of web between two rollers. Velocity dependent traction was incorporated into a uniform web for analysis. Two regimes were discussed. As the web was typically nearly planar in regime 1, the classical bending theory for plates was still applicable. The web was unstable and buckling would occur when the work done by forces acting on the web became larger than the strain energy of bending for web out-of-plane deformation. The expression for the critical rotation of roller for wrinkles occurrence was developed at regime 1. Unlike regime1, the regime 2 was velocity dependent and the wrinkles cannot be sustained if the maximum lateral compressive stress was less than the buckling stress predicted by Timoshenko [8].

Good and Beisel [6][7] further analyzed the buckling formation in orthotropic webs. Based on Lekhnisskii plate theory, the closed form equations of the critical CMD stress to generate troughs and wrinkles were developed and investigated for orthotropic webs. The beam stiffness matrix [10] incorporated with tension was utilized to define the critical rotation of a roller for troughs occurrence in the web. A set of experiments were conducted to test the validity of the trough failure criterion, the lateral deformation, the shear, and the tension stiffening assumptions.

In early 1990s, the total world production of the newsprint was 100,000 tons every day, and the newsprint machines ran at more than 787 in/s [11]. The productivity and quality of the final product on these fast running machines increase the demand of the stability of the running web. Now more and more newspapers are printed in full four colors (CMYK). For the multi-color printed product, align successive print patters on the web with precise position is one of the most important qualities. The image would appear blurred or fuzzy even one of the patterns has a slight position shift. The registration errors would be noticed if the web moves laterally on the printing machine more than 0.1 millimeters (0.004 inches) [12]. Although the printing machines are generally aligned to prevent web lateral instability, the printing equipment itself, the non-uniform web and other disturbances would cause web registration error, wrinkles, and even the crease. The web guide is usually used in R2R process to control the web lateral motion. However, the web lateral deflections are sometimes so quick or severe that the press adjustments cannot compensate for them [13].

Summary: Several examples have already shown the web lateral steering effects on registration error and web instability. The classical beam theories were generally incorporated for free web spans and the plate theories for the webs wrapping on the rollers. The steady state condition of the web was assumed and sufficient friction force between the web and the roller was enforced to avoid the slippage and moment transfer. The detailed discussion about the web lateral movement and criterions for web troughs and wrinkles would be developed and proved in the following sections.

2.2 Web Lateral Movement: Boundary Conditions Associated with Steady State Lateral Behavior

An understanding of web steady state behavior is necessary for understanding its dynamic behaviors. The web is defined as in a steady static condition when it moves along MD without any lateral movement on the roller [14]. Fu et al. [15] defined a web has a steady state behavior when the lateral velocities of the web acquired at the entry contact points to rollers approach to zero.

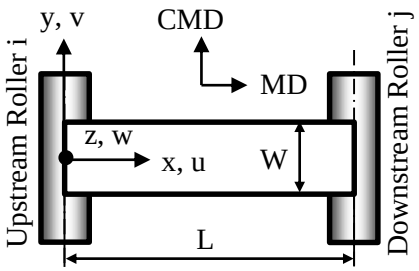

Figure 2.1 –Web Coordinate System for a Web Span Between Two Rollers

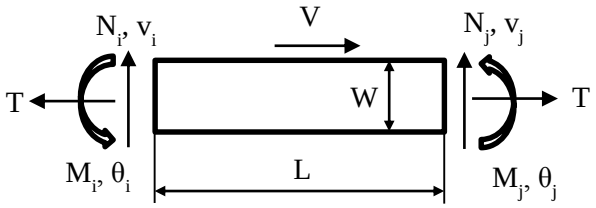

Figure 2.2 – Sign Convention for the Positive Loads, Displacements and Rotations of a Web Span

For a web span that exits from an upstream roller and enters into a downstream roller, a Cartesian coordinate system is defined for convenience. As shown in Figure 2.1, the center point at the exit line as the web leaves the upstream roller i is regarded as the origin of the coordinate system. The positive directions of x axis and y axis align with the MD and CMD directions,

respectively. According to right hand rule, the positive direction of the z axis points above and perpendicular to the web plane. The web displacements u, v, and w are along the x, y and z axes, respectively. The displacement v represents the lateral (CMD) displacement of a web. Figure 2.2 shows the sign conventions for the free web span between the upstream roller i and the downstream roller j. The terms are defined as: T (web tension), N (shear force), M (moment), θ (rotation), V (MD velocity), W (web width) and L (web span length).

In 1932, Swift [16] presented the interactions between a belt and a pulley which was one of the earliest publications on this subject. The most important development was the concept of the normal entry rule. In Figure 2.3, the steady running belt with no lateral travel should enter the pulley along Line A, which was exactly perpendicular to the rotation axis of the pulley. If instead the belt is led on at some small angle θ from Line A, the succeeding portions of this belt will enter the pulley along Line B and form over the pulley a helical track with the angle θ. The belt does not have the steady state condition due to the lateral or CMD velocity component Vsec θ, where V is the MD velocity of the belt. The only way for the belt to keep the steady state is to follow the normal entry which means to lay along with line A. Swift also discussed problems involving staggered pulleys, tapered pulleys, oblique drives, and twisted drives.

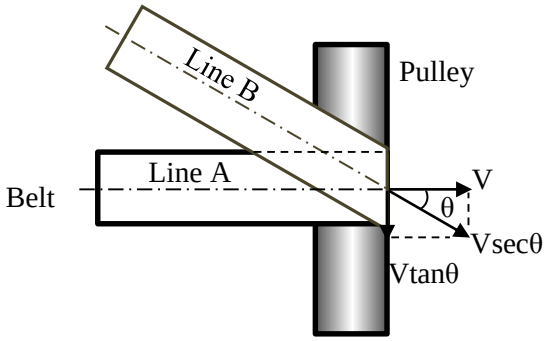

Figure 2.3 –Normal Entry of a Belt on a Pulley (Line A)

Shelton derived a fourth-order differential equation which governs the steady state lateral deformation along the elastic curve of a free web span between two rollers [14]. This elementary

beam theory equation concerned with the relatively long web span so the deflection due to shear stress is negligible:

$$v_x^{iV} - K^2 v_x'' = 0 \tag{2.1}$$

Where, the square of K is T/EI; T is web tension; E is the Young's modulus of the web; I is the area moment of inertia of web out-of-plane about the elastic axis. If the web has a rectangular cross section with thickness t and width W, I is tW3/12. In order to solve this linear ordinary differential equation, four boundary conditions for the web span with a misaligned downstream roller were defined. Two of them are for the upstream edge at exit of roller i and the others are for the downstream edge at entry to roller j. The rotate angle of the misaligned roller j is θ_j, in radians:

$$\begin{cases} 1)\ v_i = 0 \\ 2)\ v_i' = 0 \\ 3)\ v_j' = \theta_j \\ 4)\ v_j'' = 0 \text{ or } M_j = 0 \end{cases} \tag{2.2}$$

The lateral displacement of the web at the upstream roller v_i was assumed to be zero. Shelton assumed there are sufficient traction to prevent web slippage on the roller, so the second and third boundary conditions were enforced by the normal entry rule.

The fourth boundary condition was proofed by Shelton with an initial straight and uniform web cross over a roller. This web would have a finite radius of curvature if it has a residual moment as shown in Figure 2.4. If the roller was composed of many short, independent rollers, the roller on the left side should run faster than the roller on the right side, because in a unit time there is more web passes over the roller at the left side due to its longer length. However, the roller is a single object and the unique speed is expected for the whole roller. The roller would exert a moment on the web until the initial residual moment is cancelled when there is sufficient friction between the web and the roller. It turns out the initial assumption is incorrect, and the web and the roller can

reach to a steady state only the moment is zero, which turn out to be the fourth boundary condition in expression (2.2).

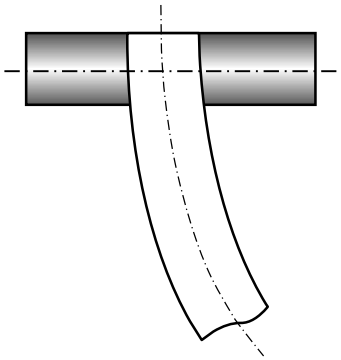

Figure 2.4 – Web with an Initial Residual Moment

The lateral deformation in a web span due to a misaligned roller can be described in expression (2.3) if inserting four boundary conditions (2.2) into equation (2.1). This achievement of Shelton's work is the basis of web handling analysis and widely used in the further web research.

$$v_x = L\theta_j[\frac{\cosh(KL)}{\cosh(KL)-1}(\frac{x}{L}-\frac{\sinh(KL)}{KL})+\frac{1}{KL}\frac{\sinh(KL)}{\cosh(KL)-1}(\cosh(Kx)-1)] \qquad (2.3)$$

Shelton designed a test apparatus to verify his boundary conditions and the corresponding lateral deformations. The moment at the downstream end of the web span was proved to be zero. Excellent correlation of the lateral deflection between the theoretical elastic curve (2.3) and experimental data was achieved for KL=2.9.

For a relatively short web span, the deflection due to shear the stresses is significant that cannot be ignored. Shelton derived the differential equation of the lateral deflection for a short web as equation (2.4) and the corresponding general solution is the expression (2.5) with the four unknown constants C1 to C4.

$$v_x^{iV} - K_e^2 v_x'' = 0 \qquad (2.4)$$

$$v = C_1\sinh(K_e x) + C_2\cosh(K_e x) + C_3 + C_4 \tag{2.5}$$

Where, $K_e^2 = \dfrac{T}{EI(1+n'\,T/AG)}$; n' is stress averaging factor, equals to 1.2 for the web has a rectangular cross section; A is the cross sectional area of the web which equals to tW; G is the web shear modulus. The slope as the web exits from the roller i is unknown, and it is nonzero due to the shear force at roller j N_j.

There are five boundary conditions in expression (2.6), four of them are for the differential equation (2.4) and one is for the algebraic relation. There is sufficient traction for the web so the normal entry rule guarantee the short web enter the misaligned roller j normally, and the moment at the entry to roller j is zero:

$$\begin{cases} 1)\ v_i = 0 \\ 2)\ v_j' = \theta_j \\ 3)\ v_j'' = 0 \\ 4)\ N_j + T\theta_j = -TK_eC_1/(1+n'T/AG) \\ 5)\ n'(N_j + T\theta_j)/AG = C_3 + C_1K_e \end{cases} \tag{2.6}$$

Shelton's solution to the differential equation (2.4) as a short web span transits a misaligned downstream roller shown as:

$$v_x = L\theta_j\Big[\frac{\cosh(K_eL)}{\cosh(K_eL) - (1+\frac{n'T}{AG})/(1+\frac{2n'T}{AG})}\frac{x}{L} - \frac{(\cosh(K_eL))(\sinh(K_eL))}{(K_eL\cosh(K_eL))(1+\frac{2n'T}{AG})/(1+\frac{n'T}{AG}) - 1} + \frac{1}{K_eL}\frac{(\sinh(K_eL))(\cosh(K_ex)-1)}{(\cosh(K_eL))(1+\frac{2n'T}{AG})/(1+\frac{n'T}{AG}) - 1}\Big] \tag{2.7}$$

The expression (2.7) would reduce to expression (2.3) if n'T/AG is equal to zero, in which case K_e is equal to K. Shelton claimed the effect of shear is negligible if K_eL is greater than 1. He did tests while the K_eL were 0.1, 0.2, 0.4, and 1. In his test, if K_eL is 0.1, a value of n'T/AG of 0.001 is significant, however, if K_eL is 1, a value of n'T/AG of 0.05 has little effect.

Shelton [17] developed a simplified model for the short web span (length/width<2) in order to acquire a simpler mathematical expression for web lateral deformation. The basic simplification for the short web span is the effect of tension on bending is insignificant, thus the elastic curve of web lateral deformation could be expressed by a polynomial in MD location x as equation (2.8) instead of exponential or hyperbolic functions as necessary for webs with large L/W.

$$v_x^{iV} = 0 \tag{2.8}$$

The simplified four boundary conditions were acquired for a short web span with a misaligned downstream roller:

$$\begin{cases} 1)\ v_i = 0 \\ 2)\ v_i' = -EIv'''/(tWG) \\ 3)\ v_j' = \theta_j \\ 4)\ v_j'' = 0 \end{cases} \tag{2.9}$$

The second boundary condition – the angle of the web leaves the upstream roller – was determined by the shearing stress – EIv'''/(tW) and web shear modulus G. The lateral displacement of the web was then defined as:

$$v_x = \frac{L\theta_j}{6(L/W)^2 + E/G}\left[\frac{E}{G}\frac{x}{L} + 6\left(\frac{L}{W}\right)^2\left(\frac{x}{L}\right)^2 - 2\left(\frac{L}{W}\right)^3\left(\frac{x}{L}\right)^3\right] \tag{2.10}$$

Shelton also studied the boundary conditions for a short web span with the upstream roller has a misaligned angle θ_i. The lateral displacement of the web can be determined by expression (2.12) with considering the boundary conditions (2.11).

$$\begin{cases} 1)\ v_i = 0 \\ 2)\ v_i' = \theta_i - EIv_i'''/(tWG) \\ 3)\ v_j' = 0 \\ 4)\ v_j'' = 0 \end{cases} \tag{2.11}$$

$$v_x = \frac{L\theta_i (L/W)^2}{6(L/W)^2 + E/G}\left[6\left(\frac{x}{L}\right) - 6\left(\frac{x}{L}\right)^2 + 2\left(\frac{x}{L}\right)^3\right] \tag{2.12}$$

Shelton considered the webs enter the misaligned rollers while all the rollers were assumed to be perfectly cylinders. However, the rollers might have unintentional taper in radius which result from machining or wearing. Yurtcu et al. [18] incorporated the beam stiffness matrix with four boundary conditions for a free web enters a tapered downstream roller. The tapered roller has nominal radius in R_0 and the slope in radius over the roller width is m. A taper in roller radius will result in MD stress variation across web width which is responsible for the development of lateral moment within the web. The boundary conditions were defined for the web span between two aligned rollers with one cylinder one taper:

$$\begin{cases} 1)\ v_i = 0 \\ 2)\ \theta_i = N_j / GA_s \\ 3)\ \theta_j = 0 \\ 4)\ M_j = -mEtW^3/12R_0 \end{cases} \tag{2.13}$$

Where, A_s is the area of beam which reacts to the shear, and it is 5tW/6 for the web with a rectangular cross section. The lateral deformation of the web was determined by incorporating the beam stiffness that developed by Przemieniecki [10] and the boundary conditions (2.13). The lateral deformation at the downstream roller v_j is proportionate to the slope of the taper radius according to expression (2.14).

$$v_j = \frac{mtW^3E}{6R_0} \frac{-60EI + (5GA_sL^2 - TL^2)(1+\phi)}{[60EI + TL^2(1+\phi)](T + GA_s)} \tag{2.14}$$

Where, ϕ is a shear parameter which is $12EI/(L^2GA_s)$. While small tapers may have produced only lateral deformations in the web, larger tapers could induce trough and wrinkle instabilities which will be discussed later. The expression (2.14) was validated by tests that small tapers can generate significant registration errors.

Summary**:** Some success has been achieved in predicting the lateral deformation of a web that was initially straight as it approaches a downstream roller that might be misaligned or perhaps tapered in radius in the CMD. Effects of shear stiffness have been considered for short spans. All of these analyses make assumptions that no slippage of the web occurs on rollers. Thus there must be ranges of operating parameters where these predictions are valid and outside that range they become invalid. For instance, consider Shelton's expression (2.3). It is valid as long as the boundary conditions in (2.2) are valid. For a web with a misaligned downstream roller, the moment in the web is maximum at the upstream roller ($M_i \sim 2EI\theta_j/L$) and decays linearly to zero as the web enters the downstream roller. How large a moment M_i can be applied prior to slippage occurring which would cause the 2nd boundary condition ($v_i'=0$) in (2.2) to become invalid? It could be argued that any non-zero M_i would cause some slippage at the exit of the upstream roller, so the curiosity then becomes how large v_i' can be in reality before expression (2.3) becomes invalid. Shelton's boundary conditions $v_i'=0$ and $v_j'=\theta_j$ are kinematic boundary conditions. These boundary conditions are valid only if they can be enforced by the friction forces that are available between the webs and the rollers.

2.3 Web Lateral Deformation Resulting from Web Camber

All webs are imperfect in the real world. A web whose length varies linearly in the CMD is said to have constant web camber. Such a web supported on a flat surface and unloaded would have the appearance of a curved beam with constant radius of curvature ρ. The radius of curvature ρ that defines a constant web camber is defined at the elastic axis of the web. When a cambered web is being transported through a web line, part of its camber will disappear due to the lateral deformation caused by the combination of web tension and the curvature of the web. Those authors that have written about cambered webs will refer to the long and short side of the web. If a sector of a cambered web is cut and laid unloaded on a flat surface, one edge of the web will be longer

than the other edge. Even when the cambered web is continuous reference will still be made to the long and short sides of the web. Some authors will refer to the slack and taut edge of the web as well. When the cambered web is under tension in transit bending stresses result which cause the short side to undergo higher MD stress than that due to web tension. Conversely the long side will have an MD stress lower than that due to web tension. Thus the short or taut edge are the same edge and the long or slack edge are also synonymous. Camber can result from the process from which the web is made but more often it is the result of viscoelastic deformation due web thickness non-uniformity in the CMD and residual winding stresses while the web is in roll storage. Constant web camber is the simplest case of web length uniformity. After 51 years of study [14] no valid closed form expression that predicts registration error due to constant web camber exist.

As a chronic problem in the web handling industry, camber can cause or compound problems such as troughs, wrinkles, slack edges or lateral motion that contributes to registration errors. Experimental data are valuable for web handling research since they can provide insight in theory development. For cambered webs, some experiments were performed to analyze their effect on the lateral deflection. Swanson [19] manufactured cambered webs with various curvatures and developed a special apparatus to measure these non-uniform webs in transit. The independent variables such as the span length, web tension, and web camber were considered to determine the response of the lateral displacement of the cambered webs and their shear forces. The ratio of web span length to its width was between 2.2 and 6.7. The test results showed that a cambered web, even in a short length deflected toward the slack edge. This meant the 4^{th} boundary condition that Shelton developed for the uniform web– the moment at the downstream end of a free web span was zero in expression (2.2) - was incorrect for cambered webs. For the cambered web, Swanson pointed that the range of v_j'' should between 0 and $1/\rho$, while ρ is the initial radius of curvature for the cambered web without any tension or velocity. He also mentioned that this boundary condition is related to the length of web span.

It is more difficult to measure the curvature of a running cambered web under tension than the web without tension lying on a flat surface. For a web has a constant camber without any tension, Shelton provided a method to measure its radius of curvature ρ [20]. As shown in Figure 2.5, the cambered web conforms to a flat surface by straightening out creases. The distance between the arc of the web and the chord is d, and l is the length of the test section of the web, the radius of curvature ρ can be defined as:

$$\rho = l^2/8d \tag{2.15}$$

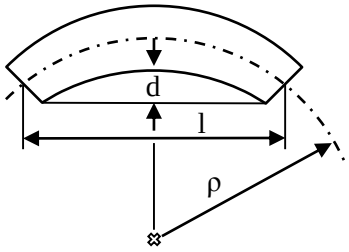

Figure 2.5 – Measurement of Web Camber

Swanson [21] continued to explore the lateral deformations of a cambered web which generated by a new method. A laterally shifting slitting system has the capability to cut an accurate, large radius web from an initially wider longitudinally advancing web. The cambered section of the web was cut and followed by a straight section. The lengths of the straight section and cambered section were set 4 times larger than the test span length L to ensure steady state operation can be observed. Dynamic lateral position data at the entry and exit points of the test spans was taken, and the static lateral position data was the average value of the dynamic data measured in the steady state region of operation. Shelton's first boundary condition in the expression (2.2) was enforced for the test web by using a web guide to maintain the zero lateral deformation at entry to the test span (i.e. v_i=0). Shelton's second boundary condition – slope at the upstream edge is zero (2.2) –

seemed incorrect according to the pictures of the upstream roller during the steady state condition. The curvature of the tensioned web varied with web tension and web-roller traction. Swanson pointed out that the web-roller traction is very important for the lateral deflection of the cambered web, especially the traction at the downstream roller.

The goal to analysis and test the cambered web is to predict the lateral deflection at given location of the web line. The closed form expression for the cambered web has been seeking for several decades. However, the difficulty of the proper boundary conditions for the free web span is the main problem.

Shelton [20] applied an initially straight web transiting a tapered roller to simulate a cambered web transiting cylindrical rollers. The web side which rides on the roller end with larger radius was assumed as the long side of the cambered web. For the tapered roller with taper in m and nominal radius in R_0, the curvature of the straight web on this roller $1/\rho_c$ is shown as:

$$1/\rho_c = m/R_0 \tag{2.16}$$

If the upstream cylindrical roller and downstream tapered roller are aligned, the four boundary conditions for solving the differential equation (2.1) can be determined as (2.17). Compared with boundary expressions (2.2), the curvature of the web herein is expressed by the slope of the roller and the nominal radius of the tapered roller.

$$\begin{cases} 1)\ v_i = 0 \\ 2)\ v_i' = 0 \\ 3)\ v_j' = 0 \\ 4)\ v_j'' = -m/R_0 \end{cases} \tag{2.17}$$

The solution to expression (2.2) is the deflection curve of a moving web in its steady state:

$$v_x = \frac{m}{R_0 K'^2}[\cosh(K'x) - 1 - \frac{\sinh(K'L)}{\cosh(K'L) - 1}(\sinh(K'x) - (K'x))] \tag{2.18}$$

Where, $K'L=(L/W)\sqrt{12T/EtW}$. For small values of K'L, the lateral displacement of the web at the downstream end would be simplified to expression (2.19). The presence of L^2 shows the span length has a huge effect on the steering as the web on a tapered roller, which also indicated a great influence on the cambered web.

$$v_j = \frac{mL^2}{6R_0} \tag{2.19}$$

If the taper m and nominal radius R_0 were fixed, the lateral displacement of the cambered web v_j should have a L^2 relation with the web length according to expression (2.19). However, Swanson proved by tests that there was no such relation for the cambered web [19], thus he pointed out that Shelton's tapered roller concept probably cannot explain the cambered web behavior.

Swanson [22] defined M_0 as the virtual moment on the web which caused web initial curvature. He established four boundary conditions for a long cambered web (length/width>10) between two rollers. Compared with Shelton's boundary conditions (2.17), only the fourth one was different ($v_j'' = -M_0/EI$). The closed form solution to the lateral deformation of the long cambered web was given by solving equation (2.1):

$$v_x = -\frac{M_0}{T}\left[1 - \cosh(Kx) + \frac{\sinh(KL)}{1\text{-}\cosh(KL)}(Kx - \sinh(Kx))\right] \tag{2.20}$$

For a relatively short cambered web, Swanson pointed out that the web does not have any lateral deflection. He disagreed with this conclusion in his later paper that very small deflections and shears do exist [19]. He also indicated the radius of curvature of the steady state web at the downstream end of the span ρ_j is not the same as the radius of curvature of the web without tension ρ. The range of curvature $1/\rho_j$ is between 0 and $1/\rho$. The four boundary conditions for a short

cambered web approaching a misaligned downstream roller were shown as expression (2.21). The lateral deflection of the cambered web curve in (2.22) was the superposition of two terms: one was linear with the misaligned angel θ_j and another one was linear with the curvature of the steady cambered web $1/\rho_j$.

$$\begin{cases} 1)\ v_i = 0 \\ 2)\ v_i' = 0 \\ 3)\ v_j' = \theta_j \\ 4)\ v_j'' = -1/\rho_j \end{cases} \tag{2.21}$$

$$\begin{aligned} v_x = L\theta_j[\frac{\cosh(KL)}{\cosh KL\text{-}1}(\frac{x}{L}-\frac{\sinh(KL)}{KL})+\frac{1}{KL}\frac{\sinh(KL)}{\cosh KL-1}(\cosh(Kx)-1)] \\ +\frac{L}{K\rho_j}[-\frac{\sinh(KL)}{\cosh(KL)-1}(\frac{x}{L}-\frac{\sinh(KL)}{KL})-\frac{1}{KL}(\cosh(Kx)-1)] \end{aligned} \tag{2.22}$$

The moment and shear at the downstream roller could be calculated as superposition of two equations based on the lateral deformation (2.22). Swanson described the techniques to manufacture the cambered web with the desired curvature, and the measurement of displacement and shear force at the downstream end of a cambered web. The tests showed the steady downstream curvature that the long span web has is only a small fraction of the curvature of the non-tension web, whereas the short span web has a higher percentage value.

The boundary conditions Swanson developed (2.21) are similar with the one Shelton provided (2.17). They both assumed that there is sufficient friction force between the web and the roller to prevent slippage, and to ensure the shape of the web conforms to the outer surface of the roller. Shelton used an initially straight web and a tapered roller to model a cambered web on a cylindrical roller and Swanson used a cambered web with a constant curvature at the downstream roller to infer the lateral deformation. However, the curvature of a moving web in roll-to-roll machinery would change due to various parameters such as web tension, and span length. Other

disturbances also increase the difficulty to measure or determine the steady curvature of the web under tension.

Olsen [23][24] believed the lateral shift of the web is caused by widthwise variations in material properties, i.e., frozen-in strain ε_i. The frozen-in strain is referred to camber in steel industry which is not accounted for by elementary beam theory. The differential equation for the lateral displacement as the cambered web passes over a misaligned downstream roller was developed by Shelton [14] and the four boundary conditions were defined similar as expression (2.21). The only difference is the fourth boundary condition: $v_j'' = -\kappa_j$, where κ_j is the web curvature at the downstream roller which is determined by ε_i. The lateral deflection curve was presented as expression (2.23).

$$\begin{aligned} v_x = L\theta_j[\frac{\cosh(K_\varepsilon L)}{\cosh(K_\varepsilon L)-1}(\frac{x}{L}-\frac{\sinh(K_\varepsilon x)}{K_\varepsilon L})+\frac{1}{K_\varepsilon L}\frac{\sinh(K_\varepsilon L)}{\cosh(K_\varepsilon L)-1}(\cosh(K_\varepsilon x)-1)] \\ +\frac{L\kappa_j}{K_\varepsilon}[\frac{\sinh(K_\varepsilon L)}{\cosh(K_\varepsilon L)-1}(\frac{x}{L}-\frac{\sinh(K_\varepsilon x)}{K_\varepsilon L})+\frac{1}{K_\varepsilon L}(\cosh(K_\varepsilon x)-1)] \end{aligned} \tag{2.23}$$

Where, K_ε is determined by web properties and web traction that can be calculated by expression (2.24).

$$\begin{aligned} K_\varepsilon &= \frac{TS}{\Omega S - H^2} \\ S = \int Etdy,\ \Omega &= \int Ey^2tdy,\ H = \int Eytdy \end{aligned} \tag{2.24}$$

The web lateral deflection from expression (2.23) is similar as the one from expression (2.22), i.e., it is the superposition of two terms: one is linear with the roller misalignment and the other one is linear with web curvature. It showed the web steerage towards the longer edge which was agree with test results [19]. In the numerical example, Olsen made a crude estimate of ε_i for paper since there is little information about the profile of frozen-in strain in paper. However, the methods to determine the ε_i for a web under tension was not mentioned.

Olsen [25] extended his model with considering the shear effects for the cambered webs. The shear angle at the upstream roller was proportional to the shear force, which was determined by the lateral displacement. The dynamic boundary conditions were used, and the numerical method was developed to solve the differential equations for web lateral deformation. The shear effect had a contribution from the shear force and frozen-in shear strain. The numerical results showed the shear effect is only insignificant for the straight web which has high ratios of length to width, and it is significant for all cambered webs. Olsen also considered the lateral mechanics of the camber web under low tensions and he claimed the cambered web moves to the slack side only when the web and the roller in the sticking condition.

Jones [26] built the finite element model to simulate a cambered web with considering the gravity effect. This model contains a web span without any rollers. For a long web span, the slope at web upstream end was assumed to be zero strain. There are other boundary conditions including the fixed upstream CMD position, zero slope and zero curvature at web downstream end. In the simulation, the lateral deflection of the cambered web would decrease if we increase web tension. Jones recommended to increase web tension in order to reduce the lateral steering of the cambered web. Several parameters such as web span, width, camber, density and modulus were studied in the simulation to explore their effects on web lateral movement. It shows the horizontal span would sag under its own weight and a cambered web would sag more at the long edge where the web was under low tension. It showed the cambered web would steer toward to the high tension side which is in the opposite direction in contrast with the experimental results from Swanson [19] and Brown [27]. Although the simulation results are not accurate to predict the lateral displacement for the cambered web, the finite element method that Jones used inspired other researchers to run simulations for the cambered webs.

Fu et al. [28] explored the steering of a cambered web by ABAQUS/Explicit finite element analysis. It showed the lateral steering towards the long side of the cambered web which

qualitatively agreed with the experimental results [19][21]. Fu's simulations made no assumption of kinematic boundary conditions for the free web span since the long web transiting a series of rollers in his models. A web guide was set to steer the cambered web enter the test span with its centerline coinciding with the zero position. Fu's analysis showed that the upstream slope v_i' is small but not zero, and the downstream moment is non-zero but the curvature as the web enters the downstream roller tends toward zero. Fu's simulations were intended to model Swanson's experiments [21] but the quantitative agreement of the simulated lateral deformations with Swanson's test results was not good.

Good conducted an improved simulation of cambered web steering by using the standard dynamic implicit solver which produced highly accurate stress solution [29]. A linear temperature variation across the web width was introduced to induce camber in the free web span. The thermally induced camber in the test section eliminated the need to simulate the web guide and provided the accuracy in desired camber. The second boundary condition that the web exits the upstream roller θ_i is always assumed to be zero, however, the FEA showed it is non-zero but very small (5.76×10^{-5} rad). The fourth boundary condition for the cambered web is the controversial one for years. Good concluded the curvature of the cambered web at downstream end is the change in curvature between the undeformed web and the deformed steady state cambered web. To determine the deformed radius of curvature at the downstream end requires a method that can establish the equilibrium of the internal forces in the deformed web and the external forces due to slip as the web enters the downstream roll and the stick behavior of the web on the roller. Only laboratory tests and dynamic simulations have shown that capability. The lateral deformation of the cambered web at the downstream end from the closed form expression compared nicely with the result from the tests and simulations.

Summary: Web camber does not appear to be a problem that can be modelled using kinematic boundary conditions. θ_i and v_j'' are neither zero nor can be predicted based upon the

undeformed web shape or other known input. It is known that the deformed curvature at the downstream roller is less than the undeformed curvature and greater than zero. It appears that $\theta_j=0$ is a valid kinematic boundary according to Fu's results [28] and it can be argued per Swift [16] that unless $\theta_j=0$ the lateral deformations cannot be at steady state. Thus if a web is cambered the lateral deformations and hence registration in a process web span cannot be predicted accurately at present. Fu and Good [28] modeled the web as shell elements (S4R). To compare their results to that of previous authors required them to produce comparable output to a beam. They used lateral deformations from nodes that would lie on the elastic axis of the web. Then, they used finite difference approximations to estimate the slope and curvature as a function of a curvilinear x coordinate that follows the elastic axis. The second derivative approximation of the curvature was numerically noisy which resulted from the use of an explicit solution procedure while it was smooth for the results from implicit solution. It also suggests that if second derivative boundary conditions are important in the solution of cambered web problems that perhaps explicit solution routines are inappropriate.

2.4 Web Moment Transfer: Boundary Conditions Associated with Steady State Lateral Behavior

Research of the uniform and non-uniform webs has been focused mainly on the lateral deformation of the web span between two rollers. Beam theory was employed for the web without considering the interactions between webs and rollers. The normal entry rule requires sufficient friction forces between webs and rollers to avoid web slippage on the roller. In Sections 2.2 and 2.3, there are several examples in which the proper boundary conditions were sought to solve the differential equation (2.1). The expressions described the lateral deformation of the elastic axis of the web throughout a web span.

In general, for webs transit over multiple rollers for various manufacture processes, the friction interaction cannot guarantee the webs on the roller have stick condition under all situations. Slippage may occur as the web on the roller, and bending moment may transfer from roller to roller.

The interaction between the web and three rollers is the simplest case to understand the moment transfer before exploring more complex situations. As shown in Figure 2.6(a), the two web spans are in one plane for illustrative purpose but in reality the web wrap around each roller with 90° wrap angle. The contact area between the webs and each roller is rectangular in shape before webs slip on the roller. There are three rollers while span a is the web span between roller A and roller B, and span b is the web span between roller B and roller C. Roller A and roller B are parallel each other and roller C has a misaligned angle θ_{bj}. This misalignment of roller C will generate the internal bending moment in the span b while the maximum occurs as the web exits from roller B and decreases to zero at roller C. The web has uniform MD stress across web width as it entry to roller C. If the internal moment at the exit of roller B is balanced by the friction between the web and roller B, most webs on roller B have sticking condition and no moment transfer to span a so the internal moment in span a is zero. However, if the misaligned angle θ_{bj} becomes so large that the traction on roller B cannot react the internal moment in span b, slippage will occur over a large percent of the contact area on roller B. The moment will transfer across roller B from span b upstream into span a as presented in Figure 2.6(b). Normal entry law cannot be guaranteed as the web enters and exits roller B. The web-roller traction may not adequate to restrain the web rotation and the lateral movement will transmit upstream into span a. In addition, the internal moment in span a will not keep zero which result in the non-uniform web tension across web width. the arrows in Figure 2.6 shows the distribution of web MD stress. The state of traction between the web and the roller has an impact on the types of moment transfer. Gehlbach et al. [30] pointed out that the misaligned angle of the roller C for moment transfer can be much greater than the critical tram error to generate web wrinkles on roller.

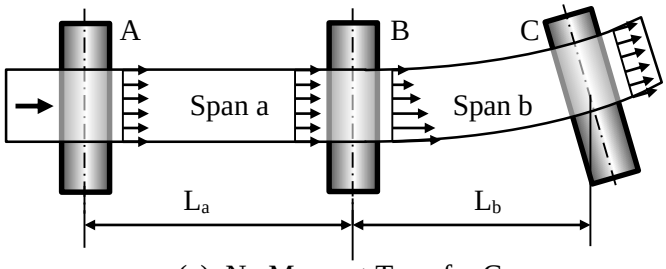

(a) No Moment Transfer Case

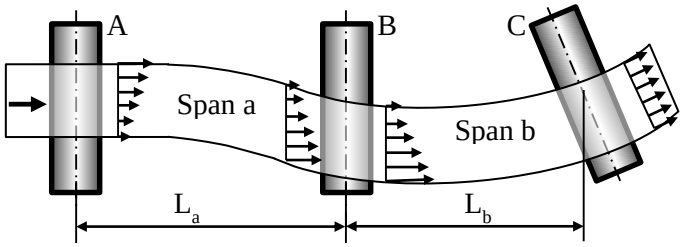

(b) Moment Transfer Case

Figure 2.6 – Lateral Deformation and Stress Distributions of the Web Before and After Slippage at Roller B due to the Misalignment at Roller C

Dobbs and Kedl [31] developed a cantilever beam model for the web with three rollers. The model is similar as the one in Figure 2.6(a). The web is totally fixed at roller A position and it bent to misaligned at roller C position due to a vertical shear force F acted on the web. The MD velocity was not considered since the web was in the steady state condition. There are two cases: Case 1 is the no moment transfer situation and Case 2 is the moment transfer situation. The normal entry was forced as the web enter and exit roller B for both cases. In Case 1, there was no moment transfer on roller B. No lateral displacement or rotation occur as the web enters or exits roller B, so the misaligned angle of roller C is totally determined by the vertical shear force F. The intermediate supporting shear force and moment on roller B can be determined in terms of F by using the beam equilibrium expressions. In Case 2, moment transfer occurred and strain would transfer from the span b to the pre-entry span a. As normal entry rule applies on all rollers, the web entering roller B has a lateral displacement without rotation. The reaction shear force and reaction moment on roller

B were governed by the internal loads and moments in span a and b. The critical moment that generate moment transfer has been developed with the experimental validation.

Dobbs and Kedl did not consider the effect of web tension on web moment transfer. The web tension is one of the key parameters for the state of the web on the roller. In addition, the relation between the shear force F and the misalignment of roller C was not provided.

$$\begin{Bmatrix} N_i \\ M_i \\ N_j \\ M_j \end{Bmatrix} = \begin{bmatrix} \frac{12EI}{L^3}+\frac{6T}{5L} & \frac{6EI}{L^2}+\frac{T}{10} & -\frac{12EI}{L^3}-\frac{6T}{5L} & \frac{6EI}{L^2}+\frac{T}{10} \\ \frac{6EI}{L^2}+\frac{T}{10} & \frac{4EI}{L}+\frac{2TL}{15} & -\frac{6EI}{L^2}-\frac{T}{10} & \frac{2EI}{L}-\frac{TL}{30} \\ -\frac{12EI}{L^3}-\frac{6T}{5L} & -\frac{6EI}{L^2}-\frac{T}{10} & \frac{12EI}{L^3}+\frac{6T}{5L} & -\frac{6EI}{L^2}-\frac{T}{10} \\ \frac{6EI}{L^2}+\frac{T}{10} & \frac{2EI}{L}-\frac{TL}{30} & -\frac{6EI}{L^2}-\frac{T}{10} & \frac{4EI}{L}+\frac{2TL}{15} \end{bmatrix} \begin{Bmatrix} v_i \\ \theta_i \\ v_j \\ \theta_j \end{Bmatrix} \qquad (2.25)$$

Good [32] incorporated the stiffness matrix [10] for the beam with considering the web tension for the free web span between rollers as shown by equation (2.25). The sign convention is indicated in Figure 2.2.

Prior to moment transfer or web edge slackness, the displacement, rotation at roller B and moment at roller C are zero, which means v_{bi}, θ_{bi} and M_{bj} are zero. The subscript b indicates the parameter is in span b, and the similar way for span a to indicated by a. The subscript i is for the upstream end in a web span and j is for the downstream end. The remained shear forces, moment and lateral displacement can be expressed by the rotation of the web prior to roller C θ_{bj} which is the misaligned angel of roller C as web enter the roller normally. The lateral deflection of the web enters roller C expressed by v_{bj}:

$$v_{bj} = \frac{4(30EIL_b + TL_b^3)}{3(60EI + TL_b^2)}\theta_{bj} \qquad (2.26)$$

The moment at the upstream end of span b M_{bi} can be determined as a function of the misalignment of roller C and known span length and web properties:

$$M_{bi} = -\left[\frac{2EI}{L_b} + \frac{TL_b}{6}\right]\theta_{bj} \tag{2.27}$$

If the traction on roller B does not have the capacity to resist the internal moment in expression (2.27), which means M_{bi} exceeds the critical moment M_r, the web would slip on roller B and moment transfer begins. For web with tension T, width W and wrap angel β, M_r is expressed by expression (2.28). The average friction coefficient μ was assumed between the web and the roller.

$$M_r = \frac{\mu T \beta W}{4} \tag{2.28}$$

After moment transfer occurs on roller B, the lateral displacement of the web enters roller B in span a v_{aj} was nonzero and it was determined by the moment at the downstream end M_{aj} as shown in expression (2.29). The moment M_{aj} can be determined by expression (2.30). In span a, other lateral displacements and rotations were still zero as the web was assumed to have the normal entry on roller A.

$$v_{aj} = -M_{aj}/\left(\frac{6EI}{L_a^2} + \frac{T}{10}\right) \tag{2.29}$$

$$\begin{aligned}
&M_{aj} = 0 && \text{when} \quad M_{bi} < |M_r| \\
&M_{aj} = -[M_{bi} - M_r] && \text{when} \quad M_{bi} > |M_r| \ \text{ and } \ M_{bi}(+) \\
&M_{aj} = -[M_{bi} + M_r] && \text{when} \quad |M_{bi}| > |M_r| \ \text{ and } \ M_{bi}(-)
\end{aligned} \tag{2.30}$$

In the meantime, the lateral displacement of the web enter roller C in span b v_{bj} will increase due to the nonzero v_{aj}. The new v_{bj} is the sum of the displacements in expression (2.26) and (2.29). The friction coefficient between the web and the roller was affected by the entrained air and it could be determined based on web and roller surface roughness. The potential for web edge slackness

was incorporated into the beam model and the critical misaligned angle of roller C $\theta_{bj,slack}$ for the onset of the slackness shown as:

$$\theta_{bj,slack} = \frac{TL_b}{W^2 tE} \tag{2.31}$$

The shear effect was not considered in the expression (2.25). The experiments were performed with quite long web span ($L_a/W>4$, $L_b/W>4$) and they proved the expressions developed herein for web shear and deformations as function of roller misalignment, moment transfer, and web edge slackness were reasonable.

Shelton [33] continued the discussion about the interaction between two web spans because of a misaligned downstream roller. The differential equations for the webs with different span length were solved: short span with length/width less than 3.5 and long span with length/width more than 3.5. Tests data reported by Good [32] were compared with the results from expressions, using lateral position and lateral reactions, and they match quite well. Suggestions were given to avoid moment transfer when design the web processing lines.

Fu et al. [15][34] examined boundary conditions which governed the lateral mechanics of the web span. Explicit finite element simulations were used to provide the validity of the assumptions made for theories developed by Shelton [15]. These simulations required some basic assumptions. For instance, the MD velocity applied on web upstream end and the MD tension on web downstream edge are uniform in simulations. The simulations involved a long web passing over 4 rollers with the 3rd roller misaligned at various levels. The path of the web was governed entirely by the frictional forces between the web and rollers. After the lateral deformations achieved steady state, the web deformations could be explored to determine if normal entry or zero curvature boundary conditions assumed by Shelton had been achieved. It was unique was that with increased roller misalignment the frictional limits associated with these boundary conditions could be explored. The validity and bounds of kinetic expressions such as (2.28) and (2.30) were also

studied. A membrane element (M2D4R) was used in this model so that only in-plane forces were transmitted and there was no bending or transverse shear stiffness. Finite element methods (FEM) were used to determine web lateral displacement and lateral velocities. From Good [32] prior to moment transfer as $M_{bi} \leq M_r$, the lateral displacement in span a v_a and span b v_b were shown as expression (2.32). The critical moment that the roller B could be resist was shown in expression (2.28).

$$\begin{aligned} v_a &= 0 \\ v_b &= -[\frac{4(30EIL_b + TL_b^3)}{3(60EI + TL_b^2)}(\frac{3x_b^2}{L_b^2} - \frac{2x_b^3}{L_b^3}) + (\frac{x_b^3}{L_b^3} - \frac{x_b^2}{L_b^2})]\theta_{bj} \end{aligned} \tag{2.32}$$

where x_b is a coordinate whose origin is at the beginning of entering span b and proceeds toward to the span end. L_b is the length of span b in Figure 2.6(b). The lateral displacements were nonzero in both spans after moment transfer begun, under the condition $M_{bi} > M_r$:

$$\begin{aligned} v_a &= \frac{M_{bi} - M_r}{(\frac{6EI}{L_a^2} + \frac{T}{10})}\ (\frac{3x_a^2}{L_a^2} - \frac{2x_a^3}{L_a^3}) \\ v_b &= \frac{M_{bi} - M_r}{(\frac{6EI}{L_a^2} + \frac{T}{10})} - [\frac{4(30EIL_b + TL_b^3)}{3(60EI + TL_b^3)}(\frac{3x_b^2}{L_b^2} - \frac{2x_b^3}{L_b^3}) + (\frac{x_b^3}{L_b^3} - \frac{x_b^2}{L_b^2})]\theta_{bj} \end{aligned} \tag{2.33}$$

where x_a is a coordinate whose origin is at the beginning of pre-entering span a and proceeds toward the span end. L_a is the length of span a. Fu explored the internal moment M in the web by analyzing the MD stresses (σ_{MD}) from the simulations after steady state lateral deformation had been achieved:

$$M = \int \sigma_{MD} y dA \approx \sum_{i=1}^{n} \sigma_{MDi} y_i A_i \tag{2.34}$$

where σ_{MDi} is the MD stress at the node i, y_i is the distance between the node i and web elastic axis, A_i are the cross sectional area of the web associate with node i. The moment applied to the web by

the friction forces in the MD M_{MD} and CMD M_{CMD} could be determined by the simulation contact shear stresses. These moments resist the internal bending moment in the free web span due to the roller misalignment.

$$\begin{aligned} M_{MD} &= \int CShear1 \cdot y \cdot dA_s \approx \sum_{i=1}^{n} CShear1_i \cdot y_i \cdot A_{si} \\ M_{CMD} &= \int CShear2 \cdot x \cdot dA_s \approx \sum_{i=1}^{n} CShear2_i \cdot x_i \cdot A_{si} \end{aligned} \tag{2.35}$$

where $CShear1_i$ and $CShear2_i$ are the contact shear stress between the web and roller in MD and CMD at node i, respectively; A_{si} is the contact area between the web and the roller associate with node i; x_i is the MD distance between the node i and the web exit of the contacted roller. This lead Fu to more accurate estimations of the moment due to friction. Laser Doppler Velocimetry (LDV) was employed to examine the web velocity variation directly without interfering with the web. This allowed the inference of moment at any location down the length of the web, even on roller B where the moment was affected by slippage and friction. The lateral displacement (2.33) and moment predictions (2.27) correlate quite well with the experimental data and FEA results.

Summary: Friction forces between webs and rollers are important because they are shown to affect the lateral behavior of the web. The maximum moment which a roller can resist without slippage has been determined with uniform friction coefficient. The classical beam theory provided the critical misaligned angle of the roller to generate moment transfer between two web spans. The finite element simulations and the experimental methods demonstrated by Fu [15][34] show how these frictional effects can be studied and when kinematic boundary conditions such as (2.2) become invalid. The simulations allow the study of lateral behavior without making assumptions of kinematic boundary conditions between the web and rollers. These simulations show promise in providing a method to attack problems such as lateral behavior due to web camber discussed earlier.

2.5 Instability of a Web in Steady State Conditions

Most webs have extremely small thickness compared with the width and length. Even small lateral stresses would induce web instabilities which are herein divided as web troughs and wrinkles. Troughs appear in free web spans between rollers and wrinkles occur as the web wrap over rollers. The troughs are sometimes acceptable if they do not interfere the following manufacture operations, while most wrinkles are catastrophe which are usually not welcome in industry and should be avoided all the time. The closed form expressions have been developed for the steady state web to have troughs or wrinkles.

Good and Beisel [6] studied the criteria to generate troughs in orthotropic webs. The web was assumed to have the instability at the lowest load or stress level. As shown in Figure 2.7, a web in the shape of a rectangular coupon has uniform surface tractions in x and y directions to generate web MD stress σ_x and CMD stress σ_y. This web has the same dimensions and sign conventions as shown in Figure 2.1 and 2.2. The simply supported boundary conditions at all edges were assumed to simulate the web span between rollers. The web is assumed in Regime 1 [1] and approaching to Regime 2, so the total potential energy equation for plate was employed and solved by Rayleigh-Ritz method. The critical CMD stress $\sigma_{y,trough}$ was derived to form uniform web troughs in y direction with half wave number n_{trough}.

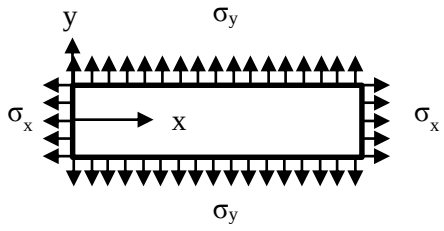

Figure 2.7 – A Coupon submitted to Uniform Edge Loads

$$\sigma_{y,trough} = -\frac{\pi t}{L}\sqrt{\frac{\sigma_x E_y}{3(1-\nu_{xy}\nu_{yx})}} \tag{2.36}$$

$$n_{trough} = W\sqrt{\frac{2}{\pi tL}}\sqrt[4]{\frac{3(1-\nu_{xy}\nu_{yx})\sigma_x}{E_y}} \tag{2.37}$$

where the subscripts x and y indicate the parameter in MD and CMD, respectively, and ν is the Poisson's ratio of the web. The negative sign of $\sigma_{y,trough}$ indicates the stress is compressive in y direction or in CMD. Note the MD stress in x direction σ_x is always positive. These orthotropic web expressions can be simplified easily for the isotropic webs [1].

There are multiple sources to induce the lateral compressive stresses in web and approaching a misaligned downstream roller is a common one. The perfect aligned rollers can only exist in theories and simulations while there are always some tram errors for rollers in reality. For a web span that has been subjected to the shear force from a misaligned roller, the critical rotation to induce troughs in the orthotropic web $\theta_{trough,ave}$ can be determined rely upon expression (2.25) and failure criterion (2.36):

$$\theta_{trough,ave} = \frac{2}{5GL}\frac{5E_x^2t^2W^6 + TL^4(3T+5GtW)(1+\phi) + E_xtL^2W^3[25GtW+2T(3\phi-2)]}{5E_x^2t^2W^6 + 9T^2L^4(1+\phi) + 2E_xtTL^2W^3(3\phi+13)} \\ ?\sqrt{\frac{3\sqrt{3}\pi tL\sqrt{E_y}\sigma_x^{3/2}}{\sqrt{1-\nu_{xy}\nu_{yx}}} - \frac{3\pi^2t^2E_y\sigma_x}{1-\nu_{xy}\nu_{yx}}} \tag{2.38}$$

where ϕ is the shear parameter equals to $12E_xI/(L^2GA_s)$ for the orthotropic web, and A_s is 5Wt/6 for the web has the rectangular cross section. The troughs would be expected across much of the web width as the downstream roller has a rotation angle $\theta_{trough,ave}$. Troughs should first appear at the web center due to the maximum flexural shear stress, which is 1.5 times greater than the average value. Thus the expression for the critical rotation to predict the onset of the trough $\theta_{trough,max}$ was determined as:

$$\theta_{trough,max} = \frac{2}{3}\theta_{trough,ave} \tag{2.39}$$

The experimental data taken over a range of typical web line conditions were compared with the results from expression (2.38). Both isotropic and orthotropic webs were used with different span lengths and tensions. It appears that expression (2.38) provides the more accurate solution over broad range of span ratios. For short and long webs, the shear and tension effects were critical [7].

Beisel and Good [35] investigated the effect of a radial taper roller on web trough formation. A lateral shear force would be induced by the tapered roller and caused a steering effect on web span. Four boundary conditions were applied for the expression (2.25) as the web transits over a tapered roller to determine the critical radial taper for web troughs m_{trough}. This expression provided the onset of troughs in web span due to a tapered downstream roller:

$$m_{trough} = \frac{2LR_0}{3W^2E}\frac{[60EI + TL^2(1+\phi)](T + GA_s)}{GA_s[10EI + TL^2(1+\phi)]} \times \sqrt{(\frac{\pi}{L})^2 \frac{tTE}{3W(1-\nu^2)} + \frac{\pi}{L}\sqrt{\frac{T^3E}{3tW^3(1-\nu^2)}}} \tag{2.40}$$

Multiple web spans were tested for polyester and acceptable agreement achieved between the tested critical radial taper and the results from expression (2.40).

The web would take the shell shape of the roller surface from the planar attitude as it moves from the free span onto the roller. The lateral stresses to generate web wrinkles would be much higher than to form troughs due to the support of the roller [6]. If the web upon the roller is under uniform lateral compression, symmetrical wrinkles with respect to the axis of the cylinder were assumed to occur at a certain compressive load. This critical lateral stress $\sigma_{y,\,wrinkle}$ for the orthotropic web to generate wrinkles with half wave number $n_{wrinkle}$ was determined by Good [6] with:

$$\sigma_{y,wrinkle} = -\frac{t}{R}\sqrt{\frac{E_x E_y}{3(1-\nu_{xy}\nu_{yx})}} \tag{2.41}$$

$$n_{wrinkle} = \frac{W}{\pi}\sqrt{\frac{2}{Rt}}\sqrt[4]{\frac{3E_x(1-\nu_{xy}\nu_{yx})}{E_y}} \tag{2.42}$$

where R is the roller radius. Morgant proved by tests that expression (2.41) was accurate for nearly perfect cylindrical shells composed of polyester film which were internally stabilized by pressure [36]. As the web passes over the roller, the web tension result in the internal pressure. The maximum compressive stress which can be supported by the friction between the web and the roller $\sigma_{y,max}$ could be determined as web has uniform MD tension T. The wrinkle cannot sustained if $\sigma_{y,max}$ is less than the critical wrinkling stress predicted by expression (2.41).

$$\sigma_{y,max} = -\frac{\mu T}{4Rt} \tag{2.43}$$

The friction coefficient between the web and the roller was reduced by entrained air [7]. So the minimum web tension required to sustain web wrinkles T_{min} was defined piecewise as a function of the entrained air film thickness:

$$T_{min} = \begin{cases} \dfrac{2t^2}{W\mu_{st}}\sqrt{\dfrac{E_x E_y}{3(1-\nu_{xy}\nu_{yx})}} & \text{when } h_o \le R_q \\ \dfrac{4t^2}{E\mu_{st}(3-h_o/R_q)}\sqrt{\dfrac{E_x E_y}{3(1-\nu_{xy}\nu_{yx})}} & \text{when } h_o \le R_q \end{cases} \tag{2.44}$$

where, μ_{st} is the static coefficient of friction between web and roller surfaces, h_0 is the air film layer due to hydrodynamic lubrication which is a function of web velocity and tension [37], and R_q is the combined root mean square roughness of web and roller surfaces. The wrinkles on rollers cannot be sustained if the air film layer in excess of 3R. Shelton [38] used the simplified expressions for isotropic webs. He also discussed the potential for the lateral slippage of a web on a roller and how friction could limit the CMD stress in the shell of web transiting a roller.

Good and Beisel [7] demonstrated by a set of experiments that the compressive stresses required to induce wrinkles were much larger than the stresses needed to induce trough. Webb demonstrated the width reduction in the web span due to web troughs is responsible for the compressive stress in the web that upon the roller and ultimately results in wrinkles [39]. There was a linear relation between the tram error to generate web troughs and the tram error to cause web wrinkles. For the isotropic webs, the ratio of the critical CMD stress to generate web wrinkles (2.41) and the critical CMD stress for troughs (2.36) was shown in expression (2.45). This ratio is a function of web span length L, roller radius R, web modulus, and web MD stress σ_x. Both Webb [39] and Good [40] verified this relation by experiments and finite element simulations.

$$\frac{\sigma_{y,wrinkle}}{\sigma_{y,trough}} = \frac{-\frac{t}{R}\sqrt{\frac{E^2}{3(1-\nu^2)}}}{-\frac{\pi t}{L}\sqrt{\frac{\sigma_x E}{3(1-\nu^2)}}} = \frac{L}{\pi R}\sqrt{\frac{E}{\sigma_x}} \tag{2.45}$$

Good and Straughan [41] presented their work for the prediction of web wrinkles due to web twist. The misaligned roller and twist roller have different positions for their pivots. In general, we define the misaligned roller has the pivot at one end of the roller which allows roller misalignment in web plane. By contrast, the pivot of the twist roller located at the center of the roller axis and the web was assumed to have a parabolic MD stress across web width, so the Rayleigh-Ritz method could be employed to determine the normal and shear stresses of the web. For webs move over a twisted roller, the wrinkles would be generated if web maximum CMD stress due to the roller twist $\sigma_{y,twist}$ (2.46) reaches to the critical CMD stress for web wrinkles $\sigma_{y,wrinkle}$ (2.41).

$$\sigma_{y,twist} = -\frac{77 S_2 L^2 W^4}{32}\left(\frac{CON1}{CON2}\right) \tag{2.46}$$

$$CON1 = 10725L^8 + 25532L^6W^2 + 76429L^4W^4 + 25532L^2W^6 + 1430W^8$$
$$CON2 = 25025(L^{12} + W^{12}) + 129740(L^{10}W^2 + L^2W^{10}) + 911998(L^8W^4 + L^4W^8) + 726044L^6W^6$$

where S_2 is A constant that defines a parabolic distribution of MD stress in the web due to the twisted roller. The critical twisted angle of the roller can be determined then, and also the web deformations at web center and edges. The experiments employed four polymer webs to verified the accuracy of these expressions.

The finite element simulations were presented for thin webs to generate instabilities [40][42]. In free spans the elements were given a "wrinkle membrane" material behavior to allow to simulate web troughs. The elements on rollers have linear elastic properties which would accept compressive stresses for the formation of troughs in web spans. The simulations demonstrated troughs with certain amplitude can be generated by disturbances such as a misaligned roller, or a tapered roller, or a hole in the web. In finite element simulations the troughs appear only when the disturbances increase until the compressive stress became more negative than that given in expression (2.41). The three examples presented proved that the existence of troughs in web spans were a necessary precursor to web wrinkles.

Gopal and Kedl [43] used finite element method (FEM) to predict web deformations and wrinkles. They assumed there was no moment transfer across the up-stream roller and only wrinkle formed in regime 1 [1] was considered. Roller diameter and wrap angle were not considered here. Two approaches were taken for the finite element analysis. In the first approach, a two dimensional membrane model was used which cannot resist compressive stresses. The lateral deflections for specific tram error matched well with the experimental data. However, this model failed to predict the wrinkles. To address this, the author developed a three dimensional model which employed the plate element. A uniform MD tension was applied for a web span to simulate the web wrapped on a roller. The web was applied a shear force at one end to simulate the effect of the misaligned roller. on the web. The critical angle for web wrinkles was determined by the bifurcation point for the

reaction force. The finite element simulation predicted the angle for wrinkles and they were in good correlation with the experimental results.

Jones et al. [44] noted that small grit particles can lift the web off the drum which could be the disturbance to initiate wrinkles. A numerical "tent model" was developed to simulate the web lift off from the roller. The critical point was found as the compressive CMD stress increased until the contact force on the grit dropped to zero. Several parameters were analyzed to affect this critical point such as grit size, MD tension, web properties, web thickness and roller size.

Baipa [45] modeled the uniform webs which had one or two circular sections thinner or thicker than the other sections with the commercial code COSMOS 2.8 and ABAQUS. The effect of the thickness and size of the non-uniformity circular were investigated for the variations of web tension. She observed web instability would occur when the web in the circular region became too different in thickness than the surrounding web.

Sandesh [46] investigated the web with voids traveling over a roller. Both experiments and simulations showed the presence of voids in webs greatly affect the web instability. The web would not have instabilities phenomena without these voids. The web with an elliptical void is more easily to generate wrinkles than the web with a circular hole.

Yurtcu [47] and Good [40] indicated that the web instabilities due to the web local non-uniformity or voids in the web is hardly to find the close form expressions. However, the linear analysis and elastic elements provided the solutions to predict the onset of web troughs and wrinkles, which is also the best way to find their effect on the web at present state.

In his PhD dissertation, Beisel [48] studied web troughs and wrinkles due to roller crown, misalignment and taper. Beisel's models combined linear and nonlinear finite element methods which he used to predict the onset of web buckling. He verified his models with the experimental data obtained in web handling research lab.

Vaijapurkar et al. [49] used advanced modeling methods to study the web and roller instability problems addressed by Beisel [48]. The explicit method was used in his FEA to study the troughs and wrinkles formation due to a crown roller. The new modeling method allowed the model using the kinetic and kinematic boundary conditions in web and roller simulations. In many cases Vaijapurkar compared his simulation results to Beisel's test results and found satisfactory agreement.

Fu and Good [50] analyzed web wrinkling due to moment transfer using dynamic explicit finite element analysis. They predicted the troughs may occur in both pre-entering span and entering span. They also proved that wrinkles could be induced by a misaligned downstream roller or a misaligned upstream roller. Low and high MD stresses with different misalignments were modeled to show the wrinkles on the misaligned roller and the upstream misaligned roller. The simulation results were consistent with the test results.

Summary: The literature demonstrates the success that has been achieved regarding trough and wrinkle instability. Known disturbances such as misaligned, tapered and twisted rollers can be modeled. Observations in production process equipment demonstrate that troughs and wrinkles can occur in steady state conditions but the disturbance cannot be identified. Thus well aligned rollers with no crown or taper can generate troughs and wrinkles in webs. What is the source of the disturbance in these cases? Conditions are not always steady state in web lines. Web often undergo changes in velocity as new rolls of web are spliced in at unwind stations. Web tension can have several different levels in different sections of a process machine. Thus webs are often subject to dynamic conditions where velocity and tension are changing. Troughs and wrinkles have been observed during these dynamic events. It is surmised but unproven that the disturbance maybe material related through the Poisson effect in such cases. Webs are often laminated to other webs in process machines. The stability of laminated webs in process machines is not addressed in the literature.

2.6 Research Objective

The research objectives of this dissertation include:

1. Both explicit and implicit methods in finite element analysis, especially their applicability in roll-to-roll processing simulations will be compared by simulating a web transits over four rollers with the third one is misaligned. Computational efficiency and output accuracy will be studied for both methods.
2. The effect of anticlastic deformation as a flat web conforms to the roller surface will be investigated by using Timoshenko's plate theory [9]. Experimental results for a straight web bend to a cylindrical roller will be compared with simulation and expression results to further verify the anticlastic bending effect.
3. Boundary conditions for the closed form expressions of web lateral deformation will be explored for a straight web approaching a misaligned roller, a straight web transiting aligned rollers, and a cambered web passing over aligned rollers. The expression results will be compared with simulation and test results to verify the accuracy of expressions.
4. Simulation of a single layer web span to generate troughs due to MD tension and CMD compression will be conducted to verify the accuracy of trough failure criterion. Different boundary conditions for the web span will be explored for trough formation.
5. The troughs failure criterion for laminated web will be developed. The critical misaligned angle of a roller will be explored for troughs and slack edges appear in a laminated. Both simulation and tests will be conducted to verify the closed form expressions.

CHAPTER III

INVESTIGATION OF PREDICTION OF FINITE ELEMENT SIMULATION METHODS

Finite element method (FEM) is the numerical technique to acquire the appropriate solutions to the boundary value problems. FEM is well-known in industry as finite element analysis (FEA). It is powerful especially when the analytical solution cannot be obtained for the complex problems. All the closed-form solutions in Chapter II require kinetic or kinematic boundary conditions to solve the governing equations, while such assumptions for the boundary conditions were not required for the FEA. FEA is a powerful and economic tool to validate the accuracy of analytical solutions. The ordinary and partial differential equations need to be solved by the numerical methods. Appropriate numerical algorithms should be chosen for the finite element software to obtain the final results with accuracy and economic.

The numerical techniques that provide the approximations to the solutions of time-dependent ordinary and partial differential equations can be divided into two parts: explicit method and implicit method. For the explicit method, the solutions of the system at a later time will be calculated based on the state of the system at the current time. The solutions of the system at a later time by implicit method should be solved by the equations involving both the state of the current time and the later one.

3.1 Explicit Method and Implicit Method in ABAQUS

The commercial finite element software ABAQUS [51] will be used in this work. There are three distinct stages for a complete FEA: preprocessing, simulation, and post-processing. The

preprocessing stage must define the model which depicts the specific problem. The settings including material properties, model dimensions, and boundary conditions are included in this state. The following state – simulation – is a background process which uses analysis products to solve the numerical problem defined by the model. All the results should be evaluated in the last post-processing stage. For instances, the stress and displacement are the fundamental variables for structural mechanical problems.

In ABAQUS, there are three main analysis products employed in the simulation stage - ABAQUS/Standard, ABAQUS/Explicit, and ABAQUS/CFD. The last one is mainly used for the fluid dynamics simulations which will not be considered here. ABAQUS/Standard determines solution to the problem by solving a system of equations implicitly at each solution "increment". In contrast, ABAQUS/Explicit employs the explicit method without any iterations. To better explain the explicit method and implicit method used in ABAQUS, the algorithmic descriptions for these two methods will be compared for the finite element equilibrium equation:

$$M^{NM}\ddot{u}^{M} + I^{N} - P^{N} = 0 \tag{3.1}$$

where $\ddot{u}^{M}$ is the acceleration vector, M^{NM} is the consistent mass matrix, I^{N} is the internal force vector, and P^{N} is the external force vector. If the system is under the static equilibrium condition, which means d'Alembert forces are constant, or vary slowly with time, then $M^{NM}\ddot{u}^{M}$ should equal or close to zero.

The explicit analysis procedure is available in ABAQUS/Explicit. The lumped mass matrix is used with the explicit central difference integration rule (3.2). This diagonal element mass is the key to the computational efficiency since it is easy to obtain its inverse.

$$\dot{u}^N\Big|_{t+\frac{\Delta t}{2}} = \dot{u}^N\Big|_{t-\frac{\Delta t}{2}} + \frac{\Delta t\big|_{t+\Delta t} + \Delta t\big|_t}{2}\ddot{u}^N\Big|_t$$
$$u^N\Big|_{t+\Delta t} = u^N\Big|_t + \Delta t\big|_{t+\Delta t}\,\dot{u}^N\Big|_{t+\frac{\Delta t}{2}} \tag{3.2}$$

where u^N is a degree of freedom (a displacement or rotation component), and $|_t$ indicates the time increment. There is no iteration during the explicit calculations, so it has no convergence problem. However, it is conditionally stable so the solution will diverge rapidly if the time increment is too large. The stable time increment Δt is estimated by:

$$\Delta t = \min\left(\frac{L^e}{c_d}\right) \tag{3.3}$$

where L^e is the characteristic element length and it is common to use the smallest element length in the model, and c_d is the dilatational wave speed of the material which is expressed by expression (3.4) for an isotropic linear elastic material.

$$c_d = \sqrt{\left(\frac{E\nu}{(1+\nu)(1-2\nu)} + \frac{2E}{2(1+\nu)}\right)/\rho_{density}} \tag{3.4}$$

If we choose a typical web material with modulus E is 712000 psi, Poisson's ratio ν is 0.4, and mass density $\rho_{density}$ is 0.049 lb/in^3, then c_d is 17,635.8 in/s. The stable time increment Δt is 1.42×10^{-5} s with the characteristic element length L^e is 0.25 in. Although the stable increment time is small, the solution to individual time increment is inexpensive since there is no iteration in explicit analysis.

In contrast to the explicit method, the implicit method in ABAQUS employs the implicit time integration operators:

$$\dot{u}^N\Big|_{t+\Delta t} = \dot{u}^N\Big|_t + \Delta t\big|_t\,\ddot{u}^N\Big|_{t+\Delta t}$$
$$u^N\Big|_{t+\Delta t} = u^N\Big|_t + \Delta t\big|_t\,\dot{u}^N\Big|_{t+\Delta t} \tag{3.5}$$

The nonlinear equations should be solved for the dynamic quantities at time $t+\Delta t$ based on the values at t and the same quantities at $t+\Delta t$. The operator available in ABAQUS/Standard for the dynamic problem uses the Hilber-Hughes-Taylor time integration by default [52]. The backward Euler operator will be used if the application classification is quasi-static. A set of nonlinear dynamic equilibrium equations are introduced by these operators and must be solved at each time increment. Newton's method is used to seek the solution iteratively.

The result from implicit method is always unconditionally stable without any limit to the increment size. However, in order to acquire the converged solution, there are three factors that should be considered for the maximum increment size in implicit method: the rate of variation of the applied external loads, the complexity of the nonlinear damping and stiffness properties, and the typical period of vibration of the structure [51]. In mechanical structure problems, the increment size for the implicit analysis is usually one or two orders of magnitude larger than the stability limit of explicit analysis. In ABAQUS/Standard, the increment size will be chosen automatically and adjust appropriately by assessing the accuracy of the solution after each increment. If few iterations are required, the increment size would increase, and it would decrease with further attempts if the convergence rate is slow. However, the convergence may not be achieved all the time. Therefore, explicit method is a good candidate for the web simulations which cannot be solved by the implicit method. For instance, the web models which contain discontinuities like wrinkles, troughs, impact, cracking etc.

There are two types of errors that resulted in numerical computation: truncation error, and round-off error [53]. The truncation error is generated by approximations such as omitting terms in the infinite series. It can be divided into two different parts: local truncation error which is the error caused by one iteration and the global truncation error which is the cumulative error produced by many iterations. The round-off error is the difference between the calculated approximation of a number and the exact mathematical value due to rounding. For a finite element model, the

truncation error of approximating the partial derivatives by finite differences usually decrease with the smaller element size, nevertheless, the round-off error generally increases with respect to the element number in the meantime. In general, the model with coarse mesh density cannot provide accurate or clean results. However, the fine mesh density implies a large number of degrees of freedom in a model, which requires great computational cost. The computational cost for the explicit simulation is approximately proportional to the model size while the implicit method shows greater cost over the explicit method for the large model according to Figure 3.1. How to obtain the results with a small error and a fast computation is vital for the finite element analysis.

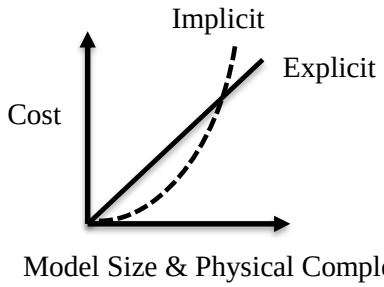

Figure 3.1 – Comparison of the Computational Cost for Implicit and Explicit Analysis

Our goal is to obtain the accurate solutions with economic computations. In web handling industry, the web would have large deformations or translations during winding and unwinding processes, and web buckling may occur due to various disturbances. The explicit method is robust to deal with complex problems so it is widely used in the previous web and roller research. Few simulation was solved by the implicit method for the web problems. As implicit method has advantages in FEA such as large increment size and unconditional stable results, it is worth to explore its practicability in web handling research.

3.2 Simulation of a Web Approaching a Misaligned Roller

A typical web and roller model was setup which will be solved by both explicit and implicit methods. The tensioned web transited over four rollers sequentially from left to right as shown in Figure 3.2. The third roller rotates a misaligned angle which would lead the web steer laterally due to the normal boundary condition [14]. The analytical solutions to the lateral steerage of the web have already been discussed in the previous chapter expression (2.3). Two solvers i.e. ABAQUS/Explicit and ABAQUS/Standard will be employed for this unique finite element model.

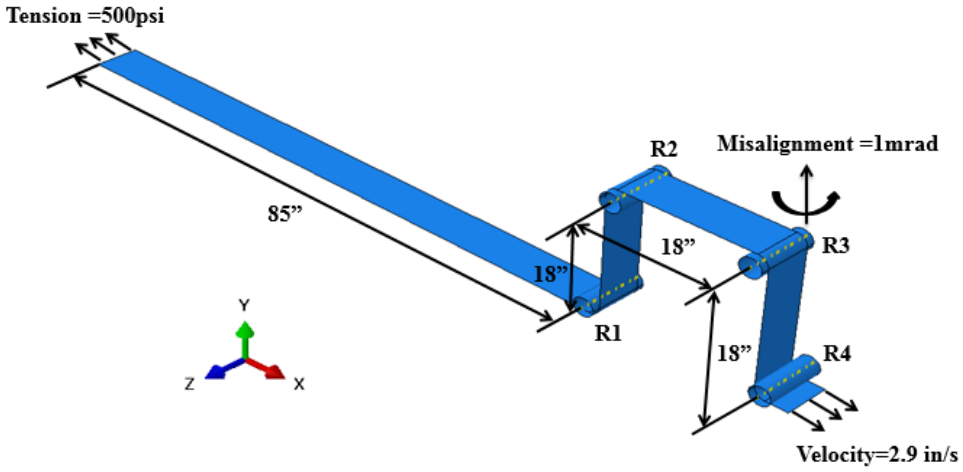

Figure 3.2 – Finite Element Model for a Web Approaching a Misaligned Roller

The web is isotropic and homogeneous with 6 inches in width and 0.001 inches in thickness. The Young’s modulus is 712,000 psi and Poisson’s ratio is 0.4. Four rollers are perfectly cylinders with 1.45 inches in radius. All rollers are aligned at the beginning and Roller3 (R3) rotates 1 mrad in the counterclockwise direction after the web reaches to the desired tension and velocity. The pre-entering span between Roller1 (R1) and Roller2 (R2) and the entering span between R2 and R3 are both 18 inches long. The ratios of the span length to web width are both 3 (W/L = 18/6). According to Shelton’s theory, this web has long web span which means the shear effect should not have large effect on the web lateral deformation.

The misalignment of R3 is the dynamic disturbance of the whole system, and the time constant τ here is the time for the web span (18") between R2 and R3 to pass over the misaligned roller R3. The lateral deformation of the web should reach to 98% of the ultimate result after four time constants. The web length before R1 was set to 85 inches, which is longer than the four span lengths ($18 \times 4 = 72$). The friction coefficient is 0.4 between the web and the rollers.

The shell element – S4R was used to generate the web model in this simulation. S4R is a 4-node, quadrilateral, stress/displacement shell element with reduced integration. Compared with solid element, shell element is more appropriate to simulate webs since the web thickness is much smaller than the length or width. Shell elements save a lot of computation compared with the solid elements due to the simplicity. The shell element has in plane and out-of-plane stiffness while membrane element only has in plane stiffness, so shell element provides outputs through web thickness while membrane element only provides output at the membrane surface. The element size for this model was to be 0.25×0.25 square inches. The four rollers are rigid bodies since they have much higher rigidity compared with the web.

There are three steps in this model. In each step, the boundary conditions and interactions between the web and the rollers can be defined separately. In the first step, the 500 psi tension was applied at web upstream end, and the 2.9 in/s velocity was applied at the web downstream end in the second step. In the third step, the third roller R3 was misaligned 1 mrad in one second. The web tension, velocity and the R3 misalignment would keep constant after they reach to the maximum values. The model with step type is Dynamic, Explicit uses explicit method and the other model with step type is Dynamic, Implicit uses Implicit method.

Multiple steps with only one or a few changes in each step help to check the model if it has any settings that are not appropriate or incorrect. In addition, restart job is allowed in ABAQUS which is very useful for large model problems. If anything wrong that interrupts the job or the job

needs to continue running with additional steps, restart module provides the ability to run a new job by using the simulation results from the old job. More steps give more choices to define the restart points.

3.3 Comparison of Implicit and Explicit Results as a Web Approaching a Misaligned Roller

Prior to compare the simulation results, the simulation cost for the explicit model and implicit model will be examined. As shown in Figure 3.1, the computational time will increase with the model size. The number of degrees of freedom is the key to the whole size of the model. The model herein has 14,496 elements and 15,125 nodes. The S4R element was used, so each element has four nodes, and each node has 6 degrees of freedom: 3 for translation and 3 for rotation. The same outputs were requested with the same frequency. Double precision was used for the explicit simulation. Although higher precision takes longer computational time, it provides more reasonable and smooth results based on previous experience. As shown in Table 3.1, the model using explicit method requires 72 hours which is 3 days to complete the job and the implicit model costs 333 hours which is about 14 days. For this case, the implicit model takes about 4.7 times computational time as the explicit model to finish the same job. The total increment number for the explicit simulation is 12,379,005 which is much larger than the increment for the implicit simulation 15,913. The nonlinearities of this web and roller model result in the difficulty for the implicit simulation to acquire the converged solutions. It indicates the total degree of freedom this model has exceeds the number at the intersection point that shown in Figure 3.1.

One advantage of explicit method is to obtain the results in a shorter time for large model compared with the implicit method. The explicit simulation has much more increment compared with the implicit simulation, however, the work per increment in implicit simulation is much more than the explicit simulation, which result in a longer total simulation time. Although the explicit method is efficient in computation for this large web and roller model, the following results show

the implicit method provides more precise results which make great contribution to the web and roller interaction analysis.

Table 3.1 – Simulation Expense for Models Solved by Explicit and Implicit Methods

	Explicit Method	Implicit Method
Simulation time (h)	72	333
Total Increment	1,237,9005	15,913

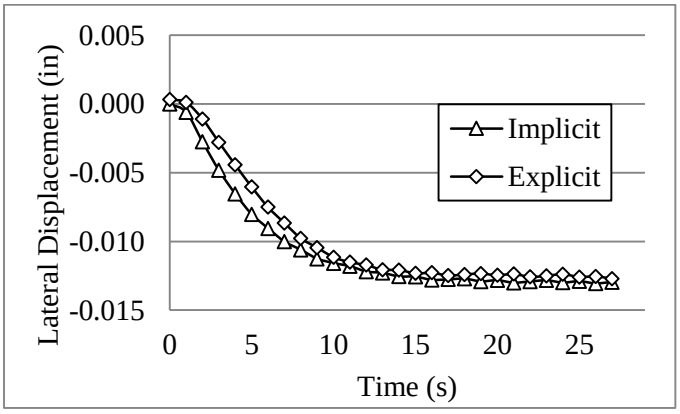

Figure 3.3 – Lateral Displacement along Web Elastic Axis at the Entry to the Misaligned Roller R3

The steady state conditions have been checked for both simulations. For the web passes over a misaligned roller, the lateral deformation as the web enter this roller is crucial. Figure 3.3 plots the lateral displacement along the web elastic axis as it approaching the entry point of the misaligned roller R3. The x axis indicates the time of the third step and the y axis indicates the web lateral displacement. Remember the R3 has zero misalignment at the beginning of this step and the misaligned angle reaches to 1 mrad in 1 second and then keeps constant until the end of the step. At the beginning of the step, the lateral displacement is 3.22×10^{-4} for the explicit simulation and it is -6.45×10^{-14} for the implicit simulation which are both close to zero. The normal entry rule should provide zero lateral displacement for both simulations and it shows the implicit displacement is more reasonable than the explicit result at the beginning of the step. The lateral displacements keep

increasing from the beginning and it takes about 20 seconds to reach the constant position for both simulations. The time constant here is the span length 18 inches divided by the web velocity 2.9 in/s or 6.2 seconds. So the web reaches to steady state after 3.2 time constants. The steady lateral displacement is -0.0127 for the explicit simulation and -0.0130 for the implicit simulation. The displacement from the closed form expression (2.3) is -0.0120 inches. The relative errors for the lateral displacement are 5.8% and 8.3% for explicit method and implicit method, respectively. To solve the differential equation (2.1) to the solution (2.3), four boundary conditions (2.2) with several assumptions were applied while none of them were required for the FEA. The more negative lateral displacement of the web from simulations may result from the slippage as the web enters or exits from rollers. However, the small relative errors mean the good agreement between the simulation and closed-form solution. It also indicated the normal entry boundary conditions are guaranteed till the end of the simulations. Although the lateral displacements have some differences before 10 seconds for the two methods, the final constant values are close to each other.

The lateral displacements are very close to zero at the beginning, it shows there is no moment transfer on R2 for both simulations. The moment transfer may occur with the increment of the misaligned angel. According to Equation (2.28) and (2.30), the moment transfer occurs only if the internal moment at the entry of the enter span M_{bi} larger than the critical moment M_r. This moment in the web can be calculated by expression (2.34). As shown in Figure 3.4(a), the internal moment at the exit of R2 are close to 1 lb-in in both simulations, which are less than the critical moment 2.83 lb-in. Thus there should no moment transfer from web span between R2 and R3 to span between R1 and R2. According to expression (2.30), the internal moment as the web reaching R2 M_{aj} should be zero. Figure 3.4(b) is the zoomed picture as the web near the entry point of R2, the moment calculated from implicit simulation is closer to zero compared with moment from the explicit method. The implicit method provided a more accurate result for the web internal moment, which calculated based on the MD stress output at web nodes.

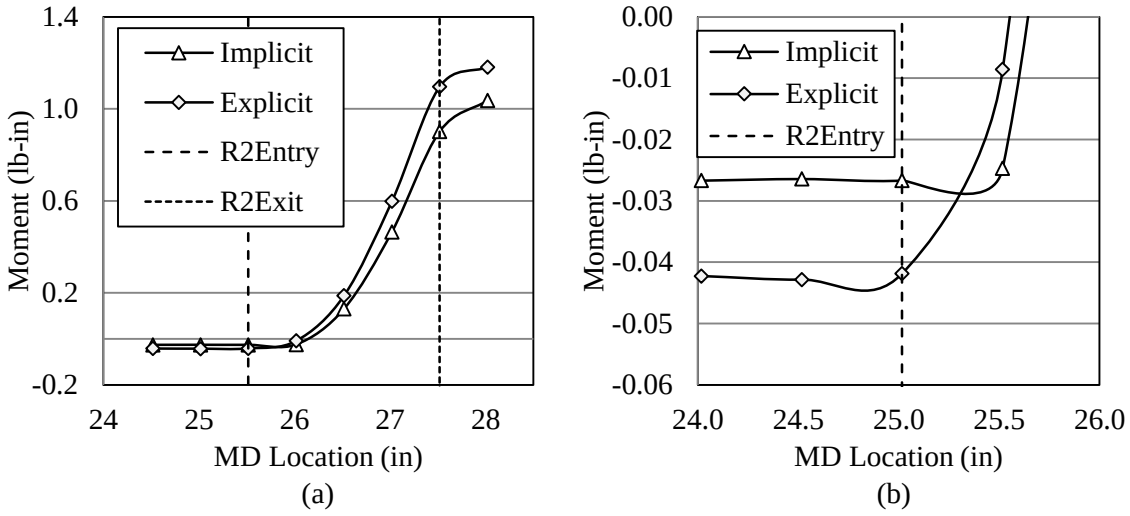

Figure 3.4 – Web Internal Moment Calculated from the MD Stresses

To further compare the results precision from these two methods, the lateral displacement along the web elastic axis was plotted in Figure 3.5(a), and a quite agreement was acquired between the explicit and implicit results. There is no lateral displacement prior web enters R2 for the implicit simulation, which is reasonable since there is no moment transfer. However, the explicit displacement at the same MD location is close to but not exactly equal to the zero. Both simulations provide smooth lateral displacement along web elastic axis. However, there are lots of numerical noised in the slope and curvature curves that comes from the explicit simulation as shown in Figures 3.5 (b) and (c). Both slope and curvature plots from the implicit simulation are smooth for all webs. As the misaligned angle of R3 is small, the linear interpolation to obtain the first derivative of the lateral displacement with respect to the MD coordinates was used for the slope, and the second derivative for the curvature. In Figure 3.5(b), the slope from implicit simulation is zero before the web enters R2 and there is a small bump before web leaves this roller. The slope keeps decreasing in the web span from R2 to the direction to approaching R3. It reached to 0.001 rad at the entry of R3 which equals to the misaligned angle of the roller.

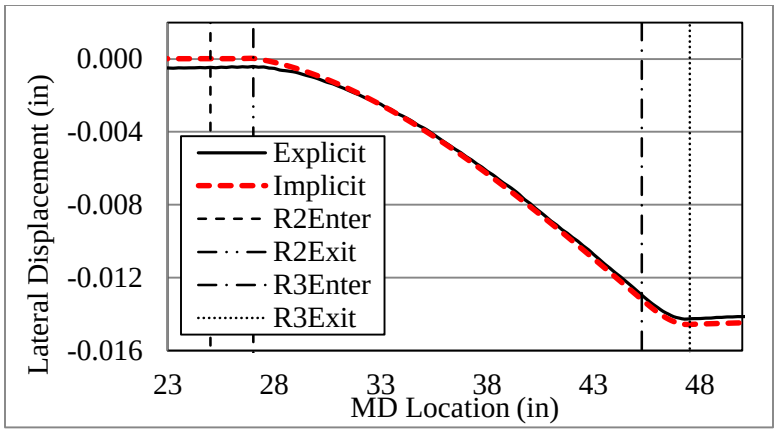

(a) Lateral displacement

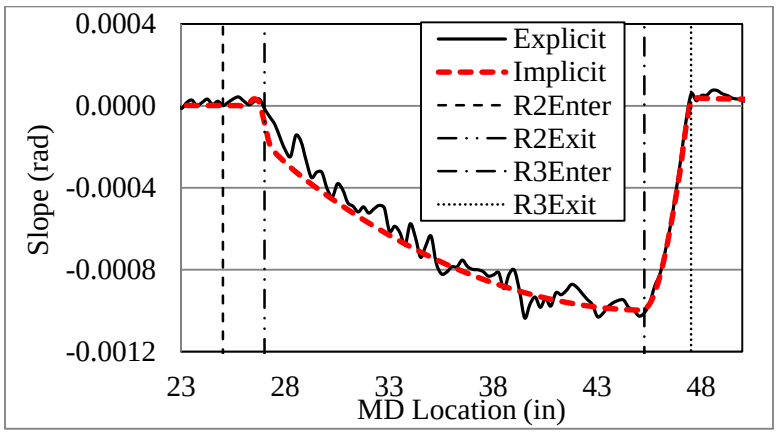

(b) Slope

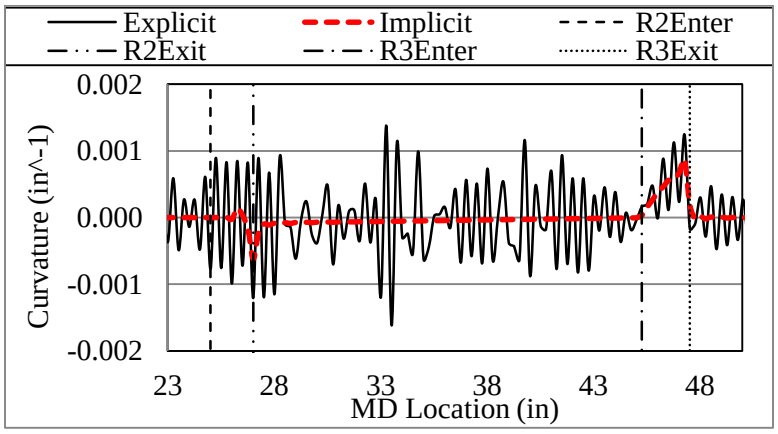

(c) Curvature

Figure 3.5 – Lateral Displacement, Slope and Curvature Along Web Elastic Axis

Although the explicit simulation provided the slope has the similar trend as the implicit plot, it does not give so much details due to the fluctuations. The numerical noises in the explicit result grow even much larger for the curvature that makes it difficult to acquire any useful information. From the implicit plot, it is easily seen that the curvature reaches to the minimum value as web exits from R2, and it keeps increased to R3. Remember from the beam theory, the second derivative of displacement is bending moment M over bending stiffness EI. Under no moment transfer condition, the web span between R2 and R3 should have the largest bending moment as web exits from R2 and it should decrease to zero at the point as web enters R3. The implicit curvature plot in the web span between R2 and R3 was identical to the trend of bending moment that resulted from roller misalignment. The first and second derivatives of the lateral deformations showed the superiority of the implicit method in FEA.

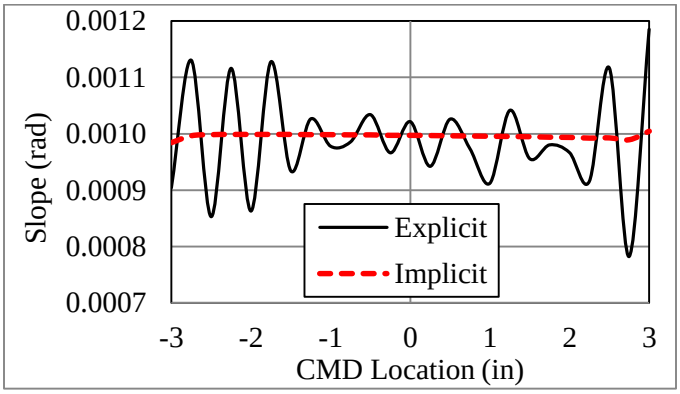

Figure 3.6 – Entry Slope to the Misaligned Roller R3

Figure 3.6 shows the slope along web width at the entry of the misaligned roller R3. The average slope from the explicit simulation is 0.000990 and it is 0.000996 from the implicit simulation, and they are both close to the roller misalignment (0.001 radians). However, there are numerical noises in the explicit plot and the implicit method provides smooth result. This difference could be described clearly by the standard deviation. The standard deviation of the explicit slope is 9.6×10^{-5} which is one order of magnitude larger than the implicit plot 3.8×10^{-6}. For the implicit

simulation, the slope from the implicit method has a symmetric profile with 0.000997 rad at the web center.

All the slopes and curvatures were the derivations of web displacements with respect to locations, and explicit simulation cannot provide smooth results for the slope or curvature. In web and roller simulations, stress is another important parameter besides deformation. In the linear elasticity, the stress can be expressed of the first derivative of the displacements:

$$\begin{aligned}
\sigma_x &= \frac{E}{(1+\nu)(1-2\nu)}[(1-\nu)\frac{\partial u}{\partial x} + \nu(\frac{\partial v}{\partial y} + \frac{\partial w}{\partial z})] \\
\sigma_y &= \frac{E}{(1+\nu)(1-2\nu)}[(1-\nu)\frac{\partial v}{\partial y} + \nu(\frac{\partial w}{\partial z} + \frac{\partial u}{\partial x})] \\
\sigma_z &= \frac{E}{(1+\nu)(1-2\nu)}[(1-\nu)\frac{\partial w}{\partial z} + \nu(\frac{\partial u}{\partial x} + \frac{\partial v}{\partial y})]
\end{aligned} \tag{3.6}$$

The web out-of-plane stress σ_z is very small due to its thin thickness, so only stresses in MD and CMD were compared. The Figure 3.7(a) and (b) showed the MD and CMD membrane stresses along web elastic axis. The red dashed lines are the outputs from the implicit simulation which are smooth for both stresses. The black lines are the explicit results that have large numerical noises just like the explicit slopes and curvatures. The implicit MD stresses were larger on the roller compared with the stresses in free span. Large MD stress on roller induced large CMD stress as shown in Figure 3.7(b). In addition, the MD stresses in free span increased a little each time as the webs pass over a roller. This tension variation in web spans may due to the slippage that resulting from web bending deformation as it enters and exits a roller. None of these details can be detected in the explicit plots. The oscillations in explicit MD and CMD membrane stresses proved implicit method has superior for the accuracy of stress output in FEA.

The non-uniformity of the CMD membrane stress from explicit simulation is shown in Figure 3.8(a). The web has spots where the stresses varies dramatically. The explicit stress across

all the web has a larger range compared with implicit result. Figure 3.8(b) proved the implicit simulation could provide smooth stress distribution for the entire web.

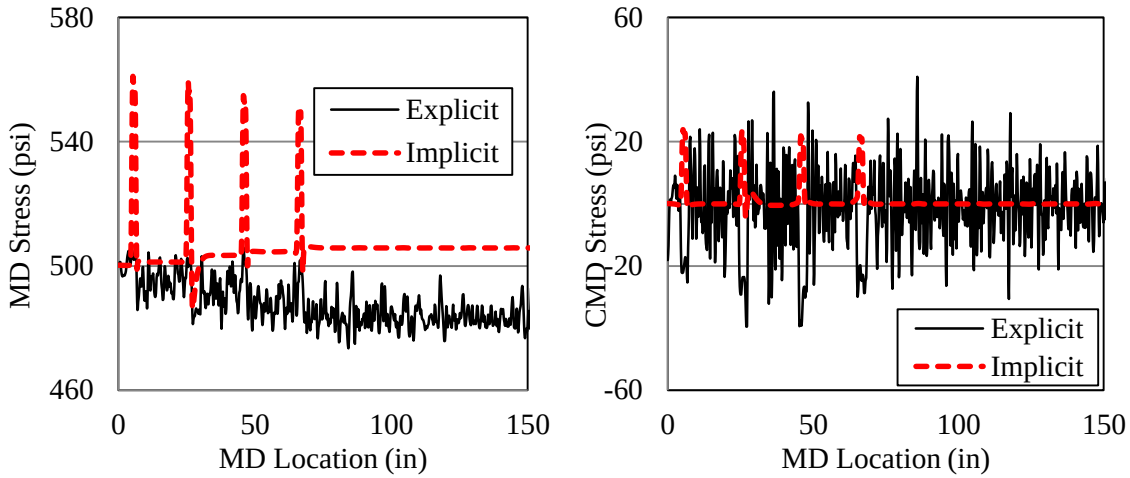

(a) MD stress (b) CMD stress

Figure 3.7 – MD and CMD Stresses Along Web Elastic Axis

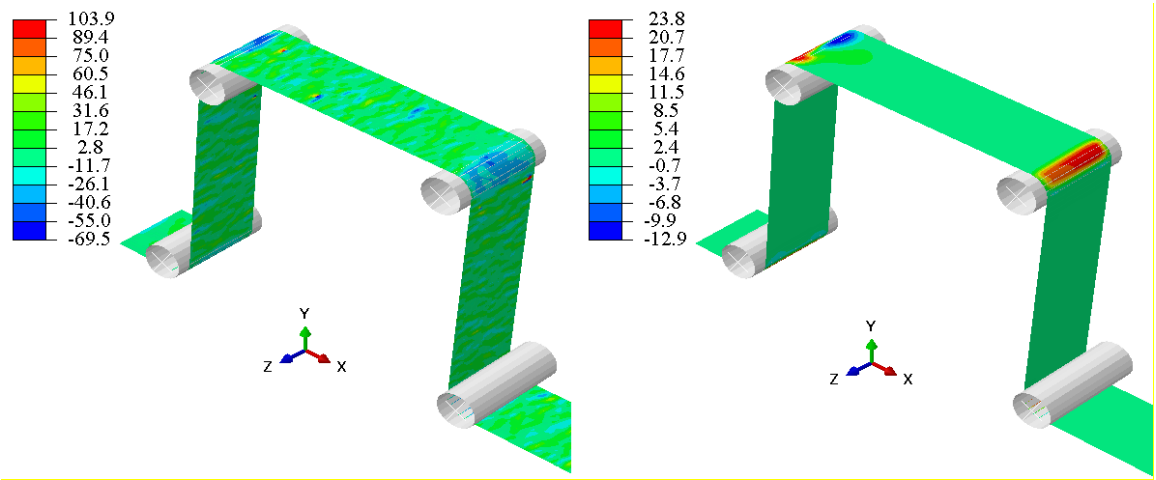

(a) CMD Stress from Explicit Simulation (b) CMD Stress from Implicit Simulation

Figure 3.8 – CMD Membrane Stresses

3.4 Conclusions

The explicit and implicit methods were discussed for the finite element analysis (FEA). The explicit method does not require iteration which makes it more robust for the models with discontinuities. The implicit method is unconditional stable without any limit to the increment size. The interactive method is required to solve the nonlinear equations.

In web and roller simulations, commercial FE software packages ABAQUS/Standard and ABAQUS/Explicit were used to study the advantages and disadvantage of implicit and explicit methods. The isotropic web with constant tension and velocity passed over four rollers and the 3rd roller was misaligned in the web plane. No moment transfer happens between rollers. The total simulation cost for the implicit simulation is much more than the explicit simulation. Both the explicit and implicit simulations provide the steady state results at the end of the simulations. However, the explicit outputs have more noises compared with the implicit outputs, especially for the high order derivatives of deformations. These numerical errors were accumulated by millions of increment during simulations. With the capability to provide the detailed and accurate results, implicit method is powerful in the FEA to solve web and roller problems. The computational cost may be sacrificed for the large models to use the implicit method. In addition, for the web and roller processes which contains the instability such as troughs and wrinkles, the implicit simulation has the possibility to converge hardly, the explicit method is preferred to be chosen under these conditions.

CHAPTER IV

IMPACT OF LARGE DEFORMATIONS ON WEBS TRANSITING ROLLERS

Webs transiting rollers in roll-to-roll (R2R) process machinery is a common occurrence. Thin webs often appear to transit over rollers nicely. The web moves from a planar state in the entering span to a cylindrical shape on the roller and then resumes the planar state in the exiting span. For the most part the web is able to do this successfully. Only when the web becomes visibly unstable in the entering span (troughs) or on the surface of rollers (wrinkles) does concern arise. The following part will try to answer what is required of the web to assume the shape of a roller.

4.1 A Flat Web Approaching a Cylindrical Roller

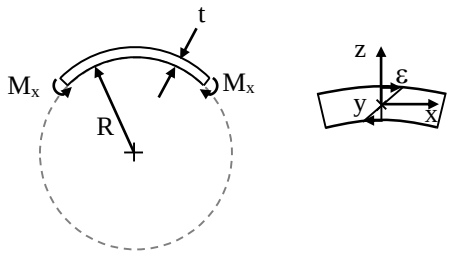

Figure 4.1 – Bending a Web to the Radius of a Roller

If the web is treated using simple plate theory, the internal moments required to make the web conform to the radius of a roller can be estimated [9]. Polyester film has a modulus E of 712,000 psi and Poisson's ratio ν of 0.3. The edge moment per unit length M_x that would be required to bend a polyester film of thickness t 0.001 in and width W of 6 in to a roller radius of

1.45 in would be expression as (4.1).

$$M_x = \frac{D}{R} = \frac{Et^3}{12R\left(1-\nu^2\right)} = \frac{712{,}000\times 0.001^3}{12\times 1.45\times(1-0.3^2)} = 4.496\times 10^{-5}\ \text{lb}-\text{in/in} \tag{4.1}$$

where D is the flexural rigidity which equals to $Et^3/(12(1 - \nu^2))$. This rather small bending moment induces a bending strain that is tensile on the upper surface of the web and compressive on the lower surface. In the absence of friction, these MD strains can be calculated per Euler theory as:

$$\varepsilon_{MD} = \frac{z}{R} = \pm\frac{0.001/2}{1.45} = \pm 3.35\times 10^{-4} \tag{4.2}$$

The bending strain and deformation of a web is more complex than this. The Poisson effect will induce CMD strains that will be compressive on the upper surface of the web and tensile on the lower surface, and will vary linearly between the web surfaces. The CMD strains will induce curvature in the web in the CMD, a curvature which is opposite in sign to the MD curvature needed to make the web conform to the roller. This phenomenon is called anticlastic bending [9][54]. In the example, an assumption of a wrap angle (WA) of π/2 radians will be added. The out-of-plane anticlastic deformation of a plate loaded with edge moments M_x (4.496×10^{-5} lb-in/in) is [9]:

$$w = -\frac{M_x}{2D(1-\nu^2)}x^2 + \frac{\nu M_x}{2D(1-\nu^2)}y^2 \tag{4.3}$$

$$w\left(\text{in}\right) = -0.3789x^2 + 0.1137y^2 \tag{4.4}$$

where x and y are input in units of in. The deformed web shape is shown in Figure 4.2. A moment was input to force the web to take the shape of a cylindrical roller. As a result of anticlastic bending, it is shown the deformed shape is not cylindrical.

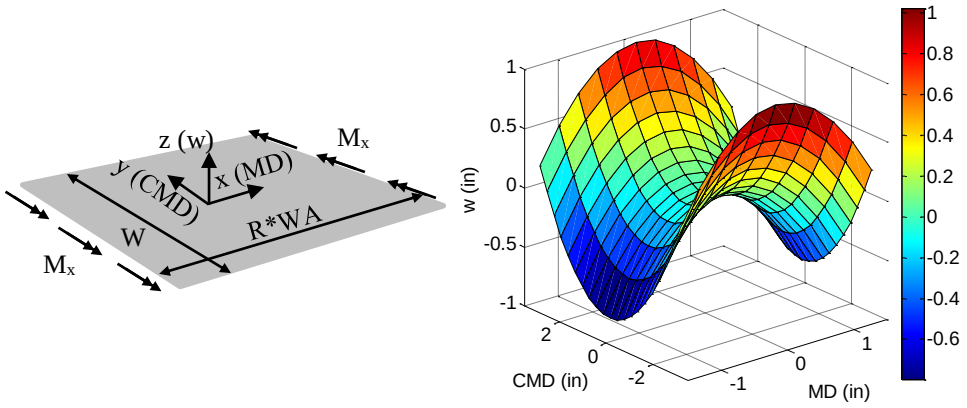

Figure 4.2 – Bending a Web to Conform to a Roller

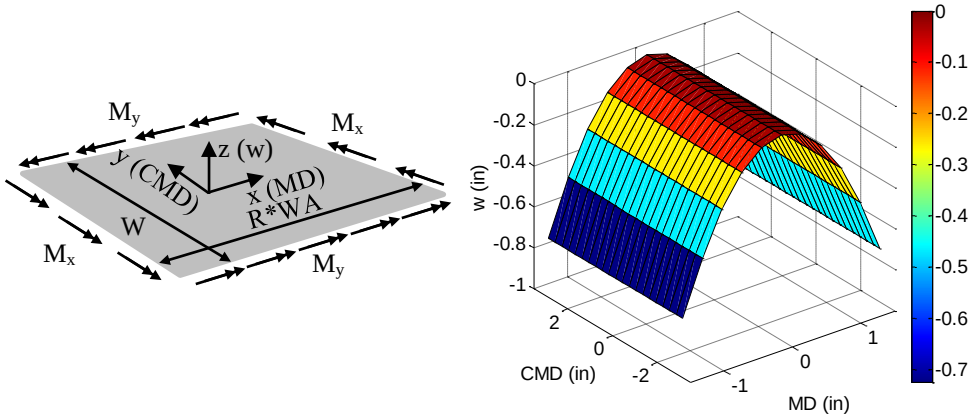

Figure 4.3 – Dual Moments Required to Make a Web Conform to a Roller

What applied moments would be required in the example to deform the web to a cylindrical shape that would be compatible with the shape of the roller? If edge moments are applied on all the edges of the plate, the equation for the out-of-plane deformation is:

$$w = -\frac{M_x - \nu M_y}{2D(1-\nu^2)}x^2 - \frac{M_y - \nu M_x}{2D(1-\nu^2)}y^2 \qquad (4.5)$$

If the edge moment M_y is set to the value νM_x (1.349×10^{-5} lb-in/in) Equation (4.5) becomes:

$$w = -\frac{M_x}{2D}x^2 = -0.3448x^2 \tag{4.6}$$

The deformation of the web has now become a cylindrical surface as shown in Figure 4.3. The radius of this cylindrical surface would be:

$$\frac{1}{r_x} = -\frac{\partial^2 w}{\partial x^2} = \frac{M_x}{D} = 0.6897 \text{ in}^{-1},\ r_x = 1.45 \text{ in} \tag{4.7}$$

Thus, the deformed web has achieved the radius of the roller in the example (1.45 in). Bending stresses have been induced in the web by the edge bending moments M_x and M_y which vary linearly through the web thickness. On the inner and outer surfaces these bending stresses are:

$$\begin{aligned} \sigma_{x,MD} &= \pm\frac{6M_x}{t^2} = \pm\frac{6\times 4.496\times 10^{-5}}{0.001^2} = \pm 270 \text{ psi} \\ \sigma_{y,CMD} &= \pm\frac{6M_y}{t^2} = \pm\frac{6\times 1.349\times 10^{-5}}{0.001^2} = \pm 81 \text{ psi} \end{aligned} \tag{4.8}$$

These stresses are tensile on the outer surface of the web and compressive on the inner surface that would be in contact with the roller surface. Note, as a result of the constant bending moments M_x and M_y, these stresses are constant over the inner and outer surface of the web. The equations for stress (4.8) neglect any frictional forces that might be present between the web and roller.

This simple example has demonstrated the duress to which a web is subjected to conform to the surface of a roller. A web under tension transiting a roller is a more complex case and will be subject to contact pressure and frictional forces. Webs do not have applied M_x and M_y moments; they only have web tension, contact pressure between the web and roller due to tension and frictional forces applied. How does the anticlastic behavior shown for discrete sheets apply to nearly continuous webs transiting rollers in process machines? A thorough examination of the dynamic interaction of a web with a roller was in order.

4.2 Finite Element Model Setup

To explore the interaction between a web and aligned rollers, a dynamic finite element simulation of a web transiting four rollers was developed as shown in Figure 4.4. As discussed in previous chapter, the implicit methods provide results with more smooth and accurate for web and roller simulations, especially for the derivatives of the displacement, stress etc. The simulation herein was run using ABAQUS/Standard operator in an implicit quasi-static mode. The web is shown at the beginning of the simulation in Figure 4.4. The web material properties, width and thickness are that of the example in the Section 4.1. The distances of the web span between rollers and the length of the span before roller R1 are the same as the example in Figure 3.2. The web span lengths between rollers L were all set at 18 in. This provided a span ratio (L/W) of 3. The rollers were modeled as rigid analytical surfaces that were free to rotate on their axes of rotation. The radius of these rollers was selected as 1.45 in identical to the roller used earlier in the example. The web was modeled with square SR4 shell elements with an edge dimension of 0.25 in which yielded converged results.

At the start of the simulation, the shell elements defining the web on the rollers are cylindrical shells with an inside radius equal to the outside radius (1.45 in) of the roller. An entry span length of web 85 in long was modeled prior to roller R1. When the simulation begins, the shells of web on the rollers transit out into the free spans. Bending stresses are induced that can induce transient motion when these sections of web pass each roller. The benefit of the long entry span length is that by the conclusion of the simulation all of these sections of the web that began on the rollers have passed downstream of roller R4 and will not affect the final results. The coefficient of the friction (COF) between the web and the rollers was set at 0.4. During the first 0.1 s of the simulation, the downstream velocity is maintained at zero while the web tension was increased to 500 psi and then held constant through the remaining 29 s of the simulation. After the

stress due to web tension stabilized, the downstream web velocity was increased from zero to 2.9 in/s in 0.5 s and maintained constant through the duration of the simulation.

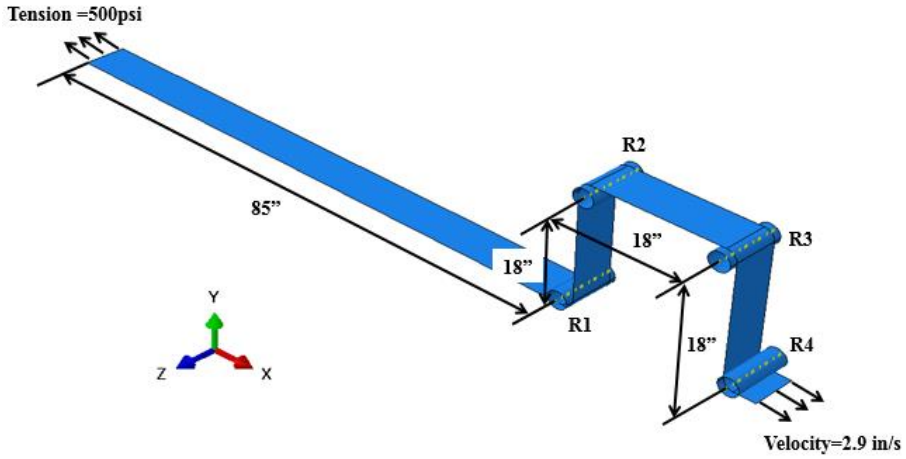

Figure 4.4 – Finite Element Model Setup

4.3 Simulation Results and Discussions

The web stresses achieve a steady state level very quickly in these simulations. The maximum CMD membrane stress on roller R3 is shown in Figure 4.5. Results are being shown for a case where Poisson’s ratio was set to 0.3. The stress is close to zero as the web begins to move, it then increases rapidly for about 2 seconds as shown in Figure 5. After 2 seconds, this stress becomes nearly constant with only small variations. The maximum CMD membrane stresses on all rollers are very similar in magnitude and in the way in which they vary through time. The time required for a point on the web to move from entry to exit of a roller is 0.784 s. This is the dynamic time constant for these simulations. After 3 time constants (2.35 s), near steady state behavior should be expected in these simulations and is shown to be the case in Figure 4.5.

The existence of the CMD tensile membrane stress shown in Figure 4.5 is interesting and indicates that the interaction of the web with the cylindrical roller has a stabilizing or spreading influence on the web. This is the first quantitative proof that cylindrical rollers have a spreading

effect on webs. Previously empirical proof was given that a misaligned cylindrical roller was superior in resisting web wrinkles than cylindrical rollers with tape wound in a spiral inward or outward pattern [54]. The origin of this tensile CMD stress will be explored further.

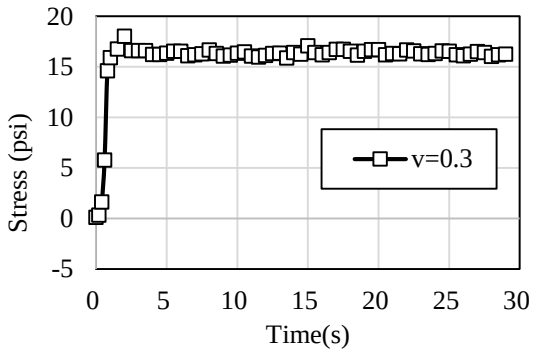

Figure 4.5 – Maximum CMD Membrane Stress on R3

The plate theory example demonstrated that a moment M_y of magnitude νM_x should be applied to the web edges to cause the CMD curvature due to the anticlastic effect to vanish and allow the web to assume a cylindrical shape while transiting the roller. From Equation (4.8), the CMD bending stresses were shown to have a linear variation through the web thickness. These stresses should be positive on the outer surface, zero on the neutral surface, and negative on the inner surface where the web in contact with the roller. These stresses should be constant across the web width provided the moment M_y is constant across the web width. After steady state conditions are achieved in the simulation, the CMD bending stresses approach 97 psi on the outer surface, 16 psi at the mid-plane, and -65 psi on the inner surface as shown in Figure 4.6. Note in Figure 4.6, the CMD stresses on the inner and outer surface are essentially constant across the web width. The 97 psi CMD stress on the outer surface is comparable to the 81 psi stress predicted in Equation (4.8). The 16 psi CMD tensile membrane stress at the mid-plane was unexpected and the -65 psi stress is comparable to the -81 psi value from Equation (4.8) for the inner surface value. The CMD stresses at the inner and outer surfaces and the mid-plane are all approximately 16 psi larger than expected from plate theory. What is clear in Figure 4.6 is that constant CMD bending stresses are

experienced across the web width in the simulation that are similar to those witnessed in the plate theory example. This demonstrates that even though webs are thin that they are subjected to considerable bending strain during transit over rollers and that the effects of anticlastic bending are present and significant. The CMD stresses shown in Figure 4.6 are very similar on all four rollers (R1 through R4).

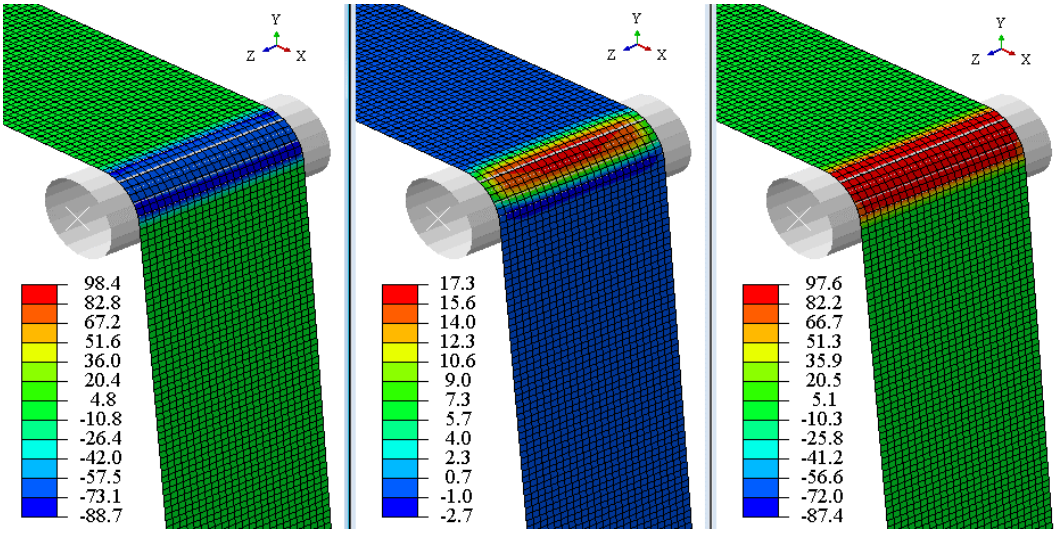

Figure 4.6 – CMD Stresses (Psi) on R3 (ν = 0.3)

To explore the origin of the CMD spreading stresses witnessed at the mid-plane of the web on the rollers, the CMD deformations were examined. When a flat web is subjected to MD tension with no CMD constraint, the web would have a uniform CMD contraction due to the Poisson effect. For the web simulated the uniform contraction expected would be 500 psi/712,000psi ×0.3 ×6 inches/2 or 0.000632 inches, again for the case where Poisson's ratio was 0.3. In the simulations conducted, the web takes the shape of a cylindrical surface while transiting over a roller but the anticlastic effects, any attempt to gain normal entry and friction forces would cause the lateral contraction to deviate from the uniform level. As shown in Figure 4.7(a), the CMD displacements appear to be uniform and exhibit symmetric width reduction of the web edges at the macro level.

However, the zoomed Figure 4.7(b) shows deviation in the CMD displacements as the web enters roller R3. The web edges contract slightly more while transiting the roller compared to the contraction in the free span. This additional contraction is shown clearly in the displacements of the web edge shown in Figure 4.8. The markers filled in red indicate the locations where the web enters or exits one of the four rollers. Although the difference of the displacements where the web on the roller and in the free span is not huge, it indicates the web has nonzero slope at edges when it enters the roller.

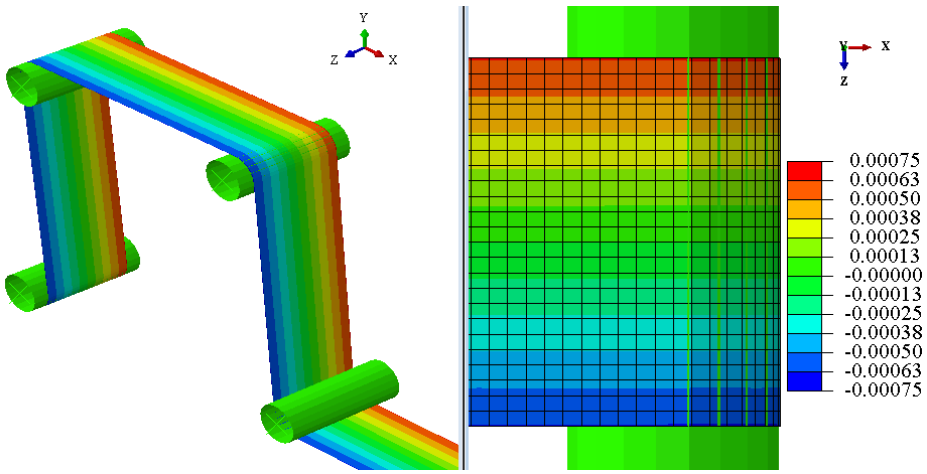

(a) Whole Model (b) Web entering R3

Figure 4.7 – CMD Displacements on R3 (in) (ν = 0.3)

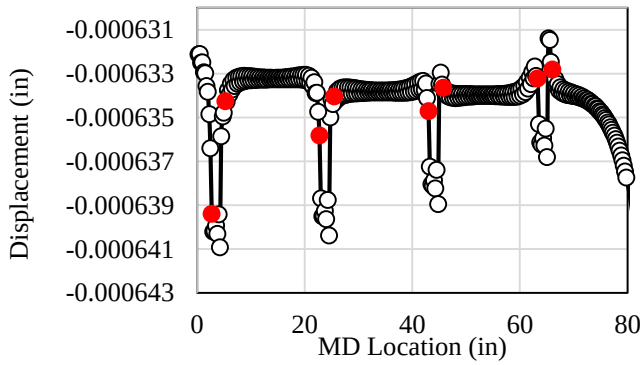

Figure 4.8 – The Lateral Displacement of the +z Web Edge (ν = 0.3)

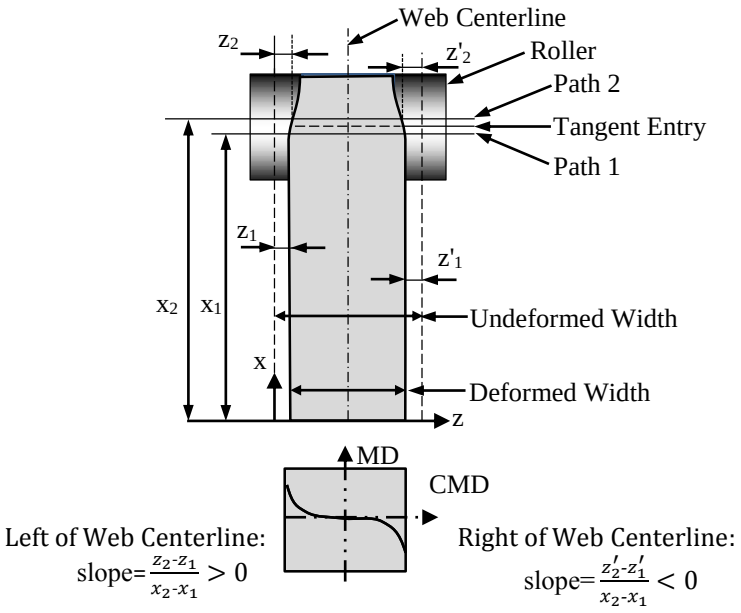

Figure 4.9 – The Entry Slope of the Web at the Roller

The slope of the web at the entry to the roller is determined by a central finite difference approximation to acquire the first order differentiation of the CMD displacements with respect to the MD coordinates. The nodes of an SR4 shell element have 6 degrees of freedom which include three translations along the xyz axes in Figure 4.7 as well as rotations about those axes. Differentiation of the lateral displacements provides superior estimate with less numerical noise than the out-of-plane rotations which are output. The web contracts in the CMD upon entry to the roller, which was evident in Figure 4.8. The slope at web entry is positive on the –z web edge and negative on the +z edge. The concept of normal entry dictates a web should enter the roller normal to the axis of rotation, which means the slope should be zero. The concept of normal entry is based completely on kinematics without regard for the frictional forces between the web and roller needed to sustain the zero slope or for the higher order deformations that occur in the web due anticlastic bending. The concept of normal entry has been applied in numerous circumstances in web lateral mechanics and dynamics investigations. In these investigations, the web is modeled as a beam. The

concept of normal entry is applied at the elastic axis of the beam at entry to a downstream roller and may be used to determine a steady state lateral behavior. The method for estimating the slope at the entry to the roller is shown in Figure 4.9. The slope is estimated at the CMD line of nodes closest to the web entry.

The result of the estimation is shown in Figure 4.10 for the case where Poisson's ratio of the web is 0.3. Note at the widthwise center of the web that the entry slope is very close to zero (the estimate was 5.5×10^{-14} rad). The slopes at the web edges were significantly larger ($\pm6.25\times10^{-6}$ rad). Also note that the integrated average of the slope over the web width would be essentially zero. Thus for analyses where the web is modeled as a beam, the normal entry boundary condition appears appropriate if sustainable by available friction. Note the signs of the slope at the web edges will promote spreading and are responsible for the CMD tensile spreading stresses witnessed on the mid-plane in Figures 4.5 and 4.6.

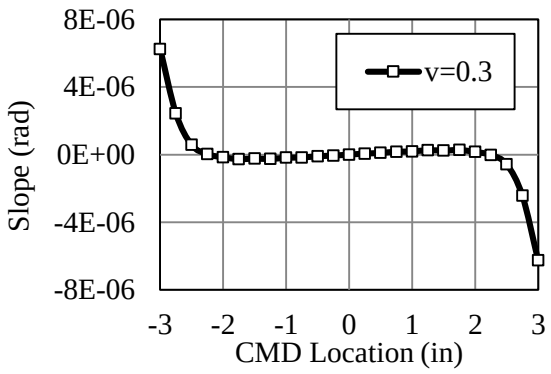

Figure 4.10 – Entry Slope at R3

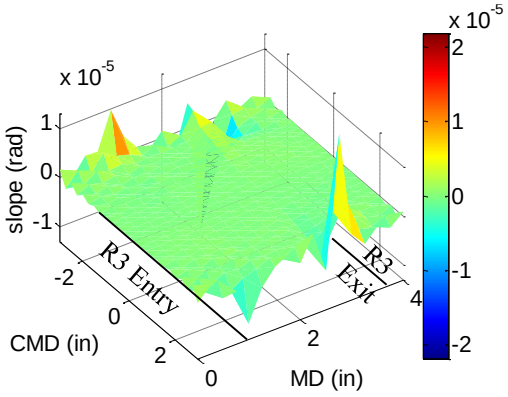

Figure 4.11 – Slope (rad) on Roller R3

The slope is shown spatially in Figure 4.11 prior to entry, on the roller and exiting roller R3. The potential for some slip always exists as a web enters and exits a roller due to the normal contact pressure being very small at the tangent entry and exit and the finite bending stiffness of the web. In Figure 4.11 slip is occurring at the entry and exit as the MD strain on the inner transitions from the membrane value in the free span, to a lower value due to the bending strain

shown in Equation (4.2) but reduced by friction and returning to the membrane value at the exit. In these same regions lateral slip and occur as well. The slope of the web is much diminished in Figure 4.11 between the entry and exit regions where stick behavior was predominant. The slip in the entry and exit regions as well as the stick behavior between those regions was evident in the contact status output from ABAQUS.

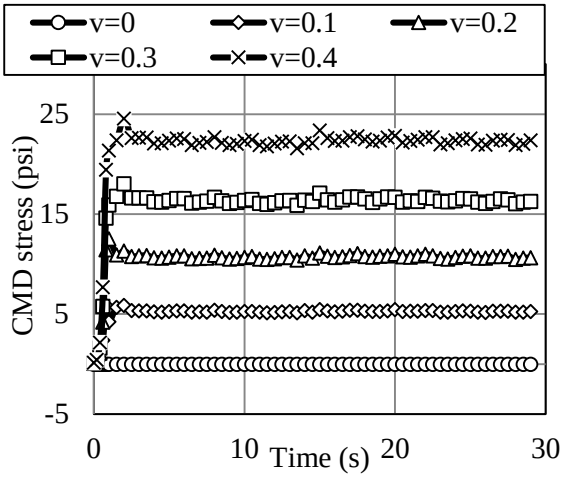

Figure 4.12 – Effect of Poisson's Ratio on CMD Membrane Stress

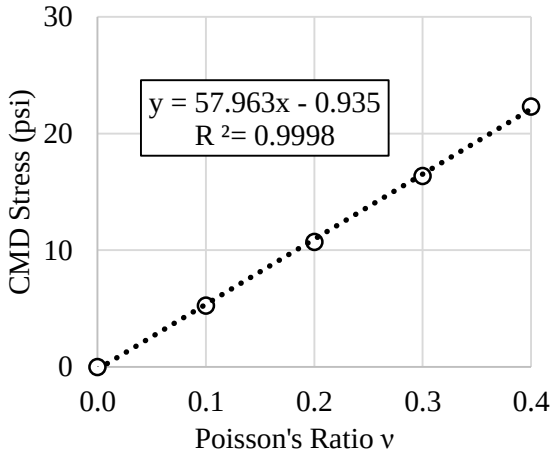

Figure 4.13 – Dependence of CMD Spreading Stress on Poisson's Ratio

The CMD spreading stresses witnessed in Figures 4.5 and 4.6 and the non-zero web entry slopes that caused those stresses were hypothesized to be the result of the anticlastic deformations described in the example in the first Section 4.1. Partial proof of the hypothesis was provided by the constant CMD stresses that were nearly constant across the web width in the simulations (Figure 4.6) and comparable to those predicted from Equation (4.8) on the inner and outer surfaces. Further proof was sought by conducting additional simulations while varying only Poisson's ratio. As Poisson's ratio approaches zero, the anticlastic deformation should vanish per Equation (4.3). The results of those simulations are shown in Figure 4.12. The CMD spreading stress did vanish when Poisson's ratio was zero. Furthermore, there appeared to be near proportionality of the CMD spreading stress as a function of Poisson's ratio. The average of the steady state CMD spreading

stresses at the mid-plane surface are shown as a function of Poisson's ratio in Figure 4.13. A linear fit of the averaged data was performed and the correlation coefficient is close to unity. Thus from the simulations it has been proven that the CMD mid-plane spreading stresses are (1) the result of anticlastic bending and (2) are proportional to Poisson's ratio.

The CMD stresses on the inner, mid-plane and outer surfaces are shown in Figure 4.14 for the case where Poisson's ratio was set to zero. The anticlastic effect is no longer present. The CMD stresses at the mid-plane and the inner and outer surfaces have vanished.

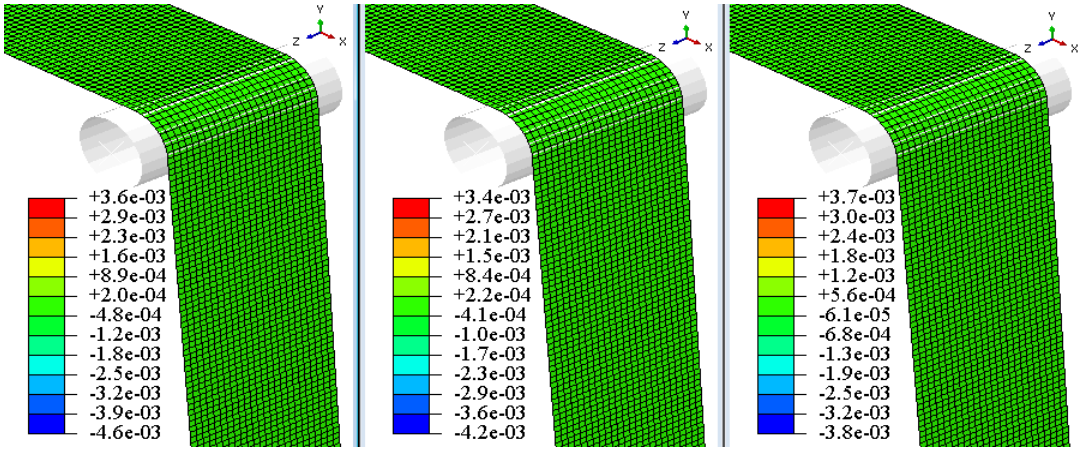

Inner surface Mid-plane surface Outer Surface

Figure 4.14 – Vanishing of CMD Stresses (Psi) on R3 for Zero Poisson's Ratio

The entry slope of the web as for various levels of Poisson's ratio is shown in Figure 4.15. Note when Poisson's ratio is zero that the entry slope is zero at all CMD locations and is indicative of why the spreading stresses for this case in Figures 4.12 and 4.14 were also zero. Note with increasing Poisson's ratio the entry slopes at the web edges are also increasing. The absolute values of the edge entry slopes are shown in Figure 4.16 as a function of Poisson's ratio. A linear curve fit of the slope data is shown that a high correlation coefficient (0.997) was obtained. Thus, the entry slope at the web edge (Figure 4.16) and the mid-plane CMD spreading stresses (Figure 4.13) have been shown to be proportional to the Poisson's ratio.

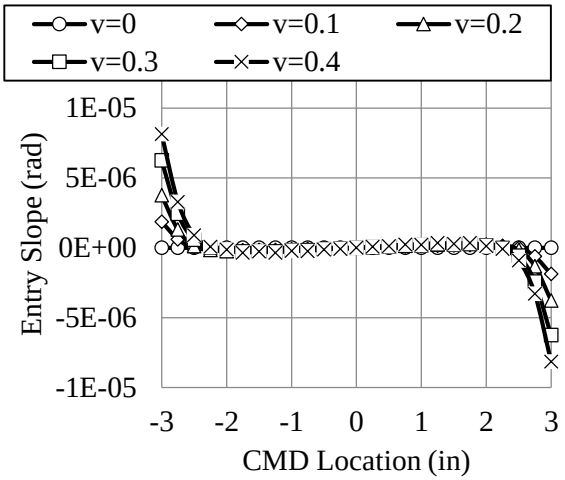

Figure 4.15 – Effect of Poisson's Ratio on Entry Slope

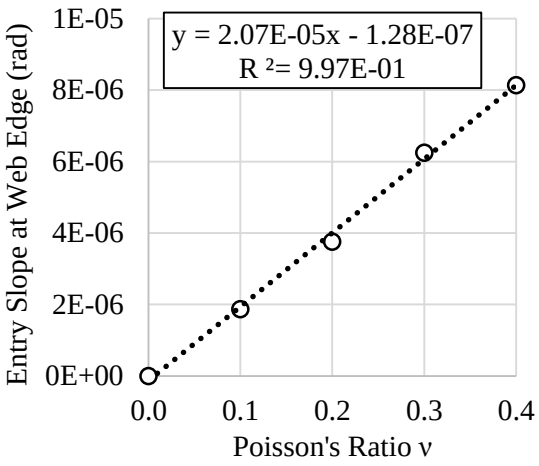

Figure 4.16 – Effect of Poisson's Ratio on Web Edge Entry Slope

The effect of friction coefficient was also studied. Air entrainment is common between webs and roller in roll-to-roll process machines and can reduced coefficients of friction. Typically, the spreading ability of rollers is diminished with decreased friction.

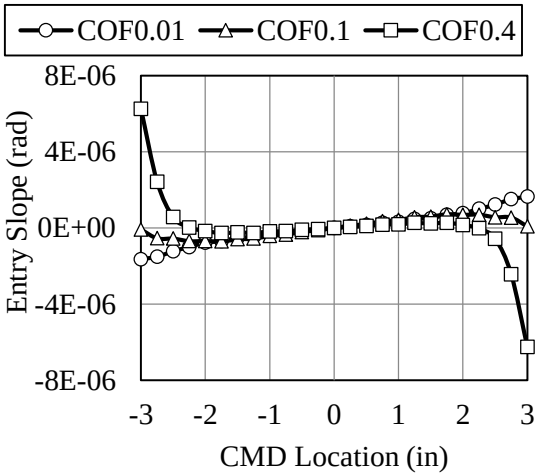

Figure 4.17 – Effect of Coefficient of Friction on Entry Slope (ν=0.3)

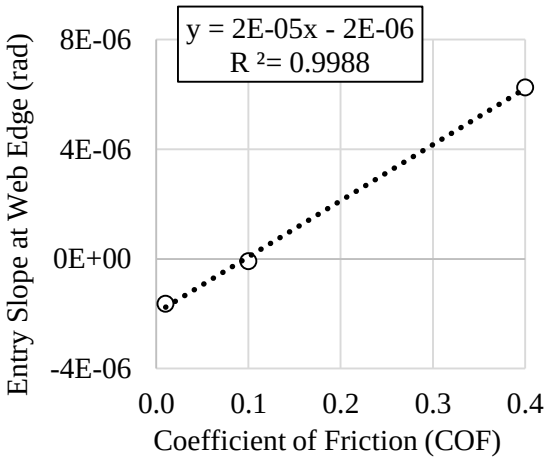

Figure 4.18 – Effect of Coefficient of Friction on Web Edge Entry Slope (ν=0.3)

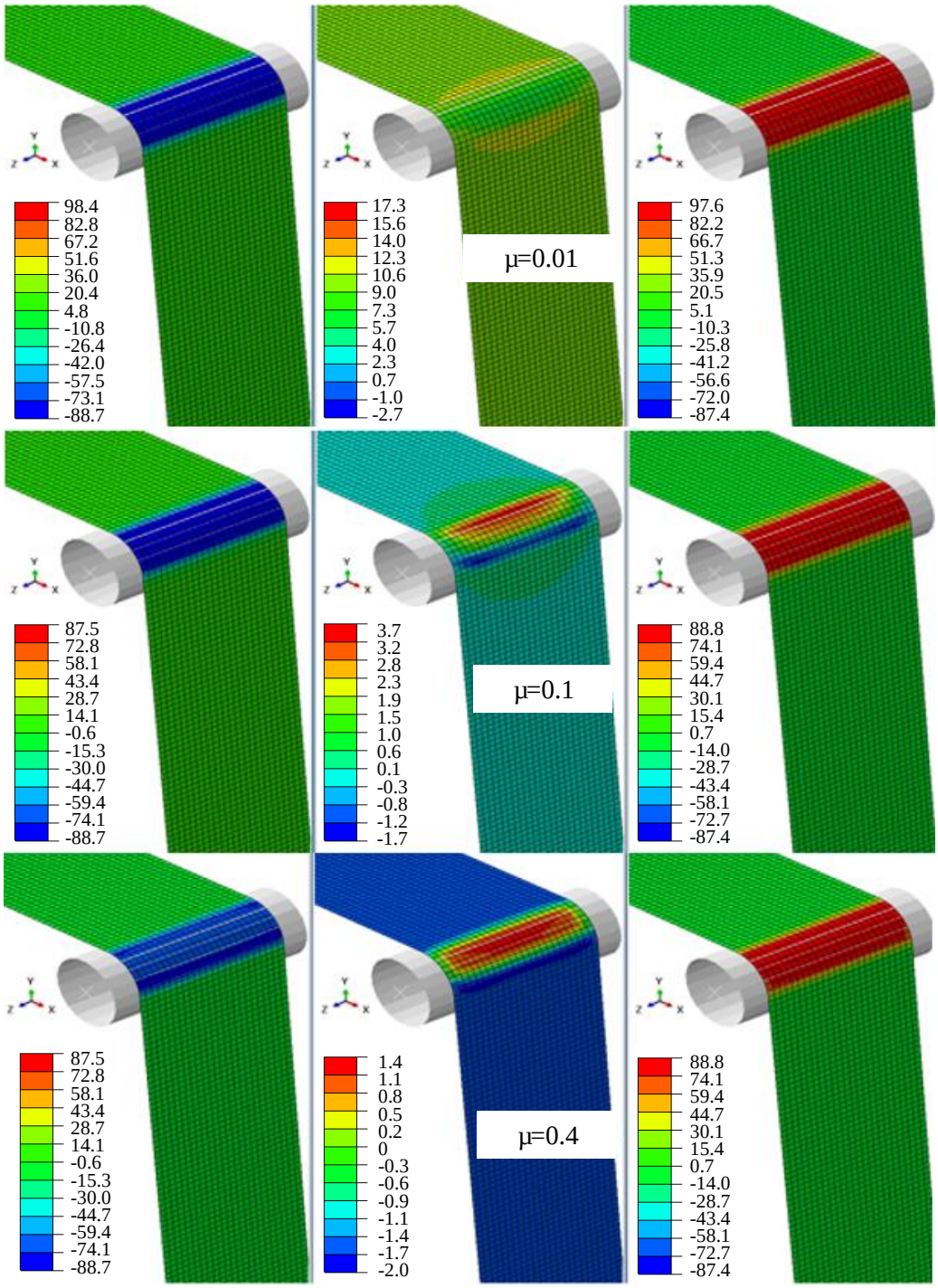

Figure 4.19 – Effect of Coefficient of Friction on CMD stress (psi), ν=0.3

In fact that is shown to the case of Figure 4.17, 4.18, and 4.19. In Figure 4.17 the web entry slopes are shown to diminish with decreased coefficient of friction. In Figure 4.18 the web edge slope is shown to diminish linearly with friction coefficient. In Figure 4.19 the CMD stresses on

the mid-plane of the web on the roller surface are shown to diminish with decreased coefficient of friction. The friction coefficient is also affecting the CMD stresses on the inner and outer surfaces. The average CMD stresses on the mid-plane and inner and outer surfaces are shown in Table 4.1. Again the decrease in CMD spreading stress is witnessed at the mid-plane. Note how the average CMD stresses converge to 80.5 psi are the coefficient of friction approaches zero. Also note this is very close to the value predicted by closed form expressions and presented in Equation (4.8). Thus the simulation results and anticlastic theory agree perfectly.

Table 4.1 – Average CMD Stresses (psi) in the Web on the Roller as a Function of Friction and Surface

μ	Inner Surface	Mid-plane	Outer Surface
0.01	-80.5	-0.5	80.5
0.1	-78	3	83
0.4	-65	16	97

4.4 Experimental Setup and Verification

The results from anticlastic theory (Equation (4.8)) and simulation results (Figure 4.6) indicate that a web with Poisson's ratio greater than zero would have a tensile CMD stress on outer surface of the web as the webs transits a roller. Good agreement was seen for the MD and CMD bending stresses on the inner and outer surfaces produced by the simulations of the 0.001 inches web and the closed form equations for the four-roller web case. Further verification was sought to determine if the stresses due to anticlastic behavior could be measured in the laboratory.

A polyester web 0.01 inches in thickness and 6 inches wide was chosen to explore the anticlastic effect in the laboratory. The modulus of elasticity of the web was measured and found to be 712,000 psi and Poisson's ratio was found to be 0.36. The strains were measured using strain gages adhered to the web surface. The strain gages[1] had a polyimide backing that was 0.31 inches

[1] CEA-06-062UT-350, Micro-Measurements, POB 27777, Raleigh, NC, 27611, USA.

square and 0.003 inches in thickness. The web was 3.3 times thicker than the strain gages and was chosen to reduce the effects of reinforcement of the web by the strain gage. The web instrumented with strain gages was positioned to transit a roller 2 inches in radius on the High Speed Web Line in the Web Handling Research Center. The coefficient of friction between the roller and the web was measured to be 0.24. As shown in Figure 4.20, the strain gauge was bonded to the web at the CMD center. The strain gages had two elements (90° tee rosette pattern) and will allow the measurement of the MD and CMD strains of the web simultaneously. Gage tabs were used as shown in Figure 4.20 such that the bending stiffness of the lead wires was minimized in the vicinity of the strain gage. The leads were connected to a multichannel strain conditioner/amplifier[2] whose output was input to a data acquisition system[3]. A fiber optic sensor[4] was used to sense when the center of the strain gage resistance grids passed the tangent entry of the web to the roller.

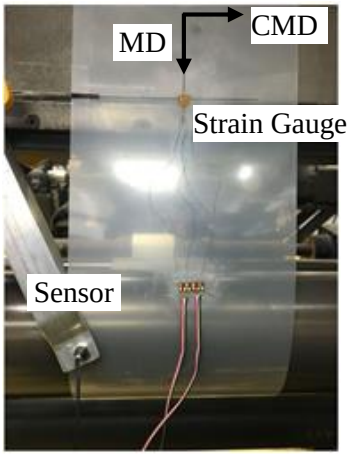

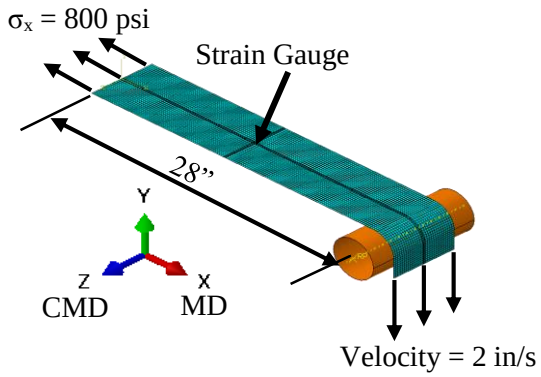

Figure 4.20 – Experiment Setup

Figure 4.21 – Simulation of Tests

A finite element (FE) simulation similar to that described earlier but with the web and roller properties used in the test was developed as shown in Figure 4.21. In the test, the strain gauge grid

[2] 2100 System, Micro-Measurements, POB 27777, Raleigh, NC, 27611, USA.
[3] PCIe 6251, National Instruments, 11500 N Mopac Expressway, Austin, TX 78759-3504, USA.
[4] FS-V11, Keyence Corporation, 500 Park Boulevard, Suite 200, Itasca, IL 60143, USA.

was centered and bonded on the web centerline. A cyanoacrylate adhesive[5] was used and the total thickness for the web, adhesive layer and the strain gauge is 0.0132 inches. In the simulation, the web was modelled with a local increase in thickness in the location of the strain gage to account for the local increase in stiffness due to the installation of the gage. The lead wires were not considered, their bending stiffness was assumed to be negligible. During tests, the web tension was maintained at 48 lb. This induced an MD membrane stress of 800 psi which was applied as a surface traction on the upstream end of the web. The downstream end of the web was brought to an MD velocity of 2 in/s consistent with the experiment.

In this simulation, the MD stress on the web outer surface rises quickly from 800 psi in the free span to 2,850 psi on the roller as shown in Figure 4.22. Theoretically the moment required to bend the test web to the radius of the test roller is:

$$M_x = \frac{D}{R} = \frac{Eh^3}{12R\left(1-\nu^2\right)} = \frac{710{,}000 \times 0.01^3}{12 \times 2 \times \left(1-0.36^2\right)} = 0.0340 \text{ lb} - \text{in/in} \tag{4.9}$$

The bending stress in the outer surface would be:

$$\sigma_{MD} = \sigma_{MD,\text{free span}} + \frac{6M_x}{h^2} = 800 + \frac{6 \times 0.034}{0.01^2} = 2{,}840 \text{ Psi} \tag{4.10}$$

This is within 0.35% of the simulation result.

The CMD stresses that result from bending the anticlastic surface so that it is compatible with the cylindrical surface of the test roller can be determined using Equation (4.8):

$$\sigma_{y,CMD} = \pm\frac{6M_y}{h^2} = \pm\frac{6\nu M_x}{h^2} = \pm\frac{6 \times 0.36 \times 0.034}{0.01^2} = \pm 734 \text{ Psi} \tag{4.11}$$

Thus if the reinforcement of the strain gauge is not considered, the CMD stress the outer surface of the web on the roller is 734 psi, zero at neutral surface and -734 psi on the inner surface

[5] MBOND-200, Micro-Measurements, POB 27777, Raleigh, NC, 27611, USA.

according to the Equation (4.11). The stress variation through the web depth is quite similar to the simulation results shown in Figure 4.23. The simulation stresses were harvested on a path half way through the wrap angle of the web on the roller. A tensile CMD spreading stress of 8 Psi was witnessed at the mid-plane in the simulation.

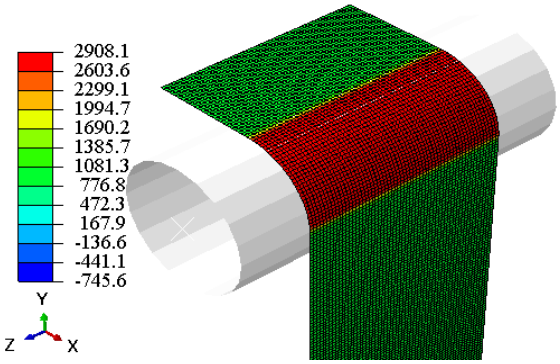

Figure 4.22 – The MD Stress (psi) on the Outer Surface

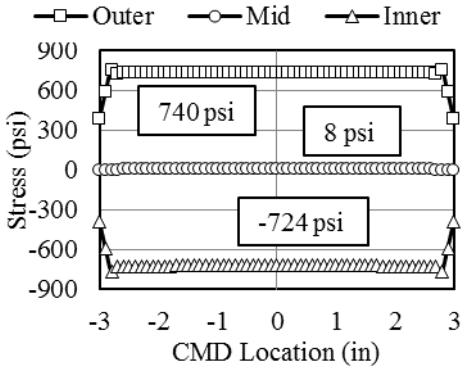

Figure 4.23 – CMD Stresses from Simulation

The MD and CMD strains of the web in the free span $\varepsilon_{MD,free}$, $\varepsilon_{CMD,free}$ and on the roller ε_{MD}, ε_{CMD} can be estimated using the constitutive Equation (4.12). As the web moves from the free span onto the roller, the MD strain on the outer surface (ε_{MD}) would increase from 1127 µin/in to 3,628 µin/in. The CMD strain on the outer surface (ε_{CMD}) changes very little, from -405.6 µin/in in the free span to -406.2 µin/in on the roller surface.

$$\varepsilon_{MD,free} = \frac{\sigma_{MD,free} - \nu\sigma_{CMD,free}}{E} = \frac{800 - 0.36 \times 0}{710{,}000} = 1{,}127\ \mu\text{in/in}$$
$$\varepsilon_{CMD,free} = \frac{\sigma_{CMD,free} - \nu\sigma_{MD,free}}{E} = \frac{0 - 0.36 \times 800}{710{,}000} = -405.6\ \mu\text{in/in}$$
$$\varepsilon_{MD} = \frac{\sigma_{MD} - \nu\sigma_{CMD}}{E} = \frac{2840 - 0.36 \times 734}{710{,}000} = 3{,}628\ \mu\text{m/m} \qquad (4.12)$$
$$\varepsilon_{CMD} = \frac{\sigma_{CMD} - \nu\sigma_{MD}}{E} = \frac{734 - 0.36 \times 2840}{710{,}000} = -406.2\ \mu\text{m/m}$$

The strains from Equation (4.12) do not account for the reinforcement of the strain gage, the friction and potential for slippage between the web and roller and the steering/spreading effects of forcing the anticlastic surface of the web to acquire the cylindrical shape of the roller. These factors were all accounted for in the simulation. In the simulation, the MD and CMD strains were recorded at the center of the strain gauge through time. As shown in Figure 4.24, the MD strains from the simulation and experiment match quite well. The CMD strain remain nearly constant, which is consistent with Equation (4.12), while the MD strains increase significantly as the strain gauge moves from the free span onto the roller. The bending strains in the outer surface of the web from tests and simulations are about 3,750 μin/in, in excess of the 3,628 μin/in from (4.12). This was expected due the added thickness of the strain gage atop the web.

The experimental MD and CMD stresses on the web outer surface can be inferred using the plane stress Equation (4.13) and the experimental strains:

$$\sigma_{MD} = \frac{E}{1-\nu^2}[\varepsilon_{MD} + \nu\varepsilon_{CMD}]$$
$$\sigma_{CMD} = \frac{E}{1-\nu^2}[\varepsilon_{CMD} + \nu\varepsilon_{MD}] \qquad (4.13)$$

The MD and CMD test and simulation stresses on the web outer surface agree well and are shown in Figure 4.25. Tensile CMD stresses of consequence are witnessed in the web on the roller, which is experimental proof that anticlastic effects exist in thin webs. From Equation (4.10), the MD stress on the web outer surface is 2,840 Psi on the roller without considering strain gauge, and

it is 800 psi in the free span as set in the simulation. In Figure 4.25, the MD stress on the roller from tests and simulation are 3,190 Psi, larger than that from Equation (4.10) due to the added thickness of the gage and the inability of Equation (4.10) to encompass the effects of friction and slippage. The CMD stresses on the web outer surface on the roller are 734 Psi from Equation (4.11) and 740 Psi from the Figure 4.20 for the case with no strain gage. The results in Figure 4.25 are slightly larger but again this was expected because of the added thickness of the strain gage.

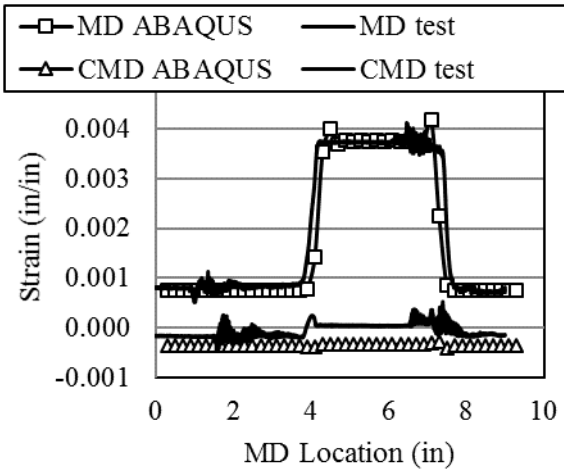

Figure 4.24 – Strain: Simulation and Test

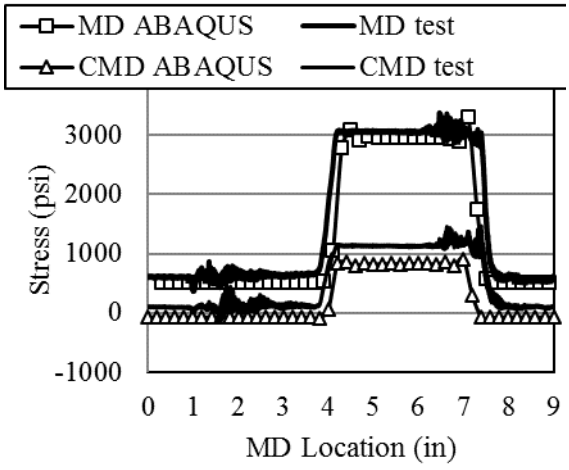

Figure 4.25 – Stress: Simulation and Test

4.5 Conclusions

Anticlastic bending produces measurable and beneficial effects for webs transiting rollers. Anticlastic effects are commonly considered negligible for thin palates such as webs. This consideration is based on the notion of small deflections where the out-of-plane deflections are comparable to the thickness of the plate. Webs transiting rollers undergo bending deformations that can be thousands of times greater than their thickness. In free space a web bent to the radius of a roller on one axis does desire to take an anticlastic shape as shown in Figure 4.2. Web tension is often sufficient to cause the web to conform and become compatible with the surface of rollers. The web tension and the resulting web deformations do result in inducing M_y internal moments

(Figure 4.3) as proven by the constant CMD stresses on the inner and outer surfaces across the web width (Figures 4.6 and 4.23). Anticlastic bending does result in non-normal entry of the web away from the CMD center of the web (Figure 4.15). This resulted in tensile CMD spreading stresses on the mid-plane of the web (Figures 4.12 and 4.23). It was shown that the slope of the web edge at the tangent entry (Figure 4.16) and the CMD spreading stresses acting at the mid-plane (Figure 4.13) were proportional to Poisson's ratio. When Poisson's ratio became zero, normal entry was achieved at all CMD locations across the web width (Figures 4.15 and 4.16) and the CMD spreading stress vanished (Figures 4.12 and 4.13) which provided evidence the behaviors were the result of anticlastic bending. The CMD spreading stresses were shown to diminish with decreasing coefficient of friction (Figure 4.17, 4.18, 4.19 and Table 4.1).

The example web studied showed the web width contracted on the order of 100 μin in Figure 4.8 from web center to edge. This may present challenges for industries concerned with the precision printing and registration of electronics.

The dynamic finite element simulations have provided perhaps the best understanding to date of the concept of normal entry of a moving web approaching contact to a downstream roller. The theory of Timoshenko [9], dynamic finite element simulation and experimental validation have proven the effects of anticlastic bending exist in common webs in roll-to-roll process machines. While the CMD mid-plane spreading stresses are beneficial in resisting web wrinkling, no simple closed form equations will allow their calculation since they are the result of slippage and non-normal entry of the web.

CHAPTER V

BOUNDARY CONDITIONS FOR LATERAL DEFORMATION OF WEBS TRANSITING ROLLERS IN ROLL-TO-ROLL PROCESS MACHINES

The lateral deformations of webs in roll-to-roll (R2R) process machines can affect the quality of the manufacturing process. The lateral registration of the web in successive R2R processes can determine whether a product will function as designed. Herein a unified theory is presented that explains how imperfections in rollers, their alignment and length nonuniformity (camber) in webs can affect the steady state lateral deformation and hence registration. Enhanced understanding of steady state lateral deformation of webs transiting free spans and rollers will provide insight for advanced control methods that account for the effects of web deformation in minimizing registration error. The validated results show that the lateral deformations can be predicted with closed form equations. In some cases the boundary conditions which are integrated into these equations must be determined using dynamic simulation.

5.1 Introduction

The lateral deformation v of a beam of bending stiffness EI subjected to tension T, lateral loads, bending moments but the absence of lateral tractions are governed by the differential equation (5.1) that can be transformed to [55]:

$$EI\frac{d^4v}{dx^4} - T\frac{d^2v}{dx^2} = 0 \tag{5.1}$$

The solution of the differential equation is of the form:

$$v = A + B\frac{x}{L} + C\cosh[\frac{\lambda x}{L}] + D\sinh[\frac{\lambda x}{L}], \quad \lambda=\sqrt{\frac{TL^2}{EI}} \tag{5.2}$$

where x is coordinate taken on the elastic axis of a beam of length L. The constant coefficients A, B, C and D depend on the boundary conditions for the problem under attack.

Spans of web between rollers in R2R process machines are often treated as beams where equations (5.1,5.2) are applicable. Shelton was first to discover how these expressions (5.1,5.2) are applicable to webs that are steered laterally by a misaligned roller [56][57]. Shelton's discovery was triggered by experimental observation. In tests he misaligned a downstream roller in a test span and measured the lateral deformation that resulted after steady state lateral conditions were achieved. Shelton limited the misalignment to ensure that moments generated at the upstream roller did not surpass the moment that could be reacted by friction between the web and roller or induce edge slackness in the web [32][33]. This confined the lateral deformations to his test and downstream web spans. From his test results, Shelton inferred the lateral deformations for long spans entering a misaligned roller were governed by boundary conditions which include (1) the lateral deformation of the web entering the test span was zero, (2) the slope of the web entering the span was zero for long spans where shear deflections were negligible, (3) that the slope of the web entering the misaligned roller was the misalignment of the roller (the normal entry condition) and (4) that the moment was zero in the web at entry to the misaligned roller. Shelton attributed the normal entry condition to Lorig [58] who stated for steady state lateral conditions that the elastic axis of the web must enter the downstream roller normally to the axis of rotation.

Idler rollers in R2R process machines are often subject to manufacturing errors that result in the outer radius of the roller not being constant. In the simplest form of this error the outer radius tapers linearly across the roller width. Yurtcu et. al. [18] studied the lateral deformations of a web

span with a downstream roller whose radius tapered linearly across the roller width. They found that the elastic axis of the web was steered laterally to a steady state position by the tapered roller. They derived the four boundary conditions (3 kinematic and 1 kinetic) needed to quantify the lateral deformations of the web in the test span.

A more complex case is that of the cambered web. A cambered web has one side longer than the other. In the simplest form this web varies linearly in length across the web width. If this web is smoothed upon a flat surface under no tension, an observer above the web surface would observe a curved web beam. The camber can be quantified by measuring the radius of curvature of the elastic axis of the unstressed web (ρ_o). Experimental investigations on cambered webs in belt form [20] and on cambered webs transiting through roll-to-roll process machines [19][21] have consistently shown that the web steers towards the longer edge. Modelling efforts have been less successful in comparison to the experiments [21][23][24][25][26][27][59][60][61] and will be discussed later.

The analyses herein will deviate from the previous analyses by considering how the mechanics of the web transiting a roller dictate the lateral behavior of the web in a free span. These considerations will be applied to the previous cases for steady state lateral deformations of web spans with a downstream misaligned or tapered roller and finally to the case of a cambered web. Validation will be provided in each case.

5.2 A Web Transiting a Misaligned Roller

A web exits an upstream roller in a web span. It will be assumed that the web entered that roller under the condition of normal entry posed by Lorig [58]. The condition of normal entry is one in which the elastic axis of the web is orthogonal to the axis of rotation of the upstream roller. The web will have zero lateral velocity on the upstream roller and the lateral position of the elastic axis of the web will be arbitrarily set at zero. Furthermore it will be assumed that the available

friction forces between the web and the upstream roller are sufficient to prevent any slippage of the web laterally or in rotation on the roller surface. With these assumptions the lateral deformation and slope of the web exiting the upstream roller can be assumed to be zero:

$$v_i = v(0) = 0 \tag{5.3A}$$

$$\theta_i = \left.\frac{dv}{dx}\right|_{x=0} = 0 \tag{5.3B}$$

The downstream roller is misaligned at an angle θ orthogonal to the plane of the web span. If the misalignment occurred instantaneously the web would begin to translate laterally on the downstream roller. Webs respond to dynamic disturbances much as a first order dynamic system would react to a step input. Webs typically have very little mass which minimize internal inertial loads and allows the approximation of a first order system. After about 4 time constants τ, where τ=L/V, L is the span length and V is the web velocity, the web would come to a new steady state lateral location on the misaligned roller and dynamic motion would cease. The web has now achieved normal entry to the misaligned roller. The slope of the web at the entry to the misaligned roller θ_j will have become equal to the misalignment θ:

$$\theta_j = \left.\frac{dv}{dx}\right|_{x=L} = \theta \tag{5.3C}$$

Furthermore due to the assumption of no slippage of the web on the misaligned roller, the slope of the elastic axis of the web will remain at θ as the elastic axis follows a curvilinear path around the misaligned roller. Since the slope is not changing, the derivative of the slope must be zero:

$$\left.\frac{d^2v}{dx^2}\right|_{x=L} = \left.\frac{d\theta}{dx}\right|_{x=L} = 0 \tag{5.3D}$$

The four boundary conditions presented in Equations (5.3A-5.3D) are sufficient to determine the four unknown coefficients A-D in Equation (5.2). The equation for the lateral deformation of the elastic axis of web in the free span between the upstream roller and the misaligned downstream roller is:

$$v = \frac{\lambda x \cosh\lambda + L(\sinh(\lambda(1 - x/L)) - \sinh\lambda)}{\lambda(\cosh\lambda - 1)}\theta \tag{5.4}$$

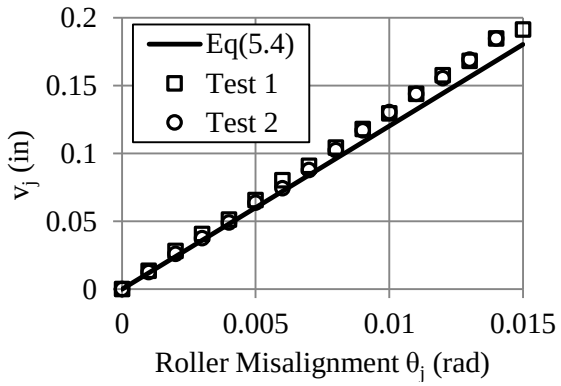

Figure 5.1 – Lateral Deformations of a Web due to a Downstream Misaligned Roller

This equation has been validated by tests [39]. A polyester web 6 inches wide and 0.001 inches in thickness was transported through a web span 18 inches in length. Young's modulus of the web was tested and found to be 712,000 GPa. Web tension was set at 3 lb. In Figure 5.1 the lateral deformations predicted by (5.4) and the test results are presented. Note the agreement between tests and (5.4) is quite good at low misalignment but that the result from (5.4) becomes less than the test data at greater misalignments. The length to width ratio of the web span is 3 and as such it might be argued that shear deformations could be significant. Also the friction forces between the web and the upstream roller surface may have been insufficient to restrain the bending moment that is maximum at that location and increases proportionately with misalignment. Thus the slope of the web exiting the upstream roller may have been greater than zero due to slippage. Either one of these sources of error could be sufficient to explain the difference seen between the

lateral deformations predicted by (5.4) and the test results. Also note that shearing deformation and slippage would both result in test results that would be greater than the prediction by Equation (5.4) since neither effect was taken into account in the derivation. Nevertheless the agreement shown in Figure 5.1 is sufficient to prove that the downstream curvature boundary condition (5.3D) is valid.

Shelton [56] was first to demonstrate the analysis of a web approaching a misaligned roller. He implemented boundary conditions (5.3A-5.3C) above. His 4th boundary condition was determined experimentally in the laboratory. He determined that the moment in the web at the entry to the downstream roller was zero.

$$M_L = 0 \tag{5.5}$$

Shelton also determined that a lateral force at the downstream roller was required to achieve normal entry (5.3C):

$$N_L = \frac{T\theta}{\cosh\lambda - 1} \tag{5.6}$$

He derived an equation equivalent to (5.4) for the lateral deformation. While the difference may seem inconsequential the argument presented is that Shelton's kinetic boundary conditions (5.5) and (5.6) were needed to sustain the kinematic boundary conditions (5.3C) and (5.3D), both of which rely on no slippage in the entry region of the web on the misaligned downstream roller.

A dynamic finite element simulation[6] code was used to provide means of visualizing the behavior discussed. The horizontal span of web in Figure 5.2(a) has identical length, width, thickness and modulus to the web described earlier in the tests. The 3rd roller in the simulation (R3) was given a misalignment of 1 mrad about the y axis in Figure 5.2(a). A web length 4 times the span length between rollers R2 and R3 was allowed to pass over the rollers in the simulation.

[6] Dassault Systems, ABAQUS Simulia, Rising Sun Mills, 166 Valley St., Providence, RI 02909-2499

Web tension was maintained 2.8 lb, slightly less than the tests conducted at 3 lb. In Figure 5.2(a) the web travels in the x direction. Note the MD stresses become uniform as the web enters roller R3. This uniformity in stress demonstrates the moment about the y axis on the elastic axis of the web is zero, hence Shelton's condition (5.5) is satisfied. The lateral deformations are shown in Figure 5.2(b). In the vertical entry span the lateral deformations are due to uniform Poisson contraction. In the horizontal test span the lateral deformations are due to a combination of Poisson contraction and lateral steering. Finally in the vertical exit span the deformations are to the steering in the horizontal span, Poisson contraction and the slight twist the span is subject to. The presence of stick and slip behavior between the web and the entry (R2) and exit (R3) rollers is shown in Figure 5.2(c). Note that stick behavior occurs over most of the contact between the web and roller R3. The MD stress variation shown across the width of the web as the web exits roller R2 results in varying degrees of capstan slippage across R2 as shown in Figure 5.2(c). The level of slippage will jeopardize the validity of boundary condition (5.3B).

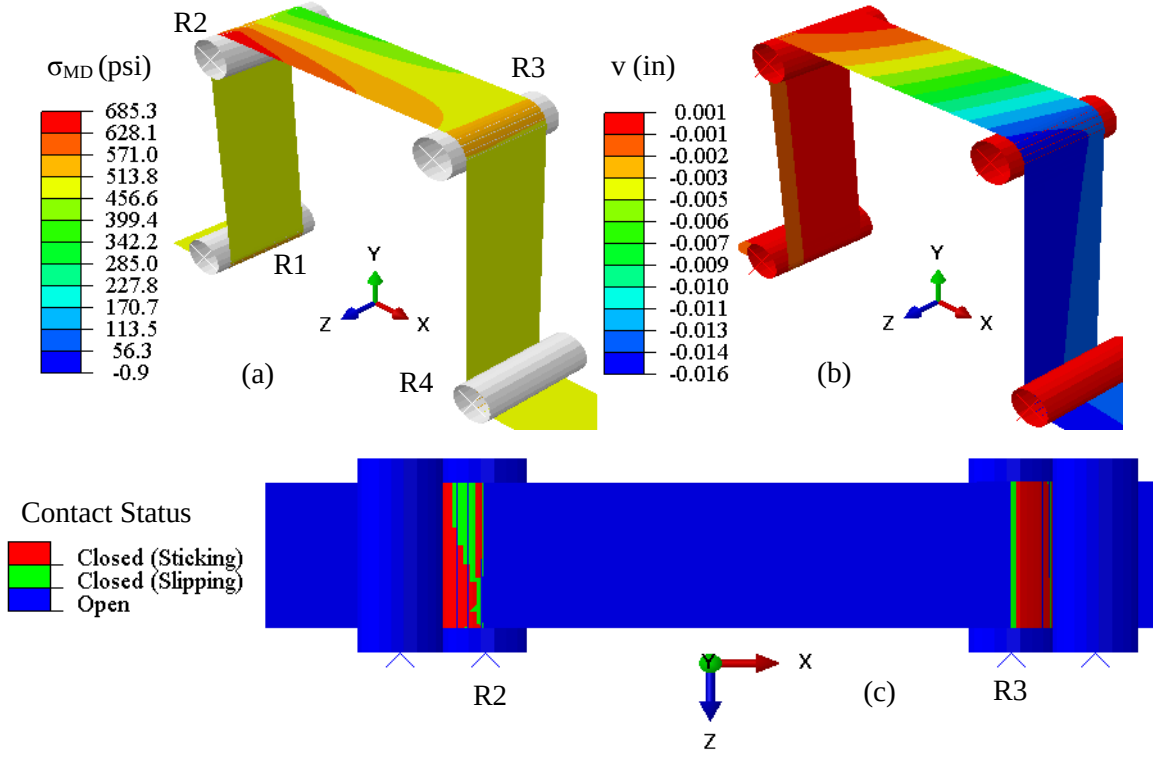

Figure 5.2 – Dynamic Simulation of a Web Approaching a Misaligned Roller

The lateral deformations for the elastic axis of the web were harvested from the whole field data presented in Figure 5.2(b) and presented in Figure 5.3. The lateral deflection of the elastic axis at the entry to R3 is -0.0129 in. In Figure 5.1 the average absolute test deflection from the two tests is 0.0130 inches, thus the simulated value is within 0.8% of the test value. Both the simulations and the tests allow slippage at the exit of R2 and relaxation of condition (5.3B). Equation (5.4) produces a deflection of -0.0120, 7.7% in error compared to the test value. For this condition, Equation (5.6) predicts a lateral force of 0.061 lb is required to enforce normal entry of the web to roller R3. The results of the dynamic simulation showed that a lateral load of 0.058 lb was required, very comparable to that predicted from Equation (5.6).

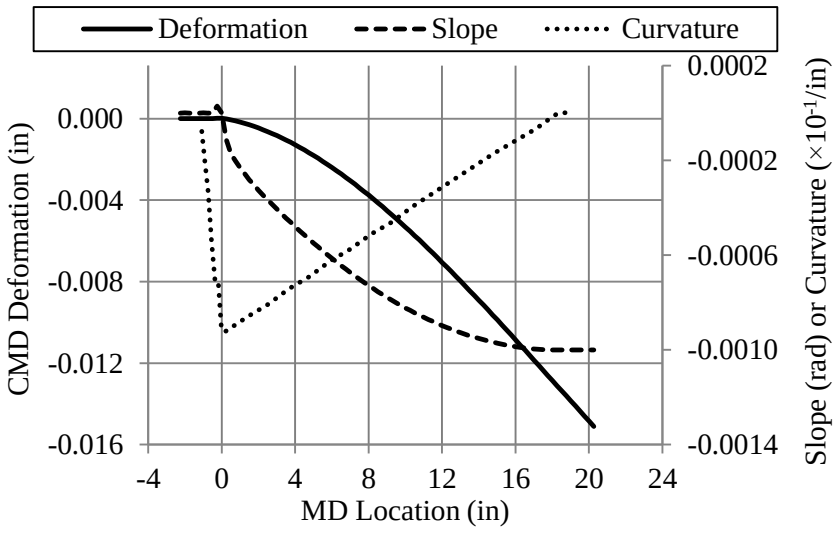

Figure 5.3 – Deformation, Slope and Curvature of the Elastic Axis of the Web after Steady State Conditions were achieved in the Simulation Shown in Figure 5.2

The dynamic simulation has none of the boundary conditions (5.3A-5.3D) enforced but the displacements, slopes and curvatures presented in Figure 5.3 show these boundary conditions are reasonable. In Figure 5.3 the web exits the upstream roller R2 at an MD location of 0 inch. The web enters roller R3 at 18 inches. The MD Location is a coordinate that follows the elastic axis of the web as it wraps around roller R2, proceeds into the horizontal span and then wraps roller R3.

The web exits R2 with no lateral deformation (5.3A) and little slope (5.3B). The web enters R3 at the slope of the misaligned roller (5.3C) with near zero curvature (5.3D).

In Figure 5.4 the rate that the steady state boundary conditions were achieved in the simulation are shown. The dynamic time constant is the span length (18 inches) divided by the web velocity (2.9 in/s) or 6.2 seconds. It appears that steady state conditions had been attained after 20 seconds of simulation or about 3.2 time constants.

The web wrapping the misaligned roller is a sector of a right circular cylinder whose inside surface matches the outside surface of the misaligned roller precisely as shown in Figure 5.5(a). That these shapes match precisely allows the web to cross much of the misaligned roller R3 without slip. The lateral force NL was required to achieve normal entry. The zero curvature allows the elastic axis to follow a circular rather than a helical path in the entry region of R3.

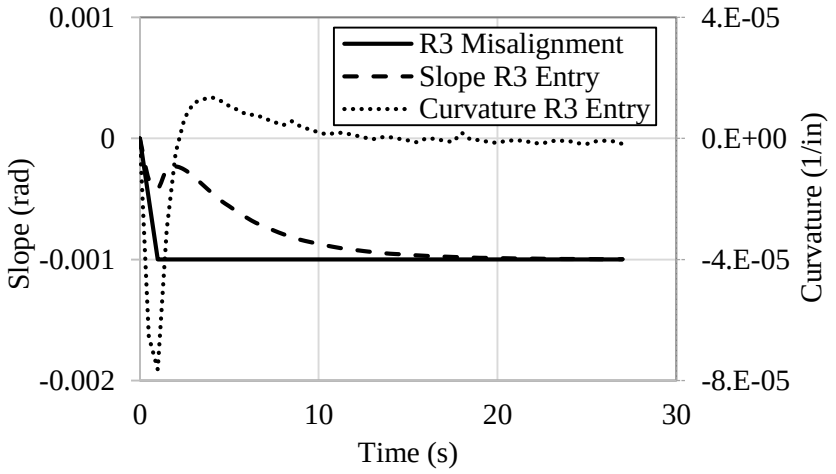

Figure 5.4 – Rate at which Steady State Boundary Conditions are attained in the Simulation shown in Figure 5.2

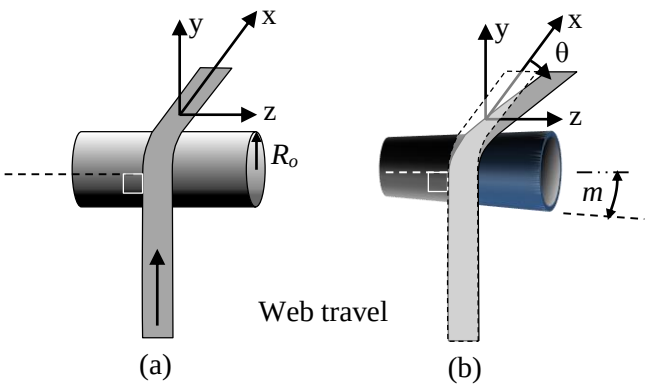

Figure 5.5 – A Web Entering (a) a Cylindrical Roller and (b) a Tapered Roller Normally

5.3 A Web Approaching a Tapered Roller

Rollers can take the shape of a truncated cone as an unintentional result of manufacturing processes. Manufacturers of rollers will quote the maximum radial taper m as an error in the radius of the roller per unit width (in the CMD). A tapered roller will steer a web in the CMD towards the larger radius end of the roller. Assume an upstream roller is a perfect right circular cylinder. Also assume the next roller downstream is a roller with linear radial taper m with respect to the CMD. The nominal radius of this roller R_0 is defined halfway across the roller width. Furthermore, assume the axes of rotation of both rollers are parallel and hence they are aligned. In Figure 5.5(a) straight web is shown entering a cylindrical roller (a) and a tapered roller (b) under normal entry conditions. Assume temporarily that the web is under no stress but that it is forced to have surface contact with the rollers and consider the geometry. The web exiting the cylindrical roller will exit normally to the exit tangent line. The web exiting the tapered roller will not exit normally but at an angle θ given by:

$$\theta = WP * m = \frac{s}{R} m \qquad (5.7)$$

where WP is the wrap angle of the web about the roller, s is a curvilinear coordinate following the elastic axis of the web, and m is the slope of the roller in terms of change in radial in./ in. width.

The earlier assumption of allowing no slippage will not allow the web to follow this path. If the web does not slip it will proceed straight over the roller as shown in the dashed configuration in Figure 5.5(b) which makes it appear similar to the web in Figure 5.5(a). Now the web must be deformed in a negative θ direction to allow the web to travel directly over the roller and exit normally from the tapered roller. To accomplish this, a constant curvature must be enacted on the web so that the straight dashed path can be followed without slip:

$$\left.\frac{d^2v}{ds^2}\right|_{x=L} = -\left.\frac{d\theta}{ds}\right|_{x=L} = -\frac{m}{R_0} \tag{5.8}$$

The four boundary conditions (5.3A) and (5.3B), (5.3C) with θ = 0 and (5.8) were used in conjunction with Equation (5.2) to determine the unknown coefficients A, B, C and D. The equation for the lateral deformation of an initially straight web approaching a tapered roller is:

$$v = \frac{mEI}{R_0 T}\left[\cosh\left[\frac{\lambda x}{L}\right] - 1 + \coth\left[\frac{\lambda}{L}\right]\left(\frac{\lambda x}{L} - \sinh\left[\frac{\lambda x}{L}\right]\right)\right] \tag{5.9}$$

From Equation (5.9), the moment and shear in the web at the entry to the tapered roller can be determined:

$$M_L = EI\left.\frac{d^2v}{dx^2}\right|_{x=L} = \frac{mEI}{R_0} \tag{5.10}$$

$$N_L = EI\left.\frac{d^3v}{dx^3}\right|_{x=L} = \frac{m\sqrt{TEI}}{R_0}\coth\left[\frac{\lambda}{2}\right] \tag{5.11}$$

This is the lateral load (5.11) required to enact normal entry (5.3C) and thus steady state lateral deformation. The moment (5.10) is required to enact the constant curvature (5.8) that will allow the elastic axis of the web to travel directly over the roller with no slip, shown in the dashed path in Figure 5.5(b). Yurtcu et al [18] developed similar equations for (5.10) and (5.11) assuming

a polynomial deformation function in (5.9) which accounted for the effects of tension and shear stiffness.

Equation (5.9) has been validated in tests as shown in Figure 5.6. A polyester web 6 inches wide and 0.001 inches in thickness was transported through a web span 20 inches in length. Young's modulus of the web was tested and found to be 712000 psi. Web tension was set at 10 lb. Four tapered rollers with tapers m of 0.00028, 0.00056, 0.00066 and 0.00075 radians with a nominal radius R_0 of 1.45 inches were machined for these tests. Reasonable agreement between the tests and Equation (5.9) is demonstrated. Note the test results are slightly larger than those predicted by Equation (5.9), a behavior similar to that witnessed for the web encountering a downstream misaligned roller in Figure 5.1.

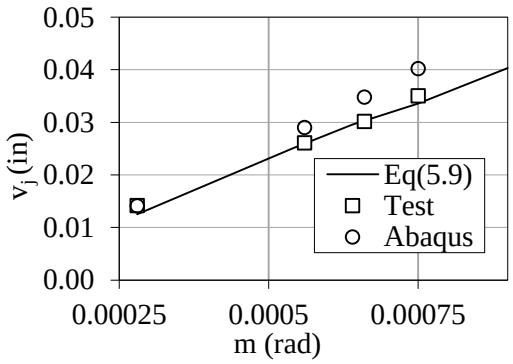

Figure 5.6 – Lateral Deformations of a Web due to a Downstream Tapered Roller

Dynamic simulations of a web transporting through a span with a downstream tapered roller were conducted[6]. The web width, thickness and span length and the material properties were identical to the test conditions. Results for the lateral deformation of the elastic axis at the entry to the tapered roller as the roller has same m in tests are shown in Figure 5.6. Simulation results are shown in Figure 5.7 for the roller taper of m = 0.00066 in/in.

In Figure 5.7(a), rollers R1, R2 and R4 are cylindrical with an outer radius of 1.45 inches. Roller R3 is the tapered roller whose nominal radius at the center is 1.45 inches and whose taper m

in this case is 0.00066 rad. The web tension was set to 10 lb. The web travels from left to right in these simulations. For the simulation to achieve steady state MD stresses and lateral deformations, shown in Figures. 5.7(a) and (b), the web had to move over 80 inches in the MD. Note how the MD stresses remain constant as the web transports over the tapered roller R3. This is an indication that the curvature of the elastic axis of the web on the roller is constant. Also note the deformation contour in Figure 5.7(b) moves directly over the roller which indicates the lateral deformation at a given CMD location is constant. This is seen in greater clarity in Figure 5.8 which shows the lateral deformation, slope and curvature of the elastic axis of the web in steady state conditions harvested from the simulation results shown in Figure 5.7. The web exits roller R2 at MD location 0 and enters R3 at 20 inches. The results shown in Figure 5.8 demonstrate clearly that the lateral deformation of the elastic axis of the web is constant as the web moves over roller R3 and is indicative of stick behavior between the web and roller surface. As the web exits R3 slippage will occur and the lateral deformations will vary in the slip region. Note the elastic axis enters R3 normally and remains normal through the entry stick region. The curvature is linear through the free span before becoming constant on roller R3. As the web enters R3 the simulation results show the web curvature is -0.000453 in^{-1}. This compares well with the curvature boundary condition for stick conditions (5.8): $-m/R_0 = -0.00066/1.45 = -0.000455$ in^{-1}, only 0.44% different. Thus the curvature boundary condition (5.8) is valid. Also the simulation shows the slope to be zero at R3 entry (hence normal entry) and boundary condition (5.3C) appears reasonable. Note the slope at the exit of R2 is small but non-zero (0.0037 rad), which contributed to the simulated deformation at the entry to R3 being greater than the test and Equation (5.9) values in Figure 5.6.

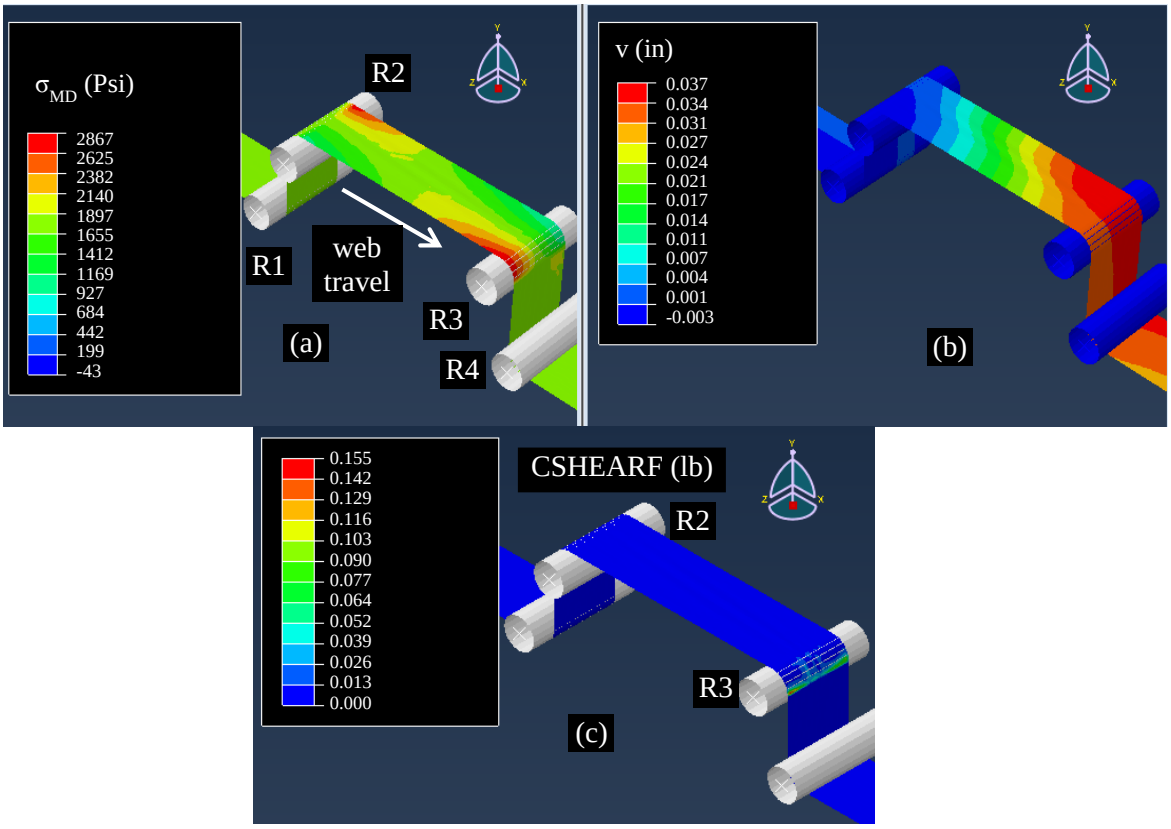

Figure 5.7 – Dynamic Simulation of a Web Approaching a Tapered Roller (m=0.00066 in/in)

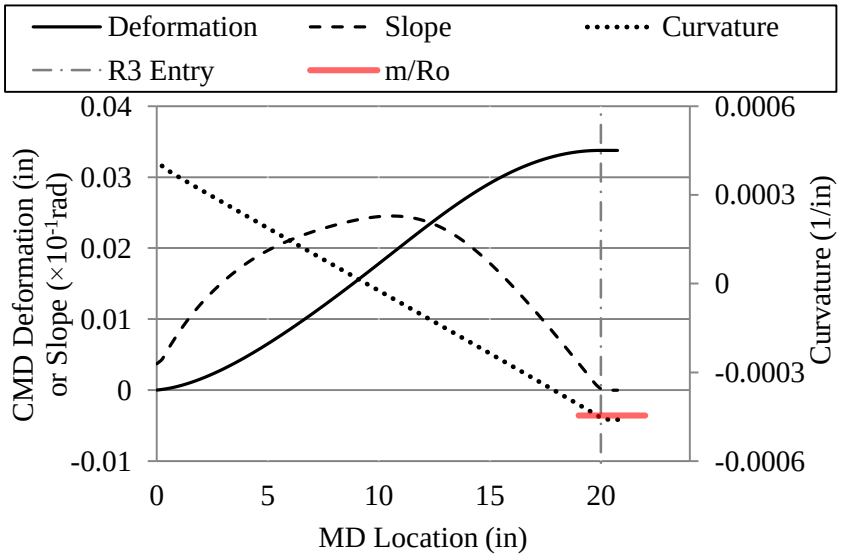

Figure 5.8 – Deformation, Slope and Curvature of the Elastic Axis of the Web after Steady State Conditions were achieved in the Simulation Shown in Figure 5.7

The behaviors of the deformation and the slope of the web on the roller in Figure 5.8 might appear to be incompatible with the curvature shown. The slope of the elastic axis was obtained by using a central finite difference formula on the lateral deformations. Note that the web enters R3 with zero slope (normal entry) and that the slope remains zero as the web transits the roller without slipping. The curvature of the elastic axis could be calculated by taking the derivative of the slope with respect to the MD and in fact this would be accurate for the web in the free span. This would yield an erroneous result of zero for the curvature of the web in contact with the roller. If the web on the roller had zero curvature it would be the unstressed web whose lateral deformation was a function of wrap angle shown in Figure 5.5(b). For the web to track directly over the roller, as required by steady state stick behavior and shown by the dashed line in Figure 5.5(b), the constant curvature of -0.000455 in^{-1} had to exist in the web on the roller. The curvature shown in Figure 5.8 was obtained by first interrogating the section force/moment field output provided by ABAQUS[6] at several points on the elastic axis. These bending moments were then divided by the bending stiffness (EI) of the web to produce the curvature shown in Figure 5.8. The web tension and bending moment in the web on the roller produces MD stresses that vary linearly in the CMD as shown in Figure 5.7(a) from 882 to 2770 psi over the web width. It is this MD stress variation over the web width that has allowed the web to conform to the linear taper of roller radius over the web width. The web has taken the shape of the conical roller surface which allows it to directly pass over the roller with no CMD slippage, as shown in the dashed web path in Figure 5.5(b).

The rate at which boundary conditions (5.3C) and (5.8) converge in time is shown in Figure 5.9. It is apparent the convergence is related to the dynamic time constant of the free span. The span length of 20 in divided by the transport velocity of the simulation (0.5 in/s) produces a time constant of 40 s. Note that convergence of boundary conditions (5.3C) to 0 radians and (5.8) to -0.000453 in^{-1} occurred essentially at 3 time constants (120 s).

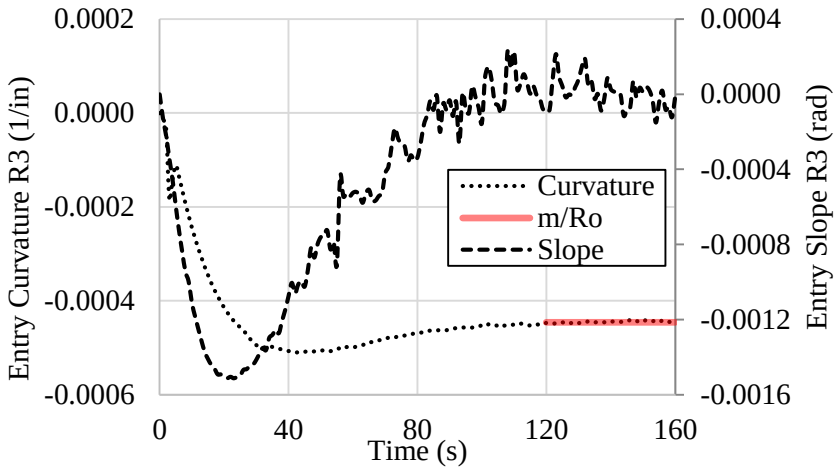

Figure 5.9 – Rate at which Steady State Boundary Conditions are attained in the Simulation shown in Figure 5.7

5.4 A Cambered Web Transiting Aligned Cylindrical Rollers

A cambered web is a web whose length varies in the CMD. If this length variation is linear and a length of the web is swept out on a flat surface the web will take the shape of a curved beam of constant radius (ρ_0) in the unstressed state. In Figure 5.10(a) an unstressed cambered web is shown with long and short sides.

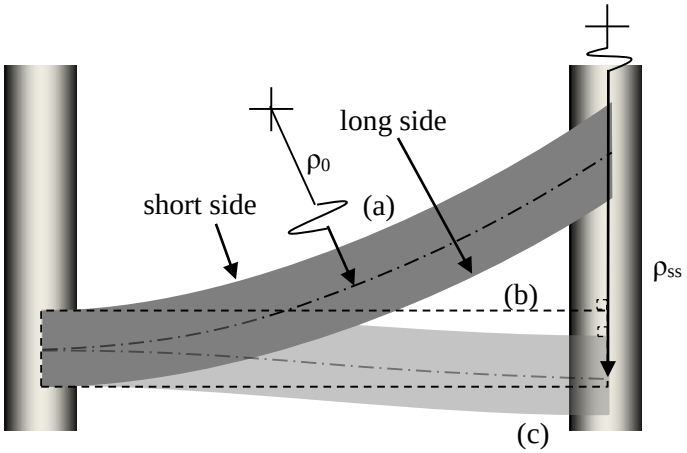

Figure 5.10 – A Cambered Web: (a) in an Undeformed State (b) Deformed to a Straight Path and (c) Deformed to Steady State Path

The camber radius ρ_0 is associated with the undeformed shape of a beam. Curvature is defined as the bending moment at some location in a beam divided by the bending stiffness (EI): $\frac{d^2v}{dx^2} = \frac{M(x)}{EI}$. There is no bending moment applied to the undeformed web and hence there is no curvature. To deform the unstressed web to the straight path would require a constant bending moment (M) of magnitude $-EI/\rho_0$ to be applied to the web (the negative sign is consistent with the convention that a negative moment causes compression on the lower surface of a beam). Hence, the straight web has curvature of magnitude $-M/EI$ or $-1/\rho_0$. It is said the cambered web steers toward the long side. Tests have shown [19][20][21] the cambered web steers laterally beyond the straight web position to a steady state position as shown in Figure 5.10(c).

The differences in these deformed states are critical when reviewing the state of the literature on cambered web steering. The downstream moment boundary condition ($M_L=0$) defined by Shelton [57] in Equation (5.5) is not applicable to the cambered web when steady state lateral deformation has been achieved. It has been assumed that the web span is bounded by two well-aligned cylindrical rollers. For steady state conditions to exist the web must normally enter the downstream roller and thus from boundary condition (5.3C) θ_j must equal zero. There will be a non-zero steady state moment at the downstream roller associated with deformed state of the cambered web as shown in Figure 10(c). That moment or curvature may be unique from the moment/curvature required to allow the web to track in a cylindrical path around the downstream roller without slipping. Several of the cambered web modeling efforts [23][24][60][61] employ Shelton's boundary condition (Equation (5.5)) and are thus incorrect. Shelton [57] proved this boundary condition was applicable to a straight web entering a misaligned roller but not for a cambered web. Swanson [19] stated the curvature was zero under high friction conditions and was equal to M_0/EI under low friction conditions based on empirical observation. Per the discussion herein the total curvature is zero only when the web is in the undeformed case of Figure 5.10(a) and to enforce curvature that would straighten the web (M_0/EI) per Figure 5.10(b) would require

high friction conditions. Swanson did state the downstream curvature was bounded in the range $[0,1/\rho_0]$ which remained valid in his later investigation [21] although the friction levels that produced these curvatures were found to be opposite of the previous investigation. Other investigations concluded that lateral steerage of cambered webs in steady state occurred as a result of higher order effects such as shear, web slackness, and trough instability [25][26][59][60][61]. Brown [27] developed a beam model to represent a cambered web span. He accounted for the shear strain being non-zero in boundary condition (5.3B) and for potential misalignment at the downstream roller. He developed an equation for the moment in the web entering the downstream roller which was found to approach EI/ρ_0 when examined for the cases herein where the surface velocities of the upstream and downstream rollers were equal.

Swanson [21] reported the results of cambered web steering tests. In these tests cambered webs were cut from a wider web using slitting blades mounted on a stage driven in the CMD by a linear motor. Camber can also be produced as a result of creep of webs in wound rolls with web thickness variation in the CMD. The advantage of Swanson's method was that sections of cambered web with radii ρ_0 could be cut for controlled tests as shown in Figure 11(a) with cut sections of straight web in between. These tests employed long web spans where the effects of shear strain on lateral deformations were minimal.

After the camber was cut, the web passed over a position guide into a test span of length L as shown in Figure 5.11(b). The position guide was used to ensure the lateral position of the web entering the test span could be held constant. The null setting for the edge sensors was established as straight web with no camber was passing through the test section. The chord length of the camber (CL) was established as the camber was cut and was set approximately 4 times the span length (L) of the test section. Webs respond to dynamic disturbances much as a first order dynamic system would react to a step input. Webs typically have very little mass which minimize internal inertial loads and allows the approximation of a first order system. After 4 times the test span length L of

either straight web or cambered web passed through the test section the measured lateral deformations (v1-v5) should have been at 98.2% of their steady state values. Thus in these tests the steady state deformations of a cambered web were being compared to the steady state deformations of a straight web. This is similar but not identical to a comparison of the steady state deformation shown in Figure 5.10(c) compared to the straight web in Figure 5.10(b). As either a section of straight or cambered web would enter the test sections each sensor output (v_i) would begin an exponential change to a steady state value of the form $v_i(1-e^{-t/\tau})$ where t is the elapsed time from the beginning of the event and τ is the dynamic time constant for the web span. As the straight web entered the test section, the measured lateral deformations from the 5 sensors (v_{1-5}) would successively approach zero. As the cambered web would enter the test section the 5 sensors would rise and saturate at unique values of lateral deformation. These values were the relative deformations between the steady state deformations of the cambered and straight webs. These tests were conducted for a polyester web 0.002 in thick and 6 in wide. The test span was adjustable but tests began with a span length L of 60 in. Young's modulus was measured at 650,000 psi. The web velocity (V) was set low 5 in/s to avoid air entrainment between the polyester and the bare aluminum roller surfaces. The dynamic time constant was $\tau=L/V=12$ s. The rollers were 2.9 in in diameter. As the testing begun no steering was witnessed for the cambered web. Steering towards the long side was witnessed when the bare aluminum rollers were covered with high friction tape (Tesa[7] 4863 or 3M[8] 5461). Thus it appeared that high friction force capability between the web and rollers is a requirement to induce measurable steering. The Tesa tape in contact with a polyester web produces a static friction coefficient of 2 and the 3M tape in contact with polyester can produce friction coefficients of 4 or greater per ASTM D1894. It should be noted that Shelton [20] covered his test rollers with 3M[8] Scotch-Tred® in earlier tests on polystyrene cambered web belts which produced high friction and steerage.

[7] Tesa Tape Inc., 5825 Carnegie Boulevard, Charlotte, N.C. 28209, USA
[8] 3M Company, 2501 Hudson Rd, Maplewood, MN 55144, USA

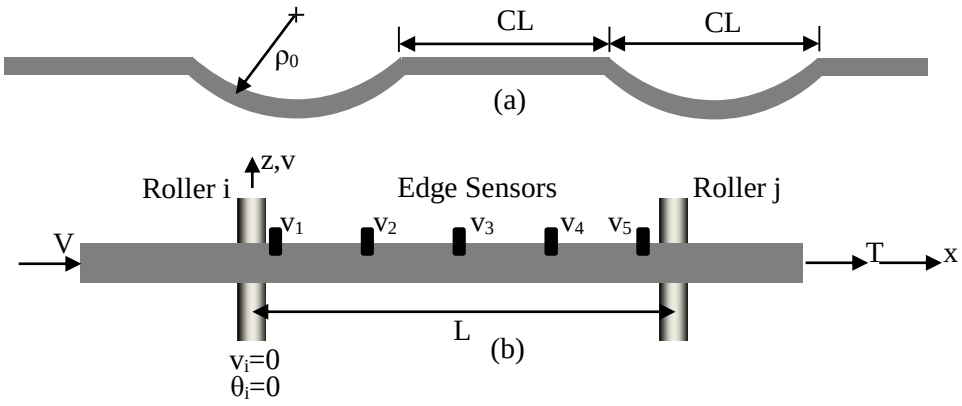

Figure 5.11 – Swanson Camber Tests: (a) Camber Slit into Web (b) Test Section where Steering was Measured

The cambered web approaching an aligned cylindrical roller has both similarity and uniqueness from the problem of a straight web entering a downstream tapered roller. The similarity is that in both cases the web is being steered due to a non-zero curvature in the web as it enters the downstream roller. The uniqueness is the source of the curvature. The straight web approaching a tapered roller had a curvature induced by the downstream roller due entirely to the geometry of the tapered roller (m/R_0) that resulted in the steering per Equation (5.9). The camber in the cambered web is the source of a variable web curvature at the downstream roller. This curvature varies with the deformation of the web.

Equation (5.2) can be used to model the lateral deformation between the steady state (Figure 5.10(c)) and straight (Figure 5.10(b)) deformed shapes. It will be assumed that the elastic axis of the web enters the upstream roller at a constant lateral deformation that can arbitrarily be set at zero ($v_i=0$, (5.3A)) as a result of the upstream position guide. Furthermore it is assumed that the elastic axis of the web enters the upstream roller normally and due to the high friction condition does not slip appreciably at the exit to the roller ($\theta_i=0$ (5.3B)). In steady-state normal entry is expected at the downstream roller ($\theta_j=0$ (5.3C)). The final boundary condition is the change in

curvature between the straight and steady-state deformed shapes of the web shown in Figs. 5.10(b) and (c), respectively:

$$\left.\frac{d^2v}{dx^2}\right|_{x=L} = \frac{1}{\rho_0} - \left.\frac{1}{\rho_{ss}}\right|_{x=L} = \left.\frac{1}{\rho_\Delta}\right|_{x=L} \tag{5.12}$$

Using boundary conditions (5.3A) and (5.3B), (5.3C) with θ=0 and (5.12) the 4 unknowns (A-D) in Equation (5.2) can now be determined:

$$v(x) = \frac{EI}{\rho_\Delta T}\left[\cosh[\frac{\lambda x}{L}] - 1 + \coth[\frac{\lambda}{2}](\frac{\lambda x}{L} - \sinh[\frac{\lambda x}{L}])\right] \tag{5.13}$$

From Equation (5.13), the slope of the web throughout the free span can be determined:

$$\theta(x) = \frac{dv}{dx} = \frac{L}{\rho_\Delta \lambda}\left[\sinh[\frac{\lambda x}{L}] - \coth[\frac{\lambda}{2}](\cosh[\frac{\lambda x}{L}] - 1)\right] \tag{5.14}$$

The curvature can be determined throughout the span as well:

$$v'' = \frac{d^2v}{dx^2} = \frac{1}{\rho_\Delta}\frac{\sinh[\frac{\lambda}{2}\frac{L-2x}{L}]}{\sinh[\frac{\lambda}{2}]} \tag{5.15}$$

Equations (5.13-5.15) represent relative changes in lateral deformation, slope and curvature between the straight and steady state deformed shapes of Figures. 5.10(b and c). If the deformed radius of curvature ρ_Δ was known, the lateral deformation (5.13), the slope (5.14) and the curvature (5.15) throughout the web span would be known. The total curvature resulting from deforming the web from the undeformed shape Figure 5.10(a) to the steady state Figure 5.10(c) can be inferred from Equations (5.12) and (5.15):

$$v''(x)_{total} = \frac{1}{\rho_0} + \frac{1}{\rho_\Delta}\frac{\sinh[\frac{\lambda}{2}\frac{L-2x}{L}]}{\sinh[\frac{\lambda}{2}]} \tag{5.16}$$

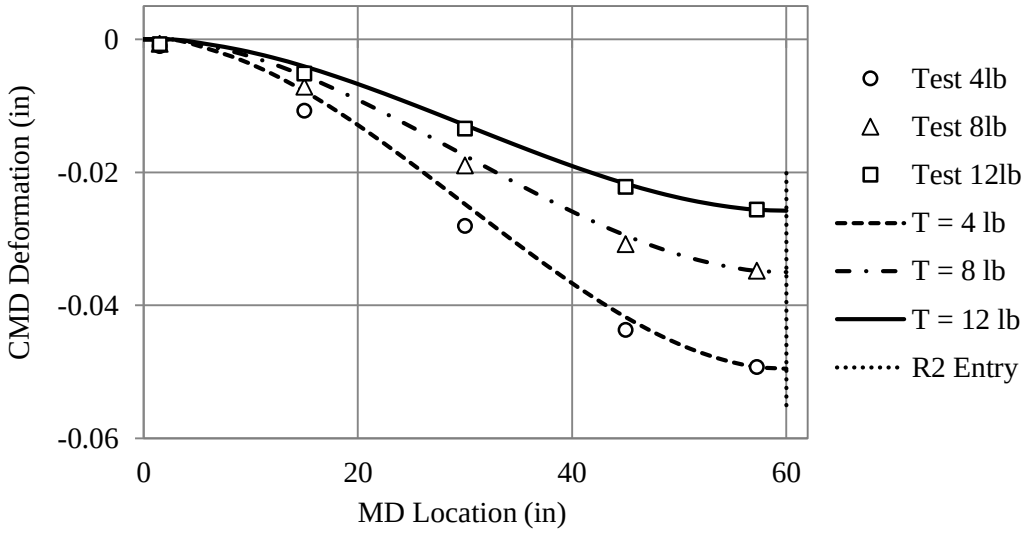

Figure 5.12 – Swanson Tests (ρ_0 = 5,906 inches) with Tesa High Friction Tape on Rollers [21]

Table 5.1 – Radii of Curvatures and Lateral Deformations at the Downstream Roller inferred from Swanson's Test Deformations [21]

T (lb)	4	8	12
v_j (in)	-0.0491	-0.0349	-0.0260
ρ_Δ (in)	-11,974	-16,847	-22,627
ρ_{ss} (in)	-11,654	-9,094	-7,992

The deformed radius of curvature ρ_Δ can be deduced from the data of Swanson [21] for the cases tested in which rollers were covered with Tesa 4863 high friction tape. The deformed radius of curvature ρ_Δ was varied in Equation (5.13) until Swanson's measured deformations at edge sensor v_5 in Figure 5.11(b) were achieved. The steady state radius of curvature at the entry of the downstream roller ρ_{ss} could be determined using Equation (5.12). Also Equation (5.13) could be used to extrapolate the test deformations to the downstream roller (v_j). These results are presented in Table 5.1. The average lateral deformations from Swanson's tests and that produced by Equation (5.13) are shown in Figure 5.12. Note that in general the test data and the deformations given by Equation (5.13) agree well and improve at higher web tension. Equation (5.13) incorporates boundary conditions (5.3A, 3B, 3C (θ_j=0)) and (5.12) and produces lateral deformations

comparable to the test data from the 5 sensors in the test span. This provides confirmation such that the boundary conditions are reasonable.

It has been shown that the lateral deformations of a cambered web depend on knowledge of a boundary condition which is the deformed radius of curvature of the web (ρ_Δ) at the downstream roller (5.13). This deformed radius of curvature is unknown. For stick conditions to exist between the web and roller at the entry to R2 the radius of curvature of the web must transition to a value equal in magnitude but opposite in sign to the radius of curvature that was initially cut into the web (ρ_0). The curvature in the web will remain constant at that value ($-1/\rho_0$) throughout the arc of contact of the web that is in stick conditions with the roller. This will allow points in the web to pass directly over the downstream roller with no lateral deformation.

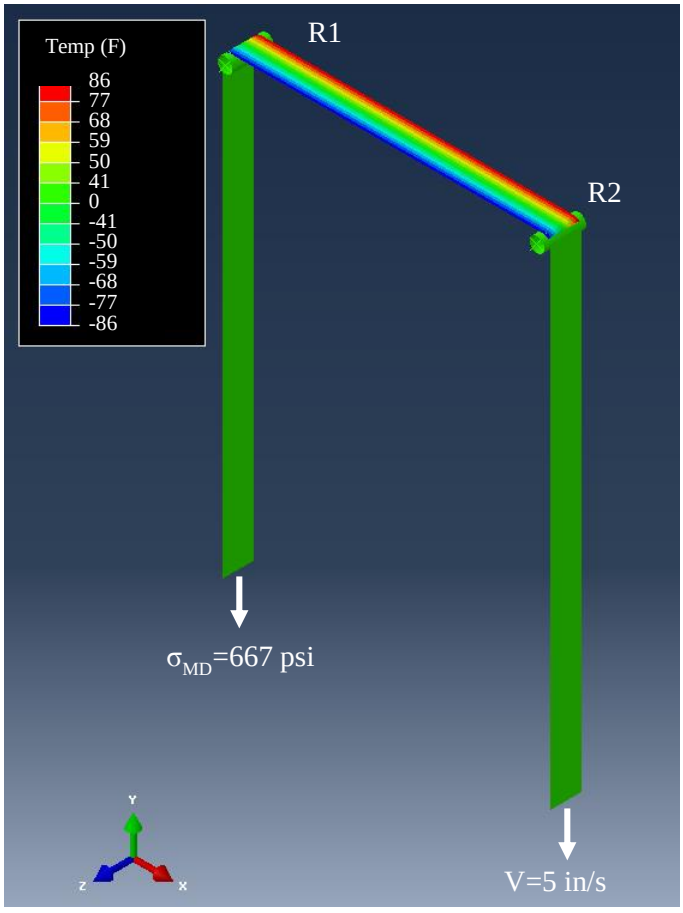

Figure 5.13 – Dynamic Simulation of Cambered Web Steering

Dynamic simulations were first conducted by Fu [28] of the Swanson camber test cases. Fu simulated a web position guide (that existed in the tests) to steer the cambered web shown in Figure 5.11(a) to a fixed lateral position prior to entering the test section. The web was then allowed to steer laterally in the test section where the lateral deformations resulting from web camber could be studied. Fu's explicit simulation of a web position guide was unique in the literature. While the simulations yielded results comparable to the test data further accuracy was sought to better define the boundary conditions. Improved simulations were conducted using the standard dynamic implicit solver in ABAQUS[6]. The simulation begins with the web achieving the constant MD stress level and velocity shown in Figure 5.13. The web thermal MD expansion coefficient (α) was set at 7.275×10^{-6} in/in/F. The CMD expansion coefficient was set at zero. A linear temperature variation across the web width was introduced to induce a web camber. The change in temperature required to induce the desired camber of 5,906 inches was $\Delta T = W/(\alpha\times\rho_0) = 6/(7.275\times10^{-6}\times5{,}906) = 139.64$ F. The temperature variation began half way through the wrap of the web about roller R1, continued through the test section and then was removed half way through the wrap of the web about roller R2. The "long" edge of the cambered web had the highest temperature of 85.82 F. This temperature variation across the web width varied from zero to the variation shown in Figure 5.13 in the first second of the simulation after the web velocity and tension had been achieved. The thermally induced camber in the test section eliminated the need to simulate the web guide and provided the accuracy in results desired.

Steady state results from the end of the simulation are shown in Figure 5.14 for the case where the web tension was 8 lb. The MD stresses shown in Figure 5.14(a) show a decreasing bending moment in the web from roller R1 to R2. The lateral deformations in Figure 5.14(b) show the web leaving roller R1 with zero lateral deformation and increasing until entry of R2, note that steering towards the longer edge occurred as demonstrated in tests. The web is shown to be in

nearly full stick behavior on R1 and R2 with small regions of slip at the exit of R1 and the entry of R2 in Figure 5.14(c).

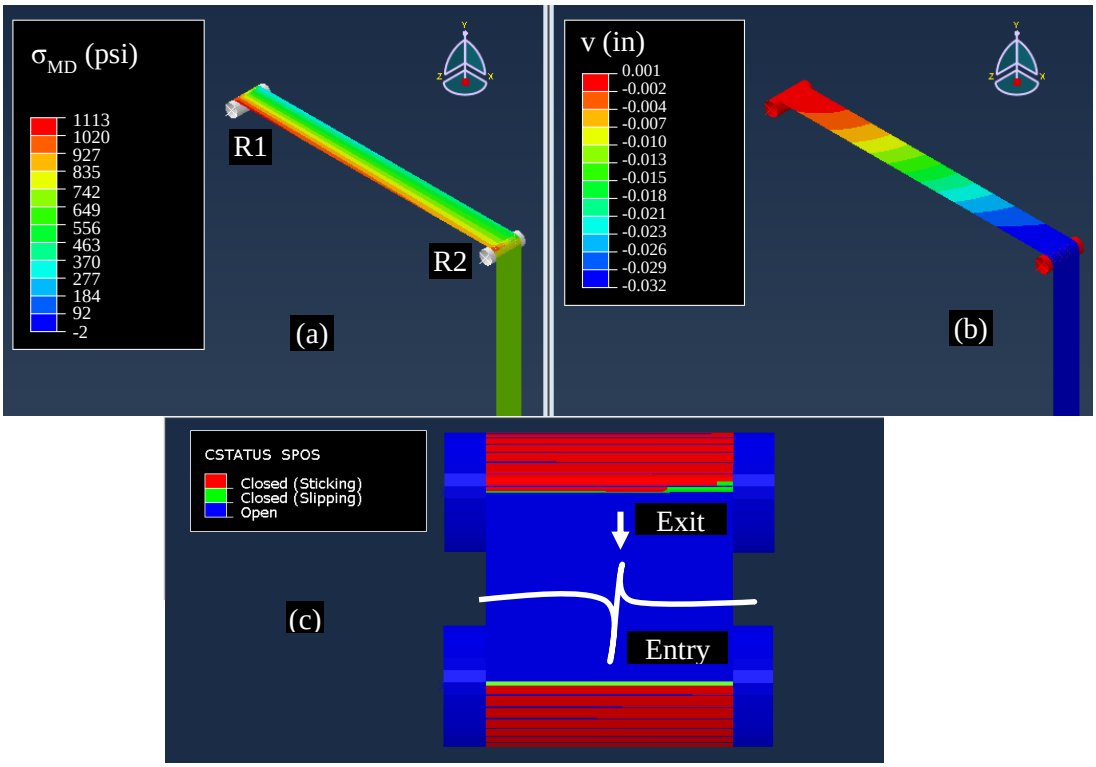

Figure 5.14 – Simulation Results at Steady State (T=8 lb)

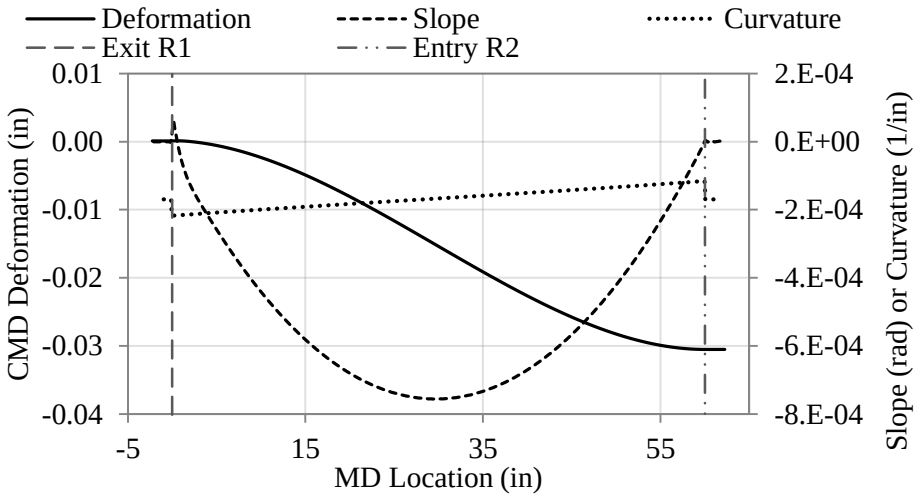

Figure 5.15 – Deformation, Slope and Curvature of Elastic Axis at Steady State (T=8 lb)

In Figure 5.15 the deformation, slope and curvature of the elastic axis of the web at steady state are shown for the simulation results of Figure 5.14. The simulation shows the lateral deformation at the exit of roller R1 is zero and thus boundary condition (5.3A) is satisfied. At the entry to roller R2 the simulation shows the lateral deformation of the web is -0.0308 inches whereas the average test results extrapolated to the entry of R2 was -0.035 inches (12% error). While the error is considerable, the shape of the lateral deformation is consistent with the test data captured by the 5 sensors in the test span shown in Figure 5.12. The simulation shows the slope of the elastic axis is slightly non-zero (5.76×10^{-5} rad) as the web exits roller R1. Thus boundary condition (5.3B (θ_i=0)) may be reasonable but not exact in this case. The elastic axis appears to enter roller R2 normally and thus boundary condition (5.3C) is satisfied as would be required for steady state behavior to be obtained. Perhaps most interesting is the curvature in Figure 5.15 where step changes in curvature occur at the exit of roller R1 and the entry to roller R2. These abrupt changes in curvature are due to MD contact shear forces between the web and roller at the exit of R1 and the entry of R2. On the rollers R1 and R2 the curvature is what would be required to deform the unstressed cambered web to a deformed straight web that can pass directly over the cylindrical rollers without slip (-1/5,906 inches = -1.69×10^{-4} in^{-1}). At the entry to R2 the curvature is -1.17×10^{-4} in^{-1}, thus the steady state radius of curvature -8,547 inches, which is within 6.0% of the steady state radius of curvature inferred from test data in Table 5.1. The deformed curvature needed for Equation (5.13) would be:

$$\left.\frac{1}{\rho_\Delta}\right|_{x=L} = \left.\frac{1}{\rho_0} - \frac{1}{\rho_{ss}}\right|_{x=L} = \left.\frac{-1}{5{,}906} - \frac{-1}{8{,}547}\right|_{x=L} = -5.23\times10^{-5}\ \text{in}^{-1},\ \rho_\Delta\big|_{x=L} = -19{,}113\ \text{in} \qquad (5.17)$$

If this curvature is input to Equation (5.13) in conjunction with boundary conditions (5.3A-3C) the lateral deformation of the web at the entry to R2 can be predicted as -0.03077 inches which compares nicely with the -0.03083 inches result from the simulation. Thus the results of the

simulation with those of Equation (5.13) agree nicely with the caveat that the simulation was required to produce the curvature boundary condition as the web entered roller R2 (5.16).

The simulations also provide explanation with regard to why the lateral steering occurs. In the derivation of the curvature boundary condition (5.12) for the cambered web, the intermediate straight web shape in Figure 5.10(b) was used. Note the straight web enters the downstream roller normally and if the straight deformed state physically occurred there would be no lateral deformation toward the long edge due to camber. The slope and lateral deformation at several instants in time from the simulation are shown in Figure 5.16. The elastic axis of the web is straight at zero seconds, but the web velocity and MD stress shown in Figure 5.13 had already been achieved at this time. The temperature variation was increased linearly from zero to the variation shown in Figure 5.13 one second later. From that time forward the web never deformed into the straight web shown in Figure 5.10(b). Thus the straight deformed web shown in Figure 5.10(b) is never a physical reality in the simulation after the camber is induced. Note the slope and the lateral deformation are exponentially reaching their steady state values through time $(1-e^{-t/(L/V)})$.

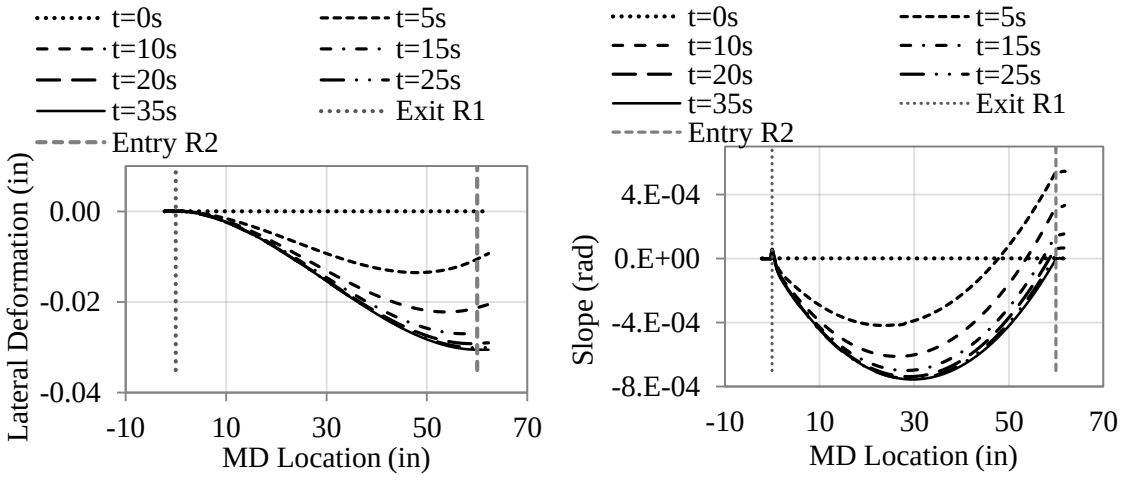

Figure 5.16 – Deformation and Slope of Elastic Axis through Time (T=8 lb)

A comparison of the lateral deformations from Swanson's tests [21], the ABAQUS simulations and Equation (5.13) are shown in Figure 5.17. The deformations from Equation (5.13) required the deformed radii of curvatures (ρ_Δ) that were determined from the ABAQUS simulations and are shown in Table 5.2. The relative errors were harvested by comparing the test data in Table 5.1. The simulations invoke no assumptions of boundary conditions whereas Equation (5.13) employs boundary conditions (5.3A), (5.3B), (5.3C) θ_j=0, and ρ_Δ (5.12) from ABAQUS in Table 5.2. Note that ABAQUS and Equation (5.13) produce very similar results throughout the web span with the agreement improving at higher web tensions.

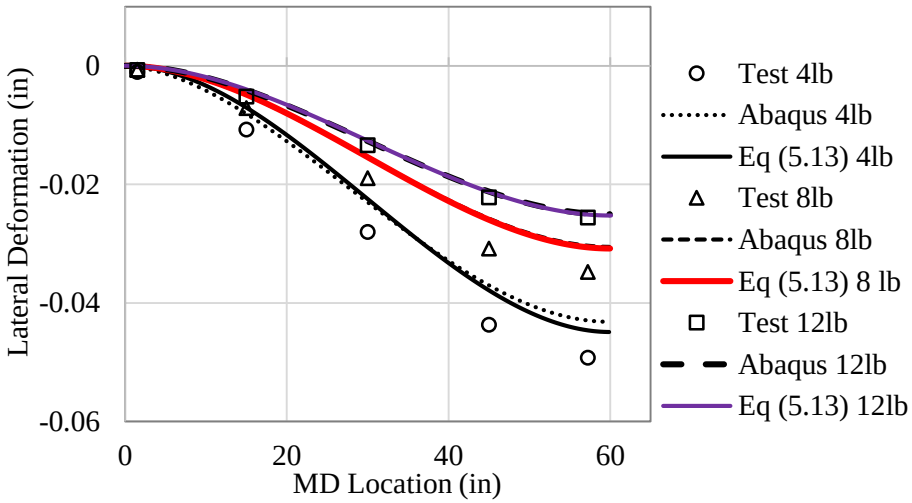

Figure 5.17 – Lateral Deformations from ABAQUS Simulations, Equation (5.13) and Test Data

Table 5.2 – Radii of Curvatures and Lateral Deformations at the Downstream Roller inferred from ABAQUS Simulation Results and Equation (5.13)

T (lb)	4	8	12
v_j (in)	-0.0445 (9.4%)	-0.0308 (11.7%)	-0.0256 (1.5%)
ρ_Δ (in)	-13,229 (10.5%)	-19,113(13.5%)	-22,954 (1.4%)
ρ_{ss} (in)	-10,669 (8.5%)	-8,547 (6.0%)	-7,952 (0.5%)

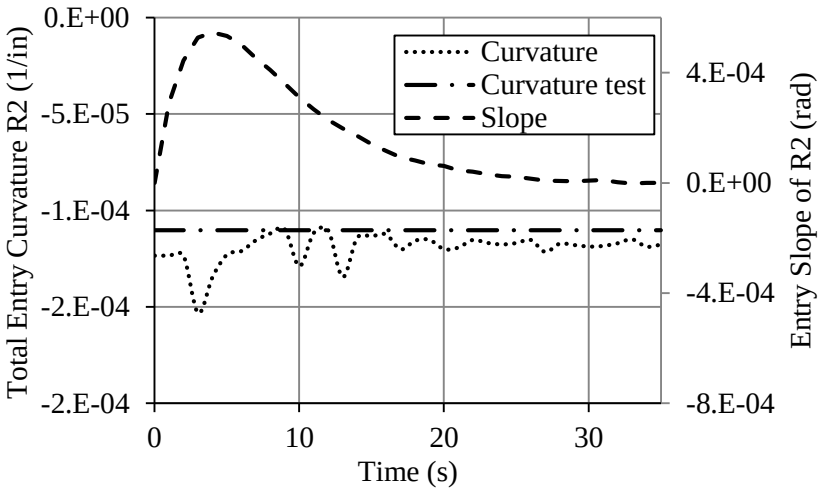

Figure 5.18 – Rate at which Steady State Boundary Conditions are attained in the Simulation shown in Figure 5.13

The total curvature and slope of the web entering the downstream roller R2 are shown in Figure 5.18. Note the web has obtained normal entry with roller R2 within 36 s which is 3 time constants of the free span. The curvature is reaching a steady state value much earlier. It is surmised that the curvature boundary condition of the web at entry to R2 involves the time constant of the web transiting the roller which is 0.46 s.

5.5 Conclusions

It has been demonstrated that Equation (5.2) can be used to model the steady state lateral deformations of a web in a free span for the cases where the downstream roller is misaligned (5.4) or tapered (5.9). The boundary conditions for the span entering the misaligned roller included (5.3A), (5.3B), (5.3C) and a zero curvature boundary condition (5.3D) at the downstream roller required for steady state conditions (i.e. no CMD velocity). The free span bounded by aligned rollers where the downstream roller was tapered linearly in radius with respect to the CMD had similar boundary conditions (5.3A), (5.3B) and (5.3C (θ_j=0)). A constant curvature boundary condition (5.8) was defined to constrain the web to track directly over the downstream roller with

no slippage or CMD velocity to attain steady state lateral behavior. In these two cases the rollers that bounded the web span and the assumption of no slip dictated the boundary conditions that produced the steady state lateral deformation of the web. The case of a cambered web has similarity to these cases in the first three boundary conditions (5.3A), (5.3B) and (5.3C (θ_j=0)). The cambered web also has a curvature boundary at the entry to the downstream roller (5.12) but differs from the other cases in that this curvature is dependent on the deformed state of the cambered web. Web tension, web material properties, initial camber and friction forces at the web entry to the downstream roller all will affect the deformed curvature which allows the web to reach steady state conditions. MD slippage is required at the web entry to the downstream roller such that the curvature can instantaneously change from the level which brought the lateral deformation to steady state ($1/\rho_{ss}$) to a level that allows the deformed cambered web to track directly over the roller with no lateral velocity ($1/\rho_0$). To determine the deformed radius of curvature at the downstream roller (ρ_Δ) requires a method that can establish the equilibrium of the internal forces in the deformed web and the external forces due to slip as the web enters the downstream roll and the stick behavior of the web on the roller. Only laboratory tests [21] and dynamic simulations (ABAQUS) have shown that capability.

CHAPTER VI

DEVELOPMENT OF A WEB TROUGH FAILURE CRITERION FOR A SINGLE LAYER WEB

A web trough is defined as the buckling of a free web span between rollers. The buckling produces out-of-plane displacement in the web, and it is a common instability phenomenon in roll-to-roll manufacturing processes. Most webs have a small thickness compared to their length or width span dimensions. Small cross machine direction (CMD) compressing stresses can generate web troughs. As troughs approach a downstream roller, they can produce CMD compressive stresses sufficient to wrinkle the web on the roller. The existence of web wrinkles is catastrophic for all web processes. Unlike wrinkles, web troughs may be acceptable in a web process. Normally troughs appear prior to wrinkles, so it is vital and useful to study web troughs.

In a web manufacturing process machine, the troughs can form due to a misaligned roller [7], or a tapered roller [35]. Web imperfections such as a local non-uniformity [45] or holes [46][62] can potentially induce troughs. Due to web tension a half wave cycle of out-of-plane buckling deformation will form in the machine direction (MD). The tension magnitude, the length, width and thickness of the web span, and the web material properties will determine the number of waves in the CMD.

A closed form expression for a trough failure criterion was developed by Shelton [63] and Good [6] . The trough criterion was used to produce expressions for the critical misalignment of the roller [7] and the critical radial taper of the roller [35] that will induce troughs into a web

span. These expressions for the misaligned roller and tapered roller have been validated by tests [48]. Shelton simplified Timoshenko's buckling expression for a simply supported rectangular plate with tension in the MD and compression in the CMD. The edges of a web spanning two successive rollers in a process machine are not supported. These edges are free and no CMD surface tractions act on these edges. Webs that have trough buckles have diminished out-of-plane deformations at their edges and thus the simple support boundary condition may be reasonable on these free edges. Shelton collected the data in the Figure 6.1 for trough wave length [63]. While it might be argued Shelton has offered some proof, it could also be argued it was not conclusive. In addition, no conclusive test results were obtained to validate the trough failure criterion that was integral to the expressions for the critical misalignment of the roller or the critical radial taper of the roller for troughs.

In this chapter, the trough failure criterion for single layer webs will be validated by employing ABAQUS/Standard simulations. Various boundary conditions for trough formation will be simulated. Both isotropic and orthotropic webs will be explored and discussed. Methods for developing expressions and simulation analysis for this single layer web will move to a more complicated case in next chapter, i.e., trough formation in a multilayer laminate.

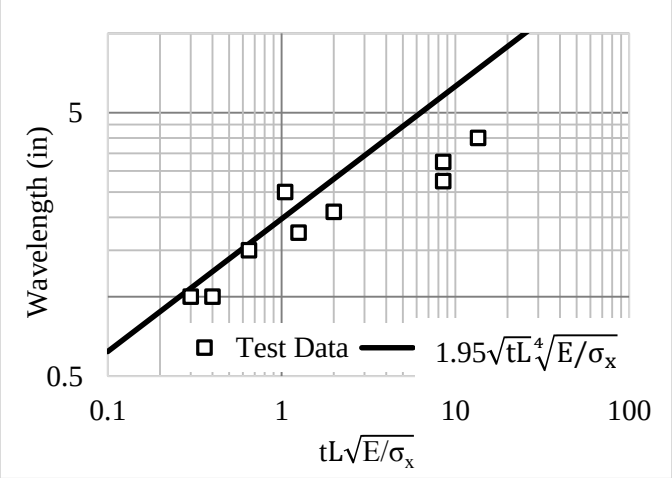

Figure 6.1 – Experimental Data for Wavelength Compared to Equation [63]

6.1 Trough Failure Criterion for a Single Layer Orthotropic Web Span

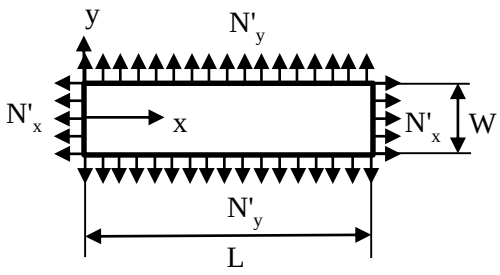

Figure 6.2 – A Web Span Under Uniform Edge Loads in MD and CMD Directions

A simple description for the development of web trough failure criterion will be presented here. For a web span between two rollers, the classical beam theory was widely applied to explore the lateral deformations [14][17][21][22]. In Chapter IV, it was demonstrated that the web has plate properties with web thickness and width considerations. For a web span under uniform MD tension N'_x at two opposite edges, the critical CMD load N'_y could be determined which introduces web troughs. Both N'_x and N'_y are the membrane forces in units of load per unit length. In order to simplify the problem, the x direction is the machine direction (MD) and the y direction is the cross machine direction (CMD). The web span in Figure 6.2 has width W and span length L. The governing equation in terms of the out-of-plane deformation of the web w is shown as [6]:

$$D_1 \frac{\partial^4 w}{\partial x^4} + 2D_3 \frac{\partial^4 w}{\partial x^2 \partial y^2} + D_2 \frac{\partial^4 w}{\partial y^4} - N'_x \frac{\partial^2 w}{\partial x^2} - N'_y \frac{\partial^2 w}{\partial y^2} = 0 \qquad (6.1)$$

The origin of the out-of-plane deformation w is on the middle plane of the web. If the web is orthotropic and the three principal axes are aligned with the MD, CMD and the out-of-plane direction, D_1, D_2, and D_3 are defined by the following equations:

$$D_1 = \frac{E_x t^3}{12(1-\nu_{xy}\nu_{yx})},\ D_2 = \frac{E_y t^3}{12(1-\nu_{xy}\nu_{yx})},\ D_3 = D_1\nu_{xy} + \frac{G_{xy} t^3}{6} \qquad (6.2)$$

The subscripts x and y denote the material directions are in x and y directions, respectively. All edges were assumed to be simply supported which means the edges do not allow out-of-plane deformation. A trial buckled deformation solution of the following form was assumed:

$$w(x,y) = A_{mn}\sin\left(\frac{m\pi x}{L}\right)\sin\left(\frac{n\pi y}{W}\right) \tag{6.3}$$

where m and n are the numbers of half wave buckles in the x and y directions, respectively. Since N'_x is a tensile load, m must be 1. A_{mn} is the amplitude of the buckled wave and dependent on the values of m and n and the traction that produced the buckle. The web was assumed to have continuous sine waves across the web width.

If expression (6.3) for w is substituted into the differential equation (6.1) with known half wave number m = 1, the critical CMD stress can be determined as expression (6.4). The edge load (N'_x or N'_y) is the average stress (σ_x or σ_y) times web thickness (t).

$$\sigma_{y,trough} = -\frac{2D_3\pi^2}{tL^2} - \frac{D_2\pi^2 n^2}{tW^2} - \frac{(tL^2\sigma_x + D_1\pi^2)W^2}{tL^4 n^2} \tag{6.4}$$

By seeking a minimum energy solution, the result may be solved for the half wave number n. Note the simply supported boundary condition at the web edges requires that the half wave number n be a positive integer.

$$n_{trough} = INT\left[W\sqrt{\frac{2}{\pi Lt}}\sqrt[4]{\frac{3(1-\nu_{xy}\nu_{yx})\sigma_x}{E_y}}\right] \tag{6.5}$$

The exact solution of the critical stress is obtained by input of the integer value of n_{trough} in (6.5) to equation (6.4), it will not vary continuously. The approximation of the critical CMD stress to induce troughs $\sigma_{y,trough}$ is simplified by neglecting the small terms:

$$\sigma_{y,trough} \approx -\frac{\pi t}{L}\sqrt{\frac{\sigma_x E_y}{3(1-\nu_{xy}\nu_{yx})}} \tag{6.6}$$

The corresponding wavelength λ is the web width divided by the continuous wave number n:

$$\lambda = \frac{2W}{n_{trough}} \tag{6.7}$$

For most webs the lateral stress and corresponding strain to cause web troughs is small and this allowed Cerda to make a claim that the web was inextensible in the CMD [64][65]. The web contracts in the CMD due to web tension and the Poisson effect, but this contraction produces little or no CMD membrane stress. Cerda's claim was that all of the Poisson contraction must result in producing out-of-plane deformations and this allowed him to estimate the amplitude of these deformations. An estimation of the amplitude of the troughs A_{mn} is developed with the support of expression (6.5) for half wave number n_{trough} using Cerda's claim:

$$A_{mn} = \sqrt{\frac{2\nu_{xy}Lt}{\pi}}\sqrt[4]{\frac{\sigma_x E_y}{3E_x^2\left[1-\nu_{xy}\nu_{yx}\right]}} \tag{6.8}$$

Expressions for the half wave number (6.5), the critical CMD load (6.4) and (6.6), wavelength (6.7), and amplitude of troughs (6.8) can be applied for the single layer web with homogeneous orthotropic material properties. It is easy to simplify these expressions for the isotropic webs. The expressions (6.4) to (6.7) were developed based on the assumptions that the web span has simple support at four edges, and uniform membrane loads were applied in MD and CMD at web edges. Cerda claimed that no lateral or CMD stress should be considered for the development of expression for the amplitude of troughs (6.8), only MD tension and Poisson's ratio dictated the contraction. The interaction between the web and the roller was not considered herein so the web was assumed to sticking on the roller without any slippage. Finite element simulations

were employed to validate the accuracy of these expressions. The model in Figure 6.2 will be simulated, and more complex examples will be explored.

6.2 Troughs in a Single Layer Isotropic Web Span with Simply Supported Edges

ABAQUS/Standard analyzer was shown to provide precise results for the three-dimensional web and roller simulations in Chapter III. This implicit method will be employed in the simulations to verify the expressions of the critical CMD stress (6.4) and (6.6), wavelength (6.7) and amplitude (6.8) for web troughs.

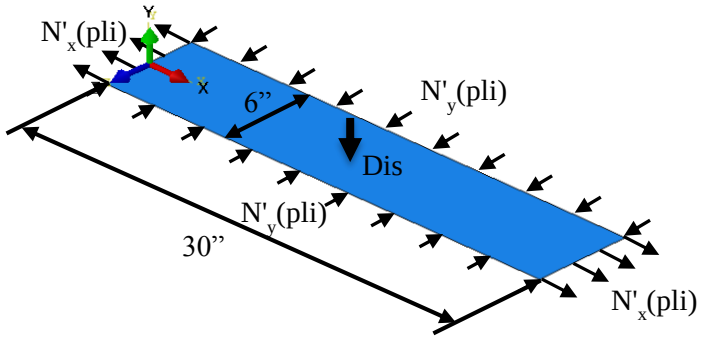

Figure 6.3 – FE Model of a Single Layer Isotropic Web Span with Simply Supported Edges

The simulation model in Figure 6.3 has the same boundary conditions as shown in Figure 6.2. The isotropic web is 30 inches long and 6 inches wide with 0.0026 inches for the thickness. The Poisson's ratio is 0.3 and Young's modulus was measured as 329,000 psi. The simple support boundary conditions were simulated as all edges could only deform in x and y directions without out-of-plane deformation. A uniform MD tension N'_x was applied on web two opposite ends (x = 0, x = 30”). The other two edges (z = ±3”) had applied the compressive load N'_y, which would keep increasing until troughs were observed.

The model in Figure 6.3 has “perfect” geometry and material properties. An imperfection must be introduced in the simulation to solve the buckling problem. A small disturbance force (Dis)

was applied at the center of the web for a short time (0.2s) to help the web generate buckles. Although the web has transient stress variation due to this external disturbance force, its effect on the web vanished with time and the web achieves steady state deformations quite soon. Several disturbance forces were tested in the simulations, and 0.001 lb was chosen to perturb the web to generate troughs while having little effect on the steady state web stress distribution.

For this single layer web, the edge loads should induce uniform web stress across web span before buckling. The MD tension N'_x was set uniformly 1.3 pli which resulted in a MD membrane stress $\sigma_{MD} = 1.3/0.0026 = 500$ psi. This uniform MD stress produces a trough wavelength 3 inches from equation (6.7). It was determined that 8 nodes per wave would be used to establish the buckled shape. Thus, the maximum size for the element length was 3/8 = 0.375 inches. A mesh density 0.125"×0.125" was tested to be the one with high accuracy and low computational cost for this model. This model has 11,809 nodes and 11,520 elements. The web was meshed by using the reduced four nodes, shell elements S4R.

In the simulations, the web edges have uniform stress distribution as the edge loads N'_x and N'_y were applied uniformly. In addition, the entire web was expected to reach the desired stress levels in equilibrium with the edge loads. The web in Figure 6.4 has no troughs with edge loads N'_x of 1.3 pli and N'_y is -0.0060 pli. The MD membrane stress in Figure 6.4(a) 500.53 psi closes to the desired value 500 psi ($N'_x = 1.3$ pli), as the relative error is only 0.11 %. The applied CMD edge load N'_y -0.0060 pli should result in a CMD membrane stress -2.31 psi. The simulation CMD stress across the whole web is -2.30 psi in Figure 6.4(b), 0.43 % in error compared with the desired value. The simulation MD and CMD membrane stresses are distributed uniformly across the whole web as expected. This provided proof the transient external disturbance force at web center does not affect the steady state stress or deformations of the web.

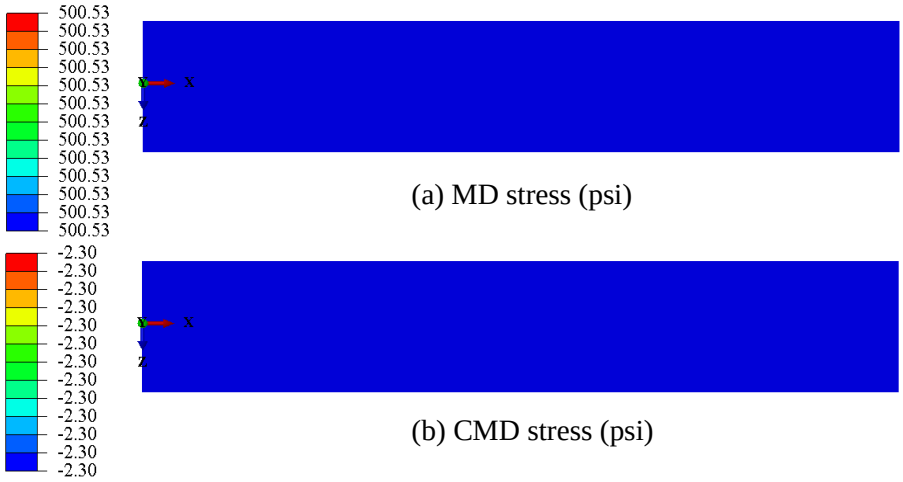

Figure 6.4 – MD and CMD Membrane Stresses (psi) Before Buckling for N'_x = 1.3 pli, N'_y = -0.0060 pli (σ_x = 500 psi, σ_y = -2.31 psi)

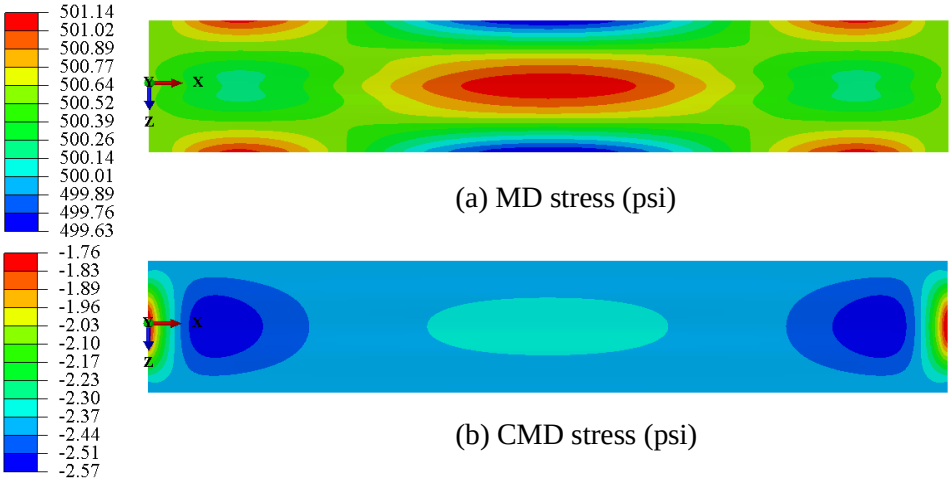

Figure 6.5 – MD and CMD Stresses (psi) After Buckling for N'_x = 1.3 pli, N'_y = -0.0062 pli (σ_x = 500 psi, σ_y = -2.38 psi)

Troughs did not appear until the CMD load increased negatively to -0.0062 pli in the simulations. Figure 6.5 shows the (a) MD and (b) CMD membrane stresses. The MD edge load was maintained as 1.3 pli. The MD and CMD membrane stresses were expected to be 500 psi and -2.38 psi, respectively. The MD stress from the simulation was close to the desired value 500 psi

with a small variation as a result of the buckling. The troughs also affected the CMD stress. The CMD stress across the whole web was no longer equal to the desired value perfectly, and the most negative stresses appear near the web ends (x = 0, x = 30") as shown in Figure 6.5(b). However, the total CMD load which was harvested by the integration of the CMD stress along web center line (z = 0) is -0.187 lb, that the average CMD stress is -0.187/(30×0.0026) = -2.397 pli, and the relative error is abs[(-2.38 - 2.397) / -2.38]×100% = 2.0%. The web has the desired MD and CMD stresses across the whole web at the macro level after web has troughs.

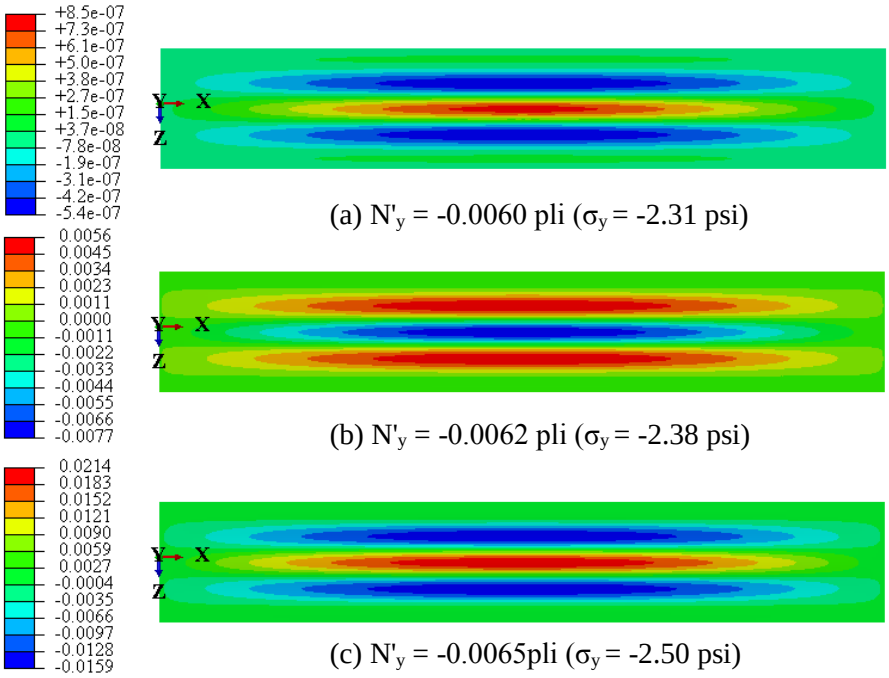

(a) N'_y = -0.0060 pli (σ_y = -2.31 psi)

(b) N'_y = -0.0062 pli (σ_y = -2.38 psi)

(c) N'_y = -0.0065pli (σ_y = -2.50 psi)

Figure 6.6 – Out-of-plane Deformations for N'_x = 1.3pli (σ_x = 500 psi)

Figure 6.6 shows the web out-of-plane deformations of the web before buckling (N'_y = -0.0060 pli) and after buckling (N'_y = -0.0062 pli, N'_y = -0.0065 pli). The MD edge load was 1.3 pli for these three cases. The web has a buckled shape when the CMD load is -0.006 pli, but the amplitudes of the troughs are very small (8.5×10^{-7} ~ -5.4×10^{-7}) compared to the web thickness and cannot be observed in the lab. The troughs become notable when the CMD load reached negatively

-0.0062 pli as shown in Figure 6.6(b). The amplitude of troughs increased with increased negative CMD load (-0.0065 pli) in the simulation results in Figure 6.6(c).

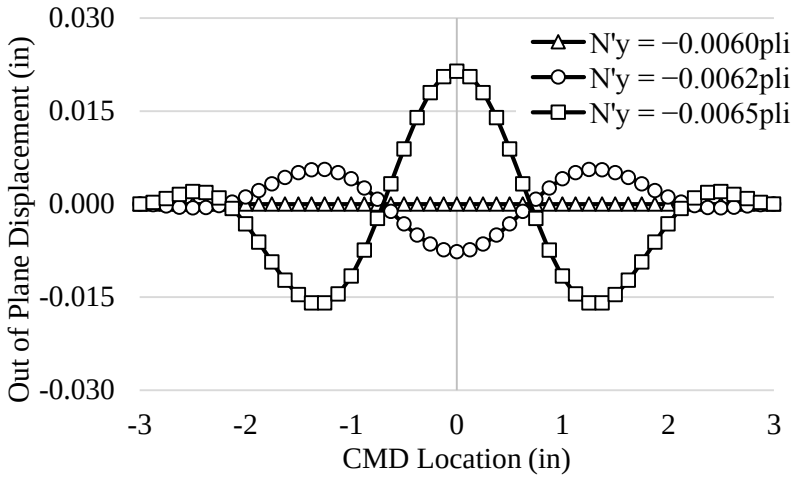

Figure 6.7 – Out-of-plane Deformations Across Web Width at x = 15" for N'_x = 1.3pli (σ_x = 500 psi)

The out-of-plane deformations across the web width were plotted for these 3 cases in Figure 6.7. The path is at web half span (x = L/2 = 15"). The web was relatively flat for the CMD load of -0.0060 pli, so the troughs in Figure 6.6(a) are negligible. The simulations indicated the web would not have troughs until the CMD load reached to -0.0062 pli. The critical CMD stress to generate troughs from equation (6.4) is -2.15 psi, which means the critical edge load is -0.0056 pli. The results from the simulation and the closed form expression are not match exactly but are quite close, with a relative error (0.0062 - 0.0056)/0.0056 ×100% = 10.71%. It noted that the mesh density 0.125"×0.125" is sufficient to depict the out-of-plane deformations of the web.

The amplitude of the troughs A and wavelength λ could be determined from the simulations. Figure 6.8 is the out-of-plane displacement across web width for MD tension 1.3 pli, and CMD compression -0.0062 pli. The trough amplitude A is 0.007 inches. The accuracy of the wavelength is limited by the mesh density. The wavelength λ is 2.50 ±0.125 inches. The amplitude from the expression (6.8) is 0.019 inches and the wavelength from expression (6.7) is 3 inches. The

wavelength from the expression and the simulation agrees well while the amplitude does not. The disagreement of the amplitude may due to the difference of assumptions used in the simulation and the expression. The lateral CMD load was applied at web edges in the simulation and no CMD stress was considered in Cerda's inextensibility assumptions that used to develop expression (6.8). In addition, the external disturbance force applied on web center may affect the shapes of troughs. More exploration will be done in the following section as the web span has different boundary conditions.

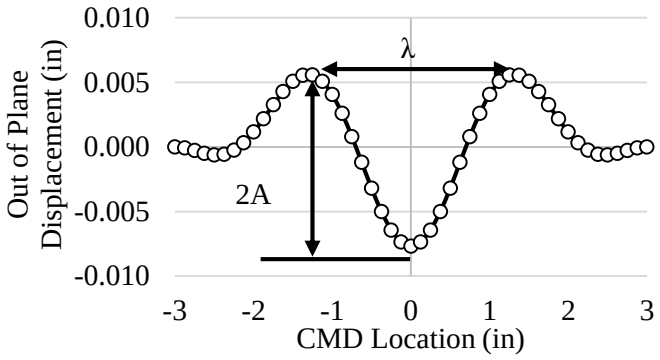

Figure 6.8 – Out-of-plane Deformations Across Web Width at x = 15" for N'_x = 1.3pli (σ_x = 500 psi) and N'_y = -0.0062pli (σ_y = -2.38 psi)

The critical CMD compressive loads were explored for various MD tensions: 1.3 pli, 2.6 pli, 3.9 pli, and 5.2 pli. The average MD stresses in webs were expected to be 500psi, 1000 psi, 1500 psi and 2000 psi, respectively. The critical CMD stresses for troughs from the simulation and the expressions were compared in Table 6.1. Expression (6.4) provides the exact stresses while expression (6.6) provides the approximate results which are in the square brackets. Both simulation and expression results showed that the web with higher MD tension requires more CMD compressive load to generate troughs. The simulation CMD stresses are lower than the expression stresses as shown in Figure 6.9(a). The exact solutions (Eq. (6.4)) from expression (6.4) have a zig zag plot which is not as continuous as the approximation solutions (Eq.-Approx.) from expression (6.6). It shows expression (6.6) is a good approximation for the critical CMD stress to induce

troughs in a single layer web. The critical CMD stresses for troughs varied from -2.38 psi (N'_y = -0.0062 pli) to -4.50 psi (N'_y = -0.0117 pli) in simulations, which are much lower than web MD stresses. Thus only small CMD compressive loads are needed to generate troughs in a web span. Unlike web troughs, the CMD compression to cause wrinkles in the web on a roller is much larger due to the web taking the shape of a cylindrical shell. If the web wrap on a cylindrical roller with radius 1.45 in, the critical CMD compressive stress for the onset of wrinkle formation is -357 psi according to expression (2.41), which is much larger than the CMD compressive stress level for web troughs.

Table 6.1 – The Critical CMD Loads for a Single Layer Isotropic Web Span with Simply Supported Edges

MD Edge Load N'_x (pli)	MD Stress (psi)	Critical CMD Compressive Stress σ_y (psi)	
		ABAQUS	Eq. (6.4) [Eq.-Approx.]
1.3	500	-2.38	-2.15 [-2.11]
2.6	1,000	-3.19	-3.00 [-2.99]
3.9	1,500	-3.88	-3.80 [-3.66]
5.2	2,000	-4.50	-4.24 [-4.23]

The wavelength from expression (6.7) will not vary continuously due to the integer value of half wave number (6.5), the approximate wavelength can be determined by using the real value of half wave number which are shown in the square brackets in Table 6.2. The approximate wavelengths (Eq.-Approx.) match well with the simulation results as shown in Figure 6.9(b). It demonstrated a large MD tension would result in a small wavelength, which indicated a large number of troughs across web width.

Table 6.2 –Wavelength for a Single Layer Isotropic Web Span with Simply Supported Edges

MD Edge Load N'_x (pli)	MD Stress (psi)	Wavelength λ (in)	
		ABAQUS	Eq. (6.7) [Eq.- Approx.]
1.3	500	2.50	3.00 [2.76]
2.6	1,000	2.25	2.40 [2.32]
3.9	1,500	2.00	2.40 [2.10]
5.2	2,000	2.00	2.00 [1.95]

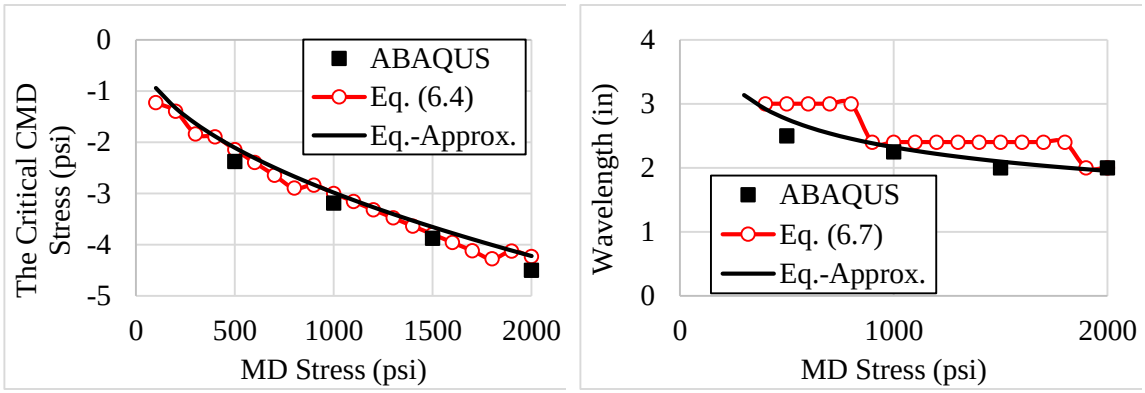

(a) Critical CMD Stress (b) Wavelength

Figure 6.9 – The Critical CMD Stress and Wavelength for a Single Layer Isotropic Web Span with Simply Supported Edges

The amplitude was not considered for this model since the external loads applied in the simulation are different with the model for developing the expression (6.8). The critical CMD load from expressions (6.4) (6.6) and wavelength from expression (6.7) compared well with the simulation outputs. For the expression results, the approximate load and wavelength are close to the exact values, the approximations will be employed for the following sections due to the simplicity of the expressions. Thus expression (6.6) will be used for the critical CMD load to induce troughs and the real value of half wave number will be employed for determining the wavelength of troughs in expression (6.7). The model for expressions (6.4) to (6.7) and the finite element model have the same kinetic and kinematic boundary conditions: all edges are simply supported, and uniform edge loads applied in MD (tension) and CMD (compression). These boundary conditions are difficult to set up in a lab on thin webs. In the lab it is much easier to clamp the web ends then apply tension by stretching web in MD. The test results showed the web would generate buckles. Models with clamped edges will be simulated in the next section. The critical CMD loads, wavelength and amplitude of troughs will be compared from the expressions, simulations and tests.

6.3 Troughs in a Single Layer Isotropic Web Span with Clamped Edges

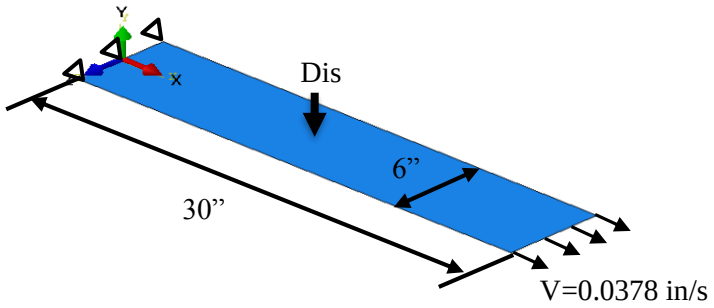

Figure 6.10 – FE Model for a Single Layer Isotropic Web with Clamped Ends

The FE model of a web span has the same width and length dimensions as the model in Figure 6.3. The web is an isotropic polyester that provided by the DuPont[9]. The Young's modulus was measured as 600,000 psi. The Poisson's ratio is 0.35, and the thickness is 0.00048". The boundary conditions are different from the model in Figure 6.3. As shown in Figure 6.10, the web has one end that was totally fixed (x = 0) and the opposite end (x = 30") was applied a MD velocity 0.0378 in/s for generating a MD tension in the web. The end with the velocity can only translate in MD (x direction), no other translation or rotation was allowed. These two opposite ends (x = 0, x = 30") were simulated to be clamped, so the CMD contraction due to Poisson effect was forbidden. The other two edges (z=±3") were free to deform. The disturbance force 0.001 lb was introduced at the planform center of the web for a short time as the model in Figure 6.10 has a "perfect" geometry and property, and the disturbance is needed to induce instability. The shell element S4R was used and mesh density 0.08"×0.08" was found to produce converged results for this model.

There are two steps in this simulation using the ABAQUS/Standard method. The Dynamic, Implicit method was chosen in the ABAQUS step module. The first step has one second, the velocity at the web end (x = 30") increased linearly from 0 to 0.0378 in/s in this step, and kept

[9] E. I. du Pont de Nemours and Company, 200 Powder Mill Rd, Wilmington, DE, 19803, USA

constant in the second step. The disturbance force increased to 0.001 lb from the beginning to 0.3 seconds, and then decreased to zero from 0.3 seconds to 0.4 seconds. The MD stress in the web increased linearly due to web elongation. The maximum MD stress in web appeared at the end of simulation due to the longest elongation.

Figure 6.11 is the final MD stress state of the web in the simulation. It showed only the MD membrane stresses at web corner exceed the yield stress 8,500 psi. According to the Saint-Venant's Principle, if we focus on the web away from the ends, the state of the web near two ends are negligible when the web has enough length. Most webs in the simulation have quite uniform MD membrane stress which proved the web is long enough to avoid the effect of large stress at four corners. Figure 6.12 plotted the MD membrane stress along web centerline (z = 0). The average stress of the web away from ends (x = 0, x = 30") is 7,211.9 psi, which is similar to the desired value 7,182 psi, within a relative error 0.42%. The desired MD stress is determined by interpreting web velocity and modulus.

Figure 6.11 –MD Membrane Stress for an Isotropic Web Span with Clamped Edges

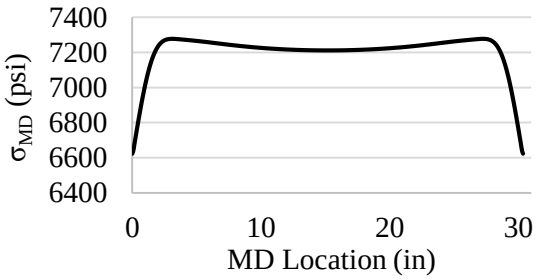

Figure 6.12 –MD Membrane Stress Along Web Centerline (z = 0)

Table 6.3 –Average MD Membrane Stresses from Simulation and Web Velocity

Step Time (s)	MD Membrane Stresses σ_{MD}(psi)		
	From Simulation	From Velocity	Relative Error
0.5	763.7	758.0	0.76%
1.1	1,192.8	1,186.2	0.56%
1.7	1,693.4	1,684.4	0.54%
2.2	2,049.4	2,038.2	0.55%
2.6	2,383.3	2,370.1	0.56%
3.0	2,683.7	2,668.7	0.56%
3.6	3,135.6	3,117.0	0.60%
4.5	3,813.3	3,788.3	0.66%
5.3	4,444.2	4,418.8	0.57%
6.1	5,010.9	4,985.8	0.50%
6.8	5,543.0	5,517.3	0.47%
7.2	5,841.6	5,815.9	0.44%
7.5	6,075.6	6,048.0	0.46%
8.0	6,456.9	6,426.0	0.48%
8.5	6,838.0	6,804.8	0.49%
9.0	7,211.9	7,182.0	0.42%

The critical CMD load (6.6), the wavelength (6.7) and the amplitude of troughs (6.8) were determined by the material properties of the web, dimensions of web span and the MD stress. Uniform MD stress was expected to be used in expressions. The accuracy of web MD stress would affect the accuracy of the expression results so it is crucial to determine the value of MD stresses. In simulation, the average MD membrane stress σ_{MD} was calculated by averaging the MD nodal stress outputs that are away from the clamped ends. Another method to determine the average MD stress in the web was based on the constant web velocity that was applied at the web end. The MD stress is the MD strain times the Young's modulus, and the MD strain is induced by the web MD elongation. This elongation is the product of MD velocity (0.0378 in/s) and time. Table 6.3 proved these two methods provide the similar values for MD stress in a web. The MD stress acquired from the simulation was chosen for the following calculations due to its high accuracy. The critical CMD

loads, wavelength and amplitude of troughs would be determined by the expressions (6.6-6.8) under various MD stress levels.

The CMD membrane stress at the end of simulation was given in Figure 6.13. The tensile stress is in grey and compressive stress is in red and orange. The positive CMD stresses appear at web two edges (x = 0, x = 30") are the consequence of the clamped boundary conditions as they are restrained from contracting from the Poisson effect. The uniform compressive stresses appear in the middle of the web which occupied the majority of the web, between these uniform stresses and the positive CMD stresses near edges are the minimum compressive CMD stress. These orange minimum stresses were induced by the positive CMD stresses at edges and the Poisson contraction in web span. These compressive stresses were sufficient to induce buckles in this web.

Figure 6.13 – CMD Membrane Stress for an Isotropic Web Span with Clamped Edges

Troughs can be observed clearly from the web out-of-plane deformation output. As shown in Figure 6.14, troughs are uniformly spread at web center and diminish towards to the web edges in the width dimension. Both ends do not have any troughs due to the positive CMD stresses and the troughs begin near the locations where the minimum CMD membrane stress appeared. The wavelength and amplitude of troughs can be determined by the out-of-plane deformation at the mid-span of the web in Figure 6.15. This figure showed the troughs have uniform wavelength and maximum amplitude at web center.

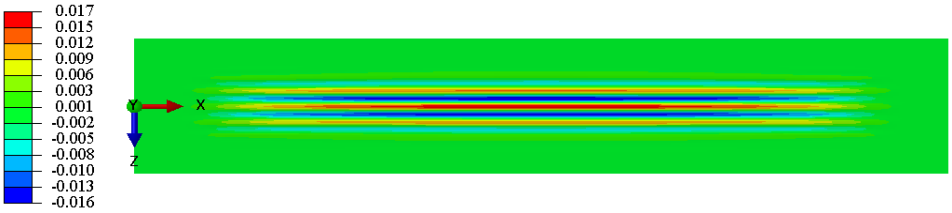

Figure 6.14 –Out-of-plane Deformation for an Isotropic Web Span with Clamped Edges

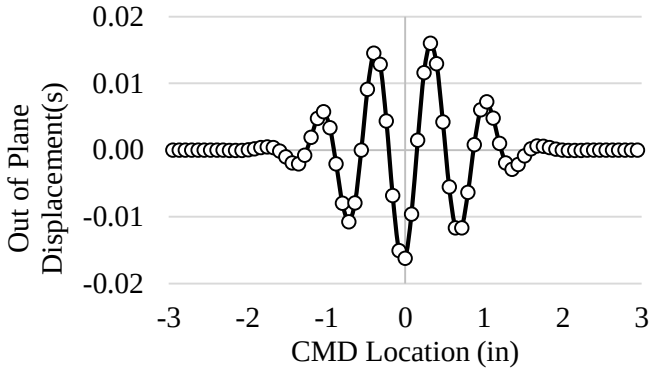

Figure 6.15 – Out-of-plane Deformation at Web Mid-span Across Web Width (x = 15")

Vindhya Nukala set up the experimental equipment and did test to measure the out-of-plane deformation for this isotropic web span with clamped edges [66]. The web was tensioned in an Instron machine[10] and the Keyence model LC-2210 laser sensor[4] was used to measure the out-of –plane deformation (w) of the web. A Yo-Yo pot 1850-0500 (displacement transducer) was used to detect the position of the laser sensor. Table 6.4 provided the wavelength and amplitude of troughs from simulation, expression and test. The MD stresses varied from 763.7 psi to 5,010.9 psi since this is the MD stress domain used in the test. Figure 6.16(a) indicated the wavelength measured in tests agree very well with the results predicted by the simulation and the expression (6.7). Note the approximate wavelength (Eq.-Approx.) from expression (6.7) uses the real value of the half wave number n in expression (6.5). The web has more trough waves under higher MD

[10] Instron Engineering Corporation, 825 University Ave, Norwood, MA, 02062-2643, USA

tensions. The amplitude of troughs under different web tensions were plotted in Figure 6.16(b). The behavior at the higher tension is similar, but the low load behavior between the test and the simulation/expression diverge. The thickness of the web herein is quite small (0.00048 inches) so the clamped boundary condition is difficult to set up perfectly in test. The web edges were bonded between two plates and then clamped into grips on the Instron[10]. The web had to be aligned in the Instron, misalignment would result in early trough formation due to unintentional shear. The simulation predicted that there is a critical MD stress for the web that troughs can formed only as web stress above this critical level. However, expression (6.8) incorporated the assumption that troughs could form as soon as MD stress becomes nonzero in the web which is not true. For a web transiting over multiple rollers, it is difficult or even unable to observe troughs when the web MD tension is low, which indicated the simulation results are reasonable.

Table 6.4 –Wavelength and Amplitude for an Isotropic Web Span with Clamped Edges

MD Stress (psi)	Wavelength λ (in)			Amplitude A_{mn} (in)		
	Eq.-Approx.	ABAQUS	Experiment	Eq. (6.8)	ABAQUS	Experiment
763.7	1.25	1.27	1.34	0.0084	6.44E-06	0.0606
1,192.8	1.12	1.02	1.19	0.0094	0.0035	0.0380
1,693.4	1.02	0.95	1.06	0.0102	0.0063	0.0227
2,049.4	0.98	0.92	1.01	0.0108	0.0075	0.0154
2,383.3	0.94	0.89	0.88	0.0112	0.0088	0.0110
2,683.7	0.91	0.86	0.82	0.0115	0.0096	0.0080
3,135.6	0.88	0.83	0.75	0.0120	0.0118	0.0075
3,813.3	0.84	0.80	0.72	0.0126	0.0140	0.0075
4,444.2	0.80	0.76	0.69	0.0130	0.0131	0.0074
5,010.9	0.78	0.74	0.70	0.0134	0.0143	0.0066

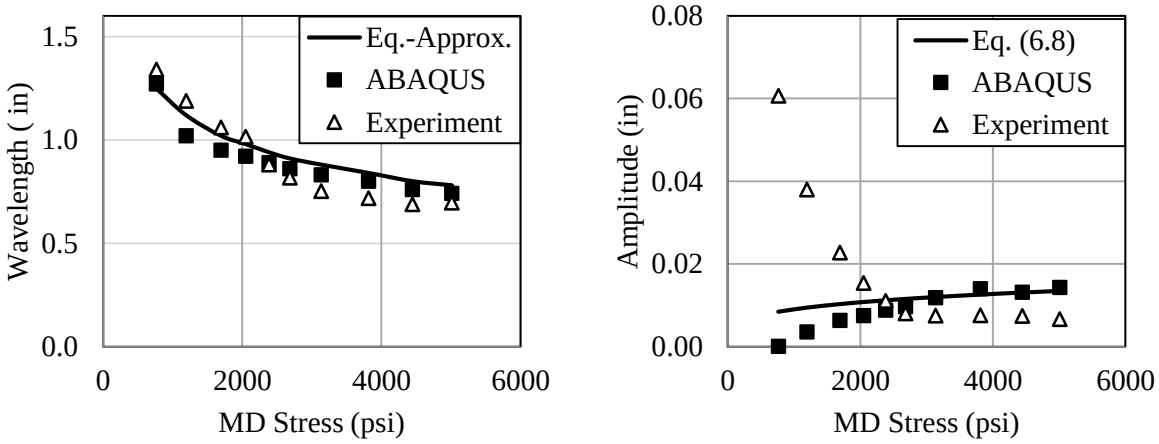

(a) Wavelength (b) Amplitude

Figure 6.16 – Wavelength and Amplitude for an Isotropic Web Span with Clamped Ends

The model used to develop the expressions (6.4-6.7) incorporated simply supported boundary conditions for all edges. The ABAQUS simulation of the web with simply supported edges showed good agreement for the critical CMD loads and the wavelength. The amplitude from the simulation has some differences with the result from the expression due to the different boundary conditions for expression (6.8). However, the good agreement of the amplitude has been obtained at high MD tensions from the simulation, expression and test as the web span has clamped edges. To summarize, expressions for the critical CMD load (6.4) and (6.6), and wavelength of troughs (6.7) have been validated to be correct by the finite element simulations as the web span has the simply supported boundary conditions at all edges. The expressions for the wavelength of troughs (6.7), and the amplitude of troughs (6.8) have been proved to be accurate by the tests and simulations as the web has two clamped ends and two free edges.

All the simulations and tests in Sections 6.2 and 6.3 used a single layer isotropic web span. Different boundary conditions were employed to validate the accuracy of expressions. The expressions (6.4) to (6.8) can be used for the orthotropic webs. The orthotropic web has more complex material properties. There are 3 independent elastic moduli for the isotropic web: Young's

modulus E, Poisson's ratio ν and shear modulus G. The elastic moduli would increase to 9 constants for the orthotropic web: three Young's moduli E_1, E_2, E_3, three Poisson's ratios ν_{12}, ν_{13}, ν_{23}, and three shear moduli G_{12}, G_{13}, G_{23}. The simulations with an orthotropic web will studied to explore the applicability of expressions (6.5) to (6.8).

6.4 Troughs in a Single Layer Orthotropic Web Span with Clamped Edges

The orthotropic web has the same width (6 in) and length (30 in) dimensions and boundary conditions as shown in Figure 6.10: two clamped ends, and two free edges. The thickness of the web is 0.00048 inches. The principal material directions of the web were assumed to aligned with the coordinate axes: MD modulus Ex is 600,000 psi, CMD modulus E_y is 300,000 psi, Poisson's ratio ν_{xy} is 0.35, and the shear modulus G_{xy} is 166,000 psi. The Poisson's ratio ν_{yx} 0.175 is determined by Maxwell's Reciprocal Theory: $\nu_{yx} = E_y\nu_{xy}/E_x$. The small disturbance force 0.001 lb was applied at the center of the web span of a very short time at the beginning of the simulations.

The orthotropic web with two clamped edges and two free edges has the similar MD stress and CMD stress distributions as an isotropic web with the same boundary conditions (Figure 6.11, Figure 6.13). In addition, the steady out-of-plane deformations of the web are also similar as the model shown in Figure 6.14. The comparison of the wavelength and amplitude from simulations and expressions was shown in Table 6.5 and Figure 6.17. The wavelengths from the simulation match well the approximate results from expression (6.7) (Eq.-Approx.). Note the real value for the half wave number has been used in expression (6.7). More MD load results in more waves across web width, as also indicated for the isotropic web in Table 6.4 and Figure 6.16(a). The amplitudes match well at a high MD tension level. At the lower MD stresses, the amplitudes from expression (6.8) are higher than results from the simulations. There is a critical MD stress predicted by the simulation that the troughs can only formed as the MD stress of this orthotropic web larger than this critical value. The isotropic web also has this critical value according to the simulation results

in Figure 6.16(b). The amplitude for the orthotropic web approaches 0.01 inches as the MD stress is 5,000 psi, the ratio of the amplitude to the web thickness is 0.01/0.00048 = 20.8 which means the troughs are easy to observe in a lab.

Table 6.5 – Wavelength and Amplitude for an Orthotropic Web with Clamped Edges

MD Stress (psi)	Wavelength λ (in)		Amplitude A_{mn} (in)	
	Eq.-Approx.	ABAQUS	Eq. (6.8)	ABAQUS
600	1.0971	0.8930	0.0065	0.0001
1,200	0.9227	0.8260	0.0078	0.0033
2,400	0.7764	0.7190	0.0092	0.0071
3,600	0.7015	0.6387	0.0102	0.0085
4,800	0.6529	0.7182	0.0110	0.0099
6,000	0.6174	0.5580	0.0116	0.0107
7,200	0.5899	0.5842	0.0122	0.0117
8,400	0.5676	0.5175	0.0126	0.0117

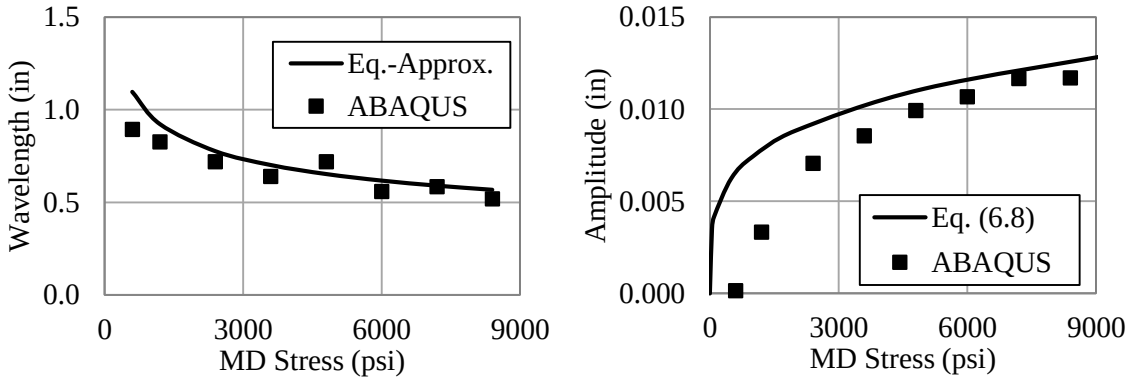

(a) Wavelength (b) Amplitude

Figure 6.17 – Wavelength and Amplitude for an Orthotropic Web Span with Clamped Edges

A nonwoven polypropylene web was selected for tests. The non-woven web was manufactured by the spun bond process which result in varied mass density across the whole web. A variation of web thickness results in the material property variations in MD and CMD directions. This nonwoven material was assumed to be an orthotropic homogeneous web at the macro level.

However, it has varied thickness across the whole web due to its non-uniformity which is difficult to build the model correctly in finite element simulations. Only test data and expression results will be compared when this non-woven web has troughs. The average thickness of this web is 0.0055 inches based on several measurements [66]. Nukala measured the average modulus and Poisson's ratio on Instron machine[10]: the MD modulus E_x is 12,000 psi, CMD modulus E_y is 1,500 psi, and Poisson's ratio ν_{xy} is 1.8. The Poisson's ratio ν_{yx} is 0.225 that determined from the relation $\nu_{yx} = E_y*\nu_{xy}/E_x$, and shear modulus G_{xy} is 1,030 psi.

The wavelength and amplitude when the nonwoven webs generate troughs were compared in Table 6.6. Both results from the expression and experiment were under varied MD tensions. The web span has two clamped edges and the MD tension was generated by the web elongation. The approximate wavelength of troughs (Eq.-Approx.) from equation (6.7) uses the real value of half wave number (6.5) and it matches quite well in Figure 6.18(a). However, the amplitude from the experiment has differences with the expression result in Figure 6.18(b). The high non-uniformity of the non-woven material was one reason for this difference. It is possible Cerda's assumption of inextensibility is not valid for low modulus webs. In addition, it is difficult to set up the test due to the thin web thickness as discussed for the isotropic web. Although the differences appear as shown in Figure 6.18(b), the amplitudes from the expression and experiment are at the same order of magnitude which means expression (6.8) may have some value to engineers.

Table 6.6 – Wavelength and Amplitude for a Nonwoven Web with Clamped Edges

MD Stress (psi)	Wavelength λ (in)		Amplitude A_{mn} (in)	
	Eq.-Approx.	Experiment	Eq. (6.8)	Experiment
72	1.88	1.69	0.062	0.053
108	1.70	1.61	0.069	0.049
144	1.58	1.51	0.074	0.045
180	1.50	1.42	0.078	0.043
216	1.43	1.33	0.082	0.043

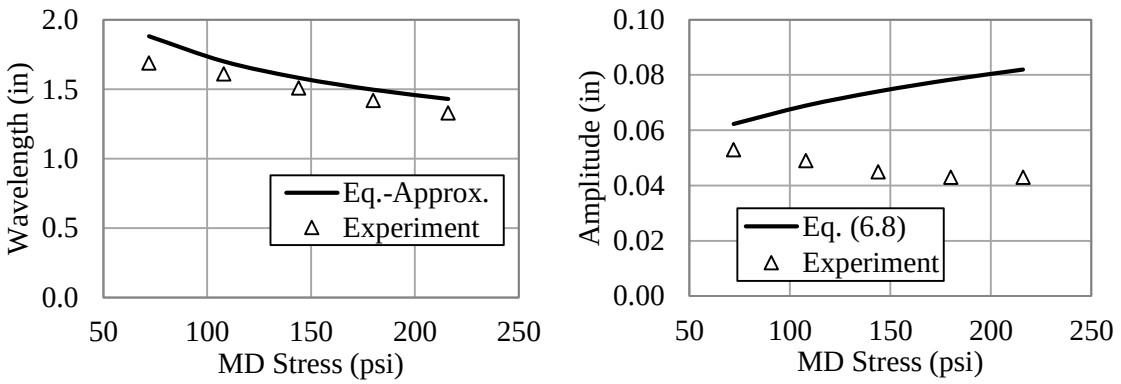

(a) Wavelength (b) Amplitude

Figure 6.18 –Wavelength and Amplitude for a Nonwoven Web Span with Clamped Edges

6.5 Conclusions

The expressions that predict troughs for a single layer orthotropic web span have been validated. The theoretical model for developing the exact (6.4) and approximate (6.6) critical CMD stress for the web to have troughs, the wavelength (6.7), and the half wave number (6.5) employed simply supported boundary conditions on all web edges. The web span had a uniform MD tension and a CMD compression applied on the edges. To develop the expression for the amplitude of troughs (6.8), Cerda's inextensibility claim was used. It requires that all of the Poisson contraction due to web tension would result in producing out-of-plane deformation of a web. The expression for amplitude was determined without considering any external CMD loads applied on the web. In reality no troughs and no amplitude is existed until the MD tensile stress and the CMD compressive stress are sufficient to induce troughs.

The expression results for the critical CMD load (6.4) (6.6), and wavelength of troughs (6.7) have been compared by the finite element simulations for an isotropic web span under uniform edge loads in MD and CMD. The simply supported edges guarantee the web do not have any out-of-plane deformations at web edges. The web span in another model has two clamped edges and two free edges, and troughs appeared along most of web span even without an external CMD

compression. The expressions of wavelength of troughs (6.7), and amplitude (6.8) of troughs have been proved to be valid by the tests and simulations for a single layer isotropic web span.

The orthotropic web with clamped edges was simulated and showed good agreement with the wavelength and amplitude of troughs from the expressions in Table 6.5. For the nonwoven material in Table 6.6, the test data indicated the expression for the wavelength (6.7) provided valid results for the orthotropic webs even the thickness of the web is not uniform. The amplitude from expression (6.8) are not exact but at the same order of magnitude compared with the tests results.

The single layer webs with isotropic and orthotropic materials have been discussed. Both single layer web and multi-layer web are widely used in the web process industry. Most researches were focused on the web with only one layer, and more attention should be paid on the laminated web. This will be the focus of Chapter VII.

CHAPTER VII

DEVELOPMENT OF A TROUGH FAILURE CRITERION FOR A LAMINATED WEB

A trough failure criterion (6.6) has been developed for a single layer web in Chapter VI. The critical CMD stress has been determined to generate troughs in a web span between two rollers. Both isotropic and orthotropic webs were simulated to validate the accuracy of the expressions for the wavelength, and amplitude of troughs which were derived from the failure criterion. Both single layer webs and laminated webs are widely used in web process industry. A large percentage of industrial products are made from laminated webs, such as all kinds of chip bags at the market, or disposable diapers that contain multi-layers of different materials. The thickness of the laminated web would increase due to the extra laminas, which results in a larger bending stiffness. The compressive CMD stress to induce troughs in the web should also increase compared with a single layer web.

In this chapter, a trough instability failure criterion for laminated webs will be developed. The closed form expressions of wavelength, half wave number and amplitude of troughs in a laminate will be developed and the accuracy will be validated by simulations and tests. Trough and slack edge behaviors will be studied for laminate web spans with a downstream misaligned roller.

7.1 Trough Failure Criterion for an Orthotropic Laminated Web Span

The simulation model for the laminated web has the boundary conditions and structure dimensions as shown in Figure 6.2. Each layer of the laminate was assumed to be homogeneous

orthotropic with unique material properties and thickness. The principal material directions are aligned with the coordinate axes shown in Figure 6.2. Edge loads N'_x and N'_y are applied at the web edges to generate uniform web tension in MD and compression in CMD. However, the unique membrane stresses will be induced in each lamina. All web edges were assumed to be simply supported. For the laminated web, the differential equation which governs the out-of-plane deformation w is shown as [70]:

$$D_{11}\frac{\partial^4 x}{\partial x^4}+2(D_{12}+2D_{66})\frac{\partial^4 w}{\partial x^2\partial y^2}+D_{22}\frac{\partial^4 w}{\partial y^4}-N'_x\frac{\partial^2 w}{\partial x^2}-N'_y\frac{\partial^2 w}{\partial y^2}=0 \qquad (7.1)$$

Where, D_{ij} is the bending stiffness of a laminated web which is determined by the material properties and the thickness of each lamina. D_{ij} is expressed by equation (7.2) when the laminated web has n layers and the thickness of the k^{th} layer is $z_k - z_{k-1}$.

$$D_{ij}=\frac{1}{3}\sum_{k=1}^{N}(Q_{ij})_k(z_k^3-z_{k-1}^3) \qquad (7.2)$$

The thickness dimension of most webs is much smaller compared with the length or width dimensions, so the plane stress condition is applicable for webs. The constitutive terms Q_{ij} in expression (7.2) can be determined using expression (7.3) for an orthotropic lamina:

$$\begin{bmatrix}\sigma_1\\ \sigma_2\\ \tau_{12}\end{bmatrix}=\begin{bmatrix}Q_{11} & Q_{12} & 0\\ Q_{12} & Q_{22} & 0\\ 0 & 0 & Q_{66}\end{bmatrix}\begin{bmatrix}\varepsilon_1\\ \varepsilon_2\\ \gamma_{12}\end{bmatrix} \qquad (7.3)$$

Where, $Q_{11}=\frac{E_x}{1-\nu_{xy}\nu_{yx}}$, $Q_{22}=\frac{E_y}{1-\nu_{xy}\nu_{yx}}$, $Q_{12}=\frac{\nu_{xy}E_y}{1-\nu_{xy}\nu_{yx}}$, $Q_{66}=G_{xy}$. E_x and E_y are the Young's moduli of a lamina in x and y directions, respectively. ν_{xy} is the Poisson's ratio that corresponds to a contraction in direction y when an extension is applied in direction x. G_{xy} is the shear modulus in xy plane.

The out-of-plane deformation w in expression (7.1) is in reference to the middle plane of a laminated web as well as the deformation in expression (6.1) for a single layer web. For example, Figure 7.1 shows the cross section of a laminated web that has two layers – Lamina1 and Lamina2. The out-of-plane deformation of the laminate w (x,y) is defined relative to the middle plane (z = 0). If both laminas have same thickness (i.e. $t_1 = t_2$), the middle plane is on the adhesive surface between these two laminas. However, if the thickness of Laminae 1 is larger than the thickness of Laminae2 (i.e. $t_1 > t_2$) as depicted in Figure 7.1, the middle plane is not on the adhesive surface but within Lamina 1. Considering the sign direction of the z coordinate, the thickness of Lamina1 is $z_1 - z_0$, and thickness of Lamina2 is $z_2 - z_1$.

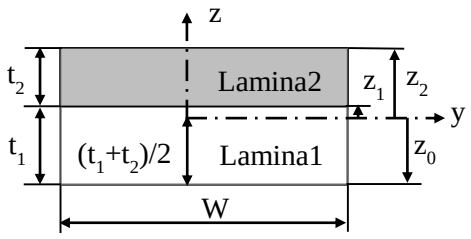

Figure 7.1 – Cross Section of a Two-layer Laminate

Expression (7.2) shows the bending stiffness D_{ij} for a laminated web which has N layers. If a laminated web has two layers as shown in Figure 7.1, D_{ij} can be expressed with equation (7.4). The subscript numbers 1, 2 outside of the brackets denote the material belong to Lamina1 and Lamina2, respectively.

$$D_{ij} = \frac{1}{3}\sum_{k=1}^{N}(Q_{ij})_k(z_k^3 - z_{k-1}^3) \overset{N=2}{=} \frac{1}{3}\left[(Q_{ij})_1(z_1^3 - z_0^3) + (Q_{ij})_2(z_2^3 - z_1^3)\right] \tag{7.4}$$

The web span between two rollers was assumed to have simply supported edges. A trial buckled deformation solution of the following form is assumed as:

$$w(x,y) = A_{mn}\sin\left(\frac{m\pi x}{L}\right)\sin\left(\frac{n\pi y}{W}\right) \tag{7.5}$$

where m and n are the number of the half wave troughs in x and y directions, respectively. Since N'_x is tensile m must be 1. A_{mn} is the amplitude of the buckled wave and dependent on the values of m and n and the traction that produced the troughs. If equation (7.5) for the out-of-plane deformation w is substituted into the differential equation (7.1), the critical CMD load to induce troughs in a laminated web will be solved as:

$$N'_{ycr} = -\frac{W^2}{n^2}\left[\frac{D_{11}\pi^2}{L^4} + \frac{D_{22}\pi^2 n^4}{W^4} + \frac{2(D_{12}+2D_{66})\pi^2 n^2}{W^2 L^2} + \frac{N'_x}{L^2}\right] \tag{7.6}$$

The derivation of equation (7.6) is based on the governing equation (7.1) and it is the first time that we know the solution to the critical CMD load to induce troughs in a laminate. The half wave number n is a positive integer since all edges of the web span are simply supported, and it can be determined by seeking a minimum energy solution to equation (7.6). The full solution to n can be simplified to expression (7.7) by ignoring the negligible terms:

$$n = INT\left[\frac{W}{\sqrt{L\pi}}\sqrt[4]{\frac{N'_x}{D_{22}}}\right] \tag{7.7}$$

With known half wave numbers m = 1 and n from (7.7), the critical CMD load N'_{ycr} to induce troughs in a laminate can be simplified to expression (7.8) and the corresponding wavelength λ can be determined as:

$$N'_{ycr} \approx -\frac{2\pi}{L}\sqrt{D_{22}N'_x} \tag{7.8}$$

$$\lambda = \frac{2W}{n} \tag{7.9}$$

The negative sign of N'_{ycr} in expression (7.8) indicates the laminated web will generate trough when subjected to sufficient CMD compressive load. The process to develop expressions (7.1-7.9) for a laminate is similar as the one for the single layer web in Chapter VI. Expression

(7.6) provides the exact critical CMD load for troughs by using the integer value of half wave number in equation (7.7), and expression (7.8) provides the approximate value.

Both expressions (7.7) and (7.8) require the bending stiffness D_{22}, which can be determined for a two-layer laminated web according to expressions (7.3) and (7.4):

$$D_{22} = \frac{1}{3}\sum_{k=1}^{N}(Q_{22})_k(z_k^3 - z_{k-1}^3) \overset{N=2}{=} \frac{1}{3}\left[\left(\frac{E_y}{1-\nu_{xy}\nu_{yx}}\right)_1(z_1^3 - z_0^3) + \left(\frac{E_y}{1-\nu_{xy}\nu_{yx}}\right)_2(z_2^3 - z_1^3)\right] \quad (7.10)$$

The critical CMD compressive load for the onset of troughs (7.6) and (7.8), the half wave number (7.7), and wavelength of troughs (7.9) have been developed for a laminated web. Uniform MD and CMD stresses were used for a single layer web in expression (6.4-6.7) while the uniform edge loads N'_x and N'_y were employed for a laminated web in expressions (7.6-7.9). The edge loads N'_x and N'_y (forces per unit length acting on the web edges) must be in equilibrium with the internal stresses in the lamina. Prior to buckling the stress will be constant but unique within each lamina. After buckling the average stress in each lamina must remain in equilibrium with the edge forces even though the stresses will vary through the thickness.

$$\begin{aligned} N'_x &= \int_{-t/2}^{t/2}\sigma_x dz = \sum_{k=1}^{N}\int_{z_{k-1}}^{z_k}\sigma_x dz \overset{N=2}{=} \sigma_{x1,avg}t_1 + \sigma_{x2,avg}t_2 \\ N'_y &= \int_{-t/2}^{t/2}\sigma_y dz = \sum_{k=1}^{N}\int_{z_{k-1}}^{z_k}\sigma_y dz \overset{N=2}{=} \sigma_{y1,avg}t_1 + \sigma_{y2,avg}t_2 \end{aligned} \quad (7.11)$$

Expression (7.5) assumed the laminate has troughs across web width with uniform wavelength and amplitude. In order to develop a closed form expression for the amplitude of troughs, Cerda's inextensible assumption will be employed [64][65]. His assumption claims all of the Poisson contraction of a web must result in producing out-of-plane deformations while producing negligible CMD membrane stresses. The reduced width of the web due to the out-of-plane deformation is W':

$$W' = \int_0^w \left(1 - \frac{1}{2}\left(\frac{\partial w}{\partial y}\right)^2\right) dy \tag{7.12}$$

The CMD strain of a laminated web due to the MD tension and CMD compression is determined as expression (7.13) when the load directions are shown in Figure 6.2 [67]:

$$\varepsilon_{CMD} = -\alpha_{22} N'_y - \alpha_{12} N'_x \tag{7.13}$$

where $\alpha_{12} = \frac{A_{12}}{A_{12}^2 - A_{11}A_{22}}$, $\alpha_{22} = \frac{A_{11}}{-A_{12}^2 + A_{11}A_{22}}$, and $A_{ij} = \sum_{k=1}^{N} (Q_{ij})_k (z_k - z_{k-1}) \overset{N=2}{=} \left[(Q_{ij})_1 (z_1 - z_0) + (Q_{ij})_2 (z_2 - z_1) \right]$.

The reduced width of the web due to the Poisson contraction is defined as W" for an orthotropic laminated web:

$$W'' = \int_0^w \left(1 - \alpha_{12} N'_x - \alpha_{22} N'_y\right) dy \tag{7.14}$$

If width reduction W' and W" are equated, equation (7.5) is substituted for w with m = 1, the amplitude squared in expression (7.15) can be determined using edges loads and the half wave number of troughs.

$$A_{mn}^2 = \frac{4\left(-\alpha_{12} N'_x - \alpha_{22} N'_y\right)}{\left(n\pi/W\right)^2 \left[1 + \sin\left(2n\pi\right)/\left(2n\pi\right)\right]} \tag{7.15}$$

Substituting equation (7.7) of half wave number n and equation (7.8) of critical CMD load N'_{ycr} into equation (7.15), the amplitude of troughs can be solved and simplified as below expression (7.16). Note the square root term is real since web length L is positive and α_{12} is negative for laminated webs.

$$A_{mn} = 2\sqrt{\frac{-L\alpha_{12}}{\pi}} \sqrt[4]{D_{22} N'_x} \tag{7.16}$$

The critical CMD load to induce troughs (7.6) and (7.8) and the associated wavelength (7.9) for a laminate have been developed. For cases where trough buckling has occurred we also have expressions that relate the reduced buckled web width to the amplitude of the troughs (7.16).

These expressions will turn into the expressions for the single layer web (6.4)(6.6)(6.7)(6.8) if all laminas in a laminated web have the same material properties. In addition, all of these expressions are for the orthotropic web which are easy to be simplified for the isotropic web. It is prudent to compare results from finite element simulations to the expressions (7.7)(7.8)(7.9)(7.16) to check their validity.

7.2 Troughs in a Two-layer Orthotropic Web Span with Simply Supported Edges

Table 7.1 – Material Properties of a Two-layer Orthotropic Laminate

	E_x (psi)	E_y(psi)	ν_{xy}	ν_{yx}	G_{xy}(psi)	t (in)
Paper	1,722,933	522,713	0.22	0.09	416,688	0.0022
Polymer	337,652	443,430	0.19	0.2	161,917	0.0016

A two-layer laminate was supplied by Avery Dennison[11] for simulations. One lamina is paper, and the second one is a polymer laminated with an adhesive. The modulus of the adhesive is much smaller than the paper or the polymer, so the adhesive properties were not considered. The thickness of the bare polymer layer is 0.0016 inches. The total thickness of the polymer with adhesive was measured as 0.0023 inches, so the thickness of the adhesive layer is 0.0007 inches. Table 7.1 shows the modulus and Poisson's ratio of each layer which were measured on the Instron machine[10]. Some material properties were measured directly such as the modulus in the MD (E_x), the modulus in the CMD (E_y), Poisson's ratio (ν_{xy}), and the thickness t. Other material properties such as Poisson's ratio ν_{yx}, and shear modulus G_{xy} were inferred from expression (7.17) [68].

$$\nu_{yx} = \frac{E_y}{E_x}\nu_{xy}$$
$$G_{xy} = \frac{\sqrt{E_x E_y}}{2\left(1+\sqrt{\nu_{xy}\nu_{yx}}\right)} \qquad (7.17)$$

[11] Avery Dennison Corporation, 207 Goode Ave, Glendale, CA 91205, USA

For a single layer web span in Figure 6.3, its symmetric shape and homogeneous properties will prevent any out-of-plane deformations in the web when only MD tension applied on the simply supported edges. However, if we replace the single layer web by a laminate which has varied material properties for each layer, the web does not have the symmetric property. To validate the accuracy of expressions (7.7-7.9, 7.16), zero out-of-plane deformation is required before the CMD compression applied on web edges. The simulation in this section will show the steady state shape of the laminated web under a MD tension.

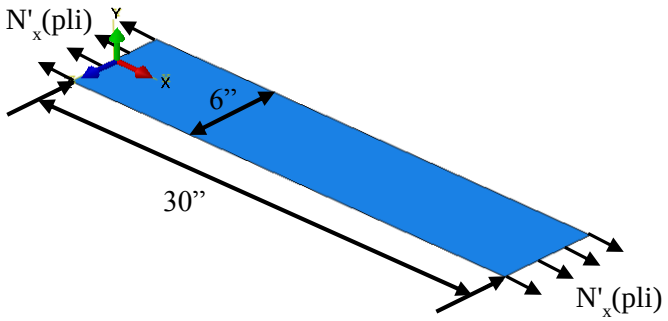

Figure 7.2 – FE Model of a Laminated Web Span with Simply Supported Edges

ABAQUS/Standard simulations were employed for the simulations to acquire high accuracy. The web span in the finite element model has simply supported edges as shown in Figure 7.2. The uniform MD edge load N'_x was applied on web two opposite ends. Material properties and the thickness of each lamina were shown in Table 7.1. The adhesive layer was not considered. A composite section was employed in the simulation to model the laminated web. The length of the web span is 30 in and the width is 6 in. The web is not “perfect” since the material properties and thicknesses of two laminas are different, the disturbance force for the single layer web in Chapter VI is not required for this laminate model. This model has 9,777 nodes and 9,366 elements. The web was meshed by using the reduced four nodes, shell elements S4R with a converged mesh density 0.25”×0.25”. This model has 9,777 nodes and 9,366 elements. This model has one step (1s) and the web load increases from zero to the maximum value in 0.2 s.

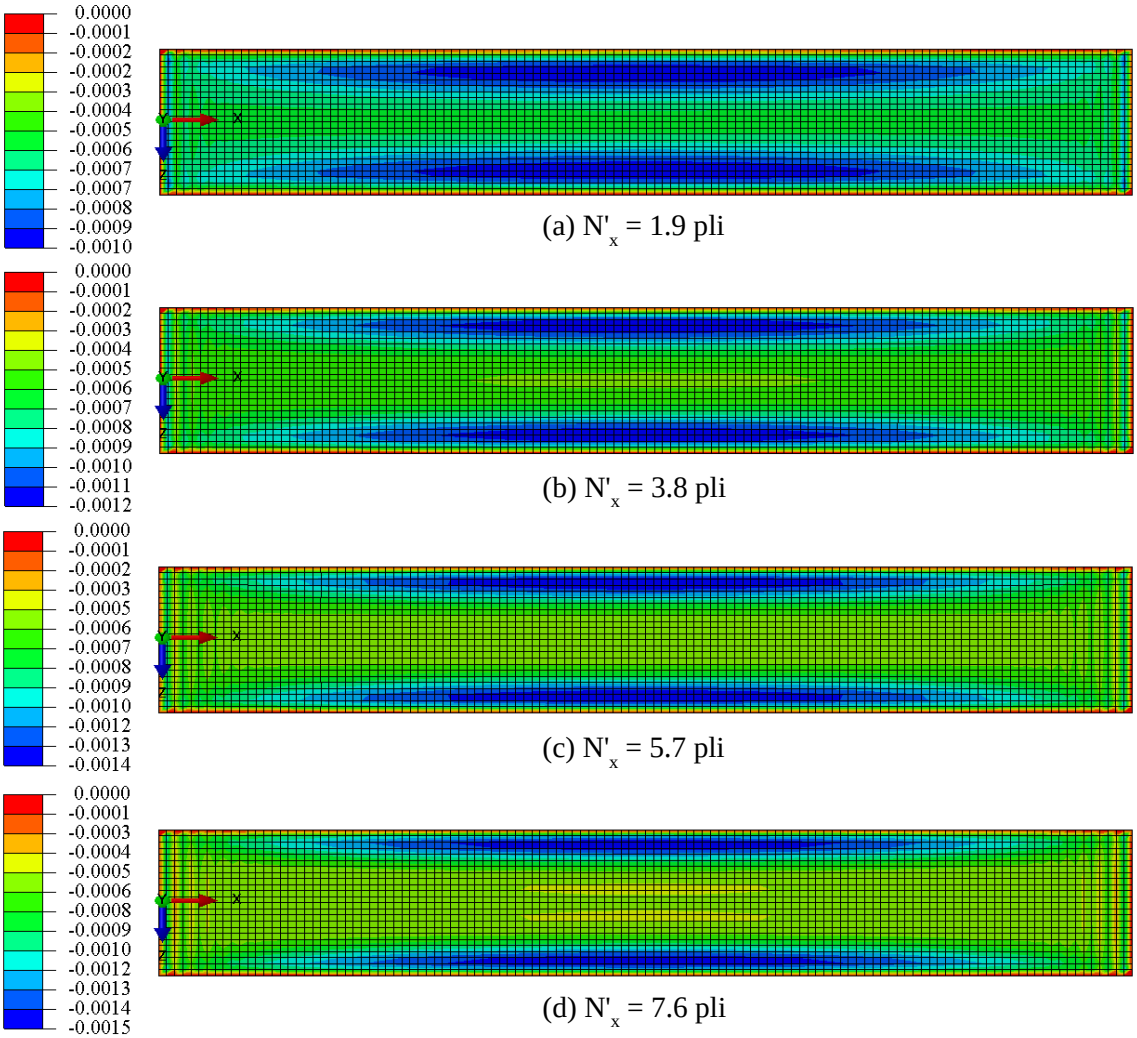

Figure 7.3 – Out-of-plane Deformations for the Laminated Web with Varied MD Tensions

Four MD tensions were applied on this model: 1.9 pli, 3.8 pli, 5.7 pli, and 7.6 pli. The steady state deformed shapes were plotted in Figure 7.3. It shows zero out-of-plane deformation appear only at web edges. Figure 7.4 is the out-of-plane deformation across web width at web center (x = 30”), it shows the web will bend more as the tension increases. The laminated web can internally produce its own disturbance to produce troughs without the CMD compression. The wavelength and amplitude of troughs in Figure 7.4 are difficult to determine since the trough waves are not uniform.

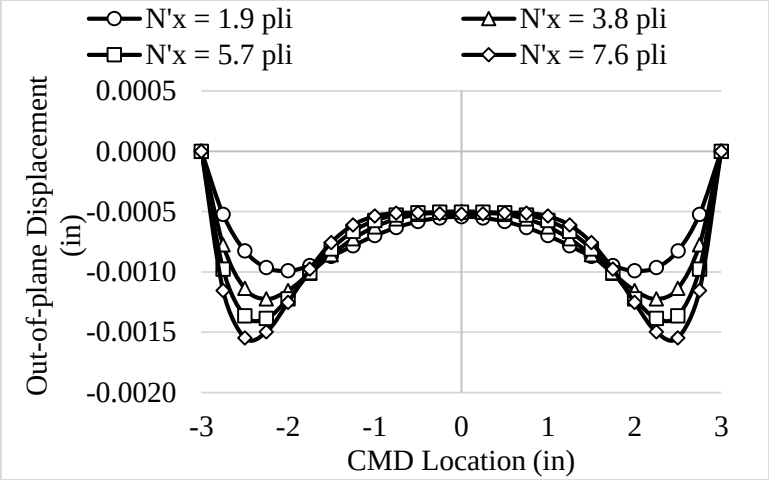

Figure 7.4 – Out-of-plane Deformations Across Web Width

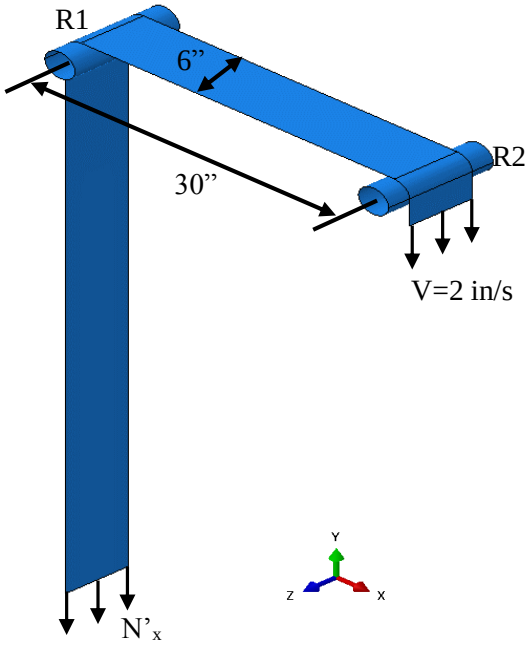

Figure 7.5 – FE Model of a Laminate Transiting Two Align Rollers

Another simulation was set up as the laminated web transit over two aligned rollers. The laminated web has the same material properties and thickness as shown in Table 7.1. In Figure 7.5, the web width is 6 in and the span length between two rollers is 30 in. The MD tension was applied at the left end of the web and velocity at the right end. The web will move from left to right in the

simulations. The two cylindrical rollers can only rotate about the z axis. The friction coefficient between the web and the roller is 0.3. The web was meshed by shell element S4R and the converged mesh density is 0.25”×0.25”. The whole web has 9,775 nodes and 9,360 elements. There are two steps in this simulation: Pretension step has 1 second, and Move step has 30 seconds. The web tension increases in the first step and then keeps constant until the end. The web velocity at the right end increases to the 2 in/s in 1 second and then keep constant.

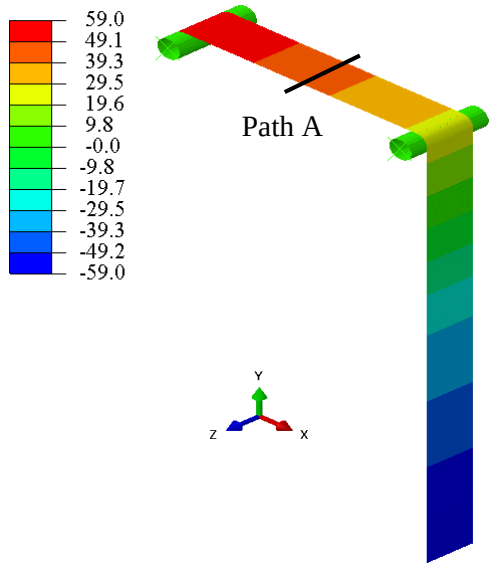

Figure 7.6 – Displacement in Y Direction for N'_x = 1.9 pli

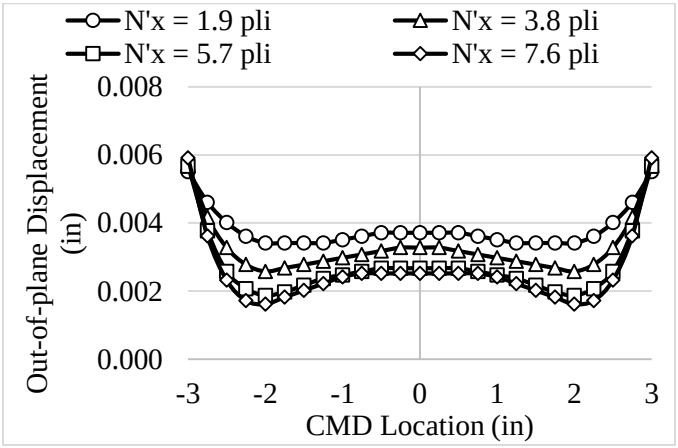

Figure 7.7 – Out-of-plane Deformations Across Web Width Along Path A

Figure 7.6 shows the y displacement of the web at the end of the simulation when the MD load is 1.9 pli. In the web span between two rollers, the y displacement is the sum of web out-of-plane deformation and the MD distance due to web tension and velocity. The MD distance is the same for web nodes on a CMD path which have the same MD locations. The web span has the similar out-of-plane deformation along the CMD path at the macro level. However, the out-of-plane deformation along Path A shows the web has troughs under varied MD tensions in Figure 7.7. Path A is indicated by the black line in Figure 7.6. The deformed shape of this laminated web span is similar to the web coupon in Figure 7.4. In Figure 7.7, the moving web with web tension 7.6 pli has a maximum distance for the out-of-plane displacement 0.0044 in, while the maximum displacement for the web coupon with simply supported edges is 0.0015 in Figure 7.4. The simply supported edges were constrained from deforming in the out-of-plane direction. The free web edges in Figure 7.5 have nonzero out-of-plane deformations in Figure 7.7.

Both simulations in this section show the fact that we can induce troughs in a laminate with the disturbance being only the difference in lamina properties. The CMD compression is not required to generate troughs for a laminated web coupon with simply supported edges. Roller imperfections such as misalignment, and taper are not required for a laminated web to have troughs. In order to acquire a plane surface for the laminated web without buckling, clamped edges will be used and discussed in next section.

7.3 Troughs in a Two-layer Orthotropic Web Span with Clamped Edges

The simulation has the same structure dimension and material as the model in Figure 7.2. There are two steps in this simulation. The web reaches to the desired MD stress level in the first step by applying MD edge load N'_x at two opposite ends. In the second step, the MD edge load keeps constant, and the CMD compression applied at other two edges increases until troughs were observed. The web in Figure 7.8 was meshed by shell element S4R with converged mesh density

0.25”×0.25”. Unlike the model in Figure 7.2 which has simply supported edges, this model in Figure 7.8 has clamped edges. All edges are not totally clamped, they are free to deform and translate in MD direction and CMD direction. However, out-of-plane deformation and rotation are not allowed at web edges.

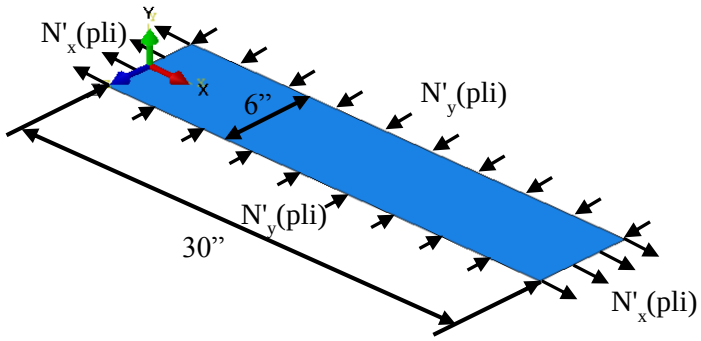

Figure 7.8 – FE Model of a Laminated Web Span with Clamped Edges

At the end of the first step, this laminated web reaches to the steady state condition with the MD load N'_x applied at web edges (x = 0” and x = 30”). Figure 7.9 is the out-of-plane displacement of the laminated web when N'_x is 1.9 pli. The web has a nearly plane surface as the deformation range is very small (-1.0×10^{-14} to 1.0×10^{-14} in). The clamped edge boundary condition provides us the desired shape of the laminate.

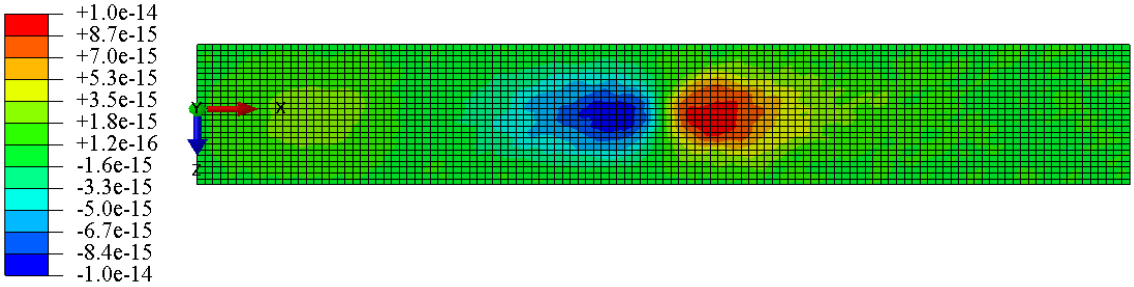

Figure 7.9 – Out-of-plane Deformations of the Laminated Web with Clamped Edges (N'_x = 1.9 pli)

The MD stress level in each lamina affected by the edge load N'_x and the material properties. The laminated web has two layers as shown in Figure 7.10. Lamina1 is the paper and Lamina2 is the polymer. There are 6 surfaces across web thickness where ABAQUS reported stresses. Although the surfaces z3 and z4 share the same plane, they belong to different lamina.

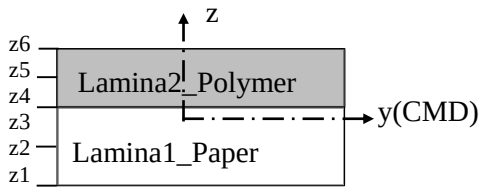

Figure 7.10 – Six Surfaces of a Two-layer Laminate

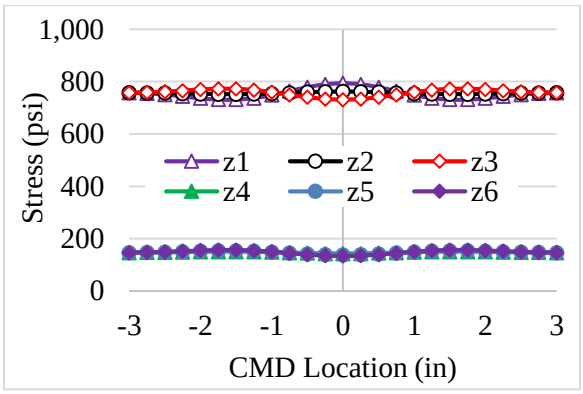

Figure 7.11 –MD Stresses of a Laminate Across Web Thickness at x = 30" (N'_x = 1.9 pli, N'_y = -0.0167 pli)

The uniform MD edge load N'_x was applied on the edges of the laminated web. The webs were strain matched at the laminator, so the lamina have common MD strain but different MD stresses due to their unique properties. The strain match condition of two laminas causes the lamina with a higher modulus to have a higher MD stress level as the laminate under the same MD load N'_x. The paper lamina has a higher modulus in MD and CMD compared with polymer (Table 7.1). The MD stresses in the paper were plotted on surfaces z1 to z3 in Figure 7.11 and are larger than the stresses in the polymer (i.e. z4 to z5). The ratio of the stresses in paper and in polymer 750/150

= 5.0 is close to the ratio of the MD modulus of the paper and polymer 1,722,933/337,652 = 5.1. The total load at one end of the web (x = 30") was calculated as 11.396 lb by integrating the MD stress over web width and thickness, which is 11.396/6 = 1.899 pli. This uniform load in very close to the MD edge load applied on the web 1.9 pli, within a relative error 0.05%.

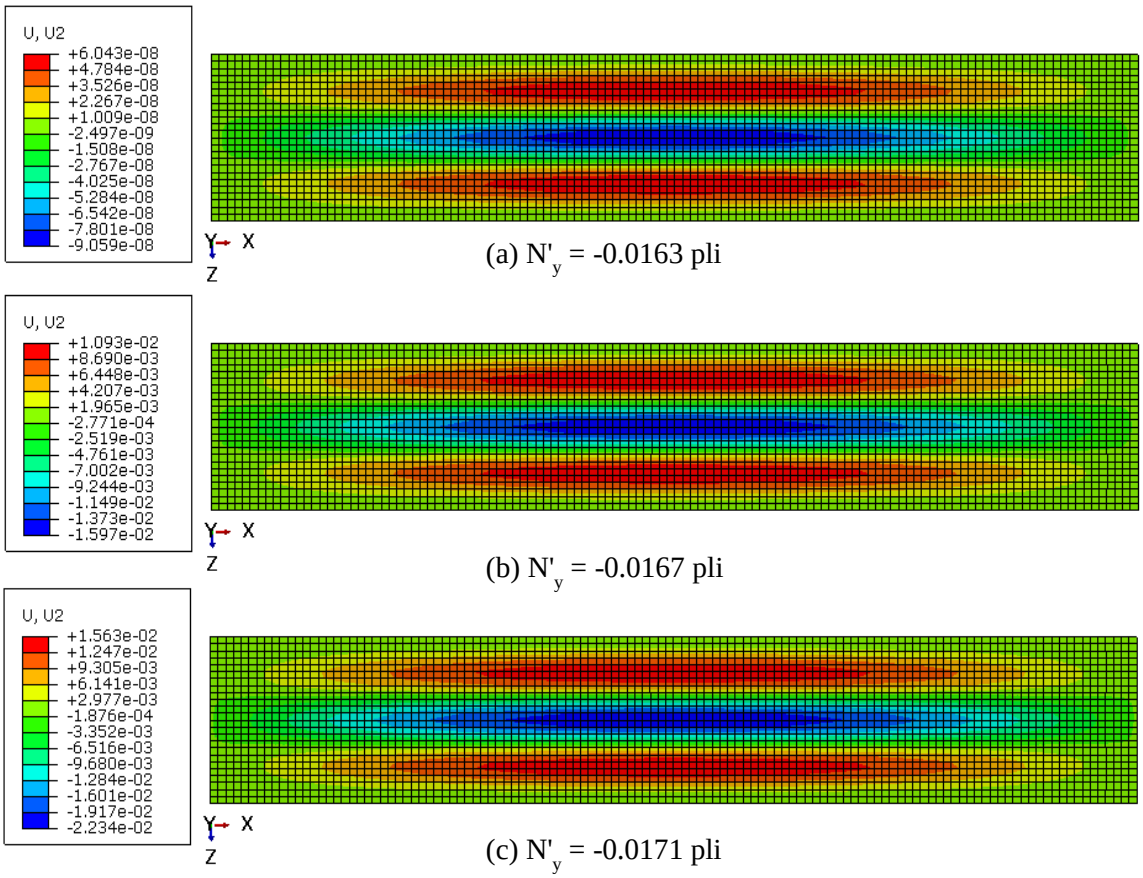

Figure 7.12 –Out-of-plane Deformations of a Laminate (N'_x = 1.9 pli)

The trough formation in this laminate is dependent on the compressive CMD load N'_y applied at web edges. As shown in Figure 7.12(a), the laminated web has out-of-plane deformations even under a small CMD compression -0.0163 pli, however, these deformations are very small compared to the laminate thickness, the range is between -9×10^{-8} to 6×10^{-8} in. The clear troughs were presented in Figures 7.12 (b) and (c) with more compression in CMD. Figure 7.13 plotted the out-of-plane displacements across web width at mid-span (x = 15") for three CMD compressions:

-0.0163 pli, -0.0167 pli, and -0.0171 pli. The critical CMD compressive load N'_{ycr} was found to be -0.0167 pli for the onset of troughs when the MD edge load is 1.9 pli. After buckling, the trough amplitude grew larger with increased CMD compressive load.

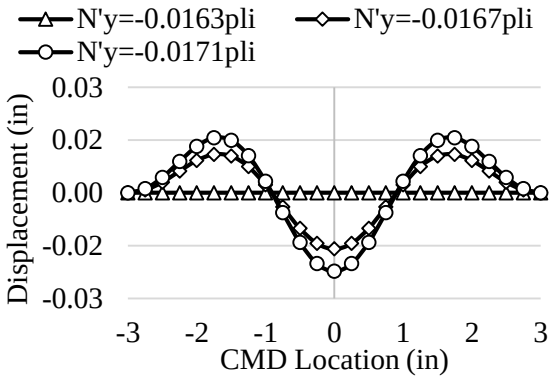

Figure 7.13 –Out-of-plane Deformations Across Web Width (N'_x = 1.9 pli)

Table 7.2 – The Critical CMD Loads for a Two-layer Laminate

MD Edge Load N'_x (pli)	Critical CMD Compressive Load N'_y (pli)	
	ABAQUS	Eq. (7.6) [Eq.-Approx.]
1.9	-0.0167	-0.1041 [-0.0138]
3.8	-0.0232	-0.0226 [-0.0195]
5.7	-0.0274	-0.0243 [-0.0238]
7.6	-0.0312	-0.0290 [-0.0275]

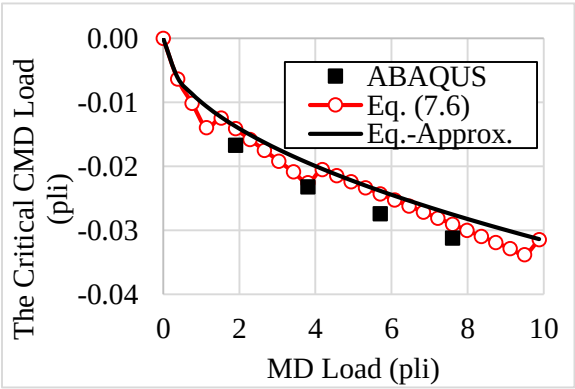

Figure 7.14 – The Critical CMD Loads for Troughs in a Two-layer Orthotropic Web Span with Clamped Edges

The critical CMD compressive loads for various MD tensions were acquired in simulations and compared with the closed form results as shown in Table 7.2. It is not a perfect match, but the agreement is good. Note the boundary conditions for the model to develop the expressions are not the same with the model in the simulations. This clamped laminated web in simulation requires a larger CMD compression to induce troughs. Equation (7.6) provides the exact critical CMD load for troughs considering the positive integer of half wave number in expression (7.7). The values in square brackets (i.e. Eq.-Approx.) are the approximate results from expression (7.8). The exact result is not as continuous as the approximate result as shown in Figure 7.14, but they are similar for all MD tensions. Considering the simplicity of equation (7.8), the approximate critical CMD load for troughs will be employed for following sections.

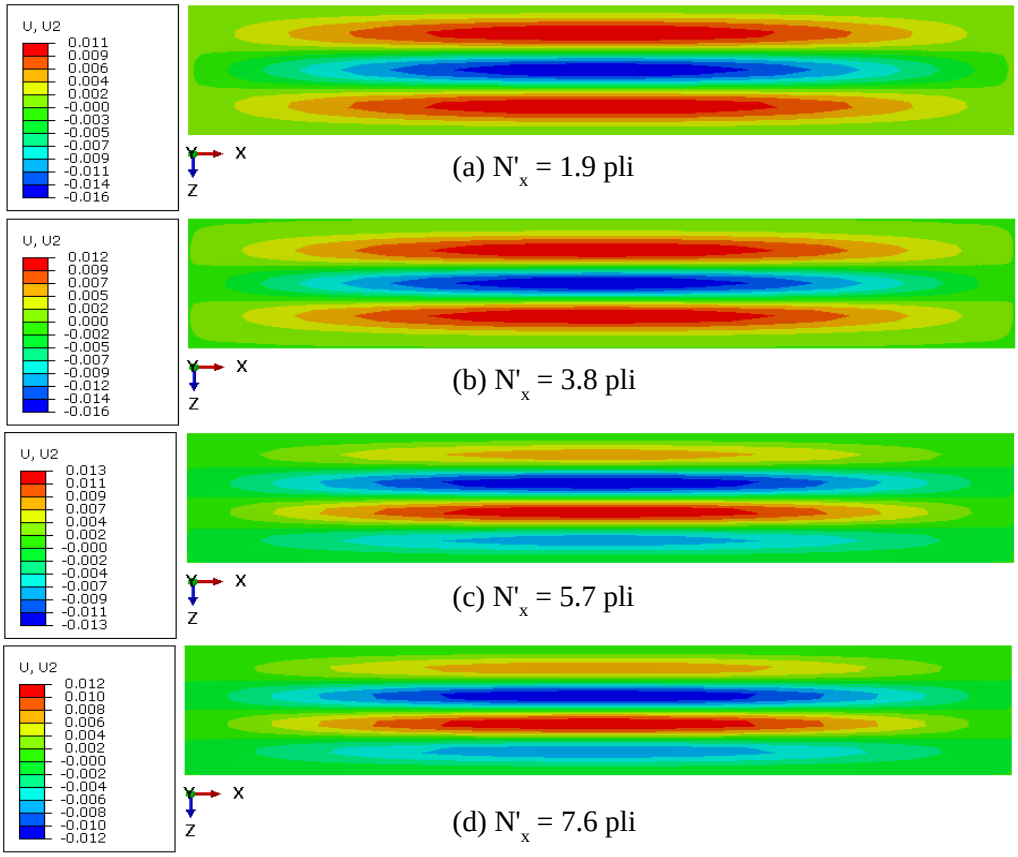

Figure 7.15 – Troughs in a Laminate Under Various MD Tensions

To generate troughs in a laminate, more CMD compression was required if the MD tension increased. The single layer web demonstrated similar phenomenon as shown in Table 6.1. The buckling occurs in a laminate away from edges as presented in Figure 7.15. The largest trough amplitude appears at web center for various MD tensions, while the wavelength of troughs is uniform across web width.

Table 7.3 –Wavelength and Amplitude of Troughs for a Two-layer Laminate with Clamped Edges

MD Edge Load N'_x (pli)	Wavelength λ (in)		Amplitude A_{mn} (in)	
	Eq. (7.9) [Eq.- Approx.]	ABAQUS	Eq. (7.16)	ABAQUS
1.9	4 [3.61]	3.50	0.0106	0.0135
3.8	4 [3.04]	3.00	0.0125	0.0139
5.7	3 [2.74]	2.75	0.0139	0.0132
7.6	3 [2.55]	2.75	0.0149	0.0119

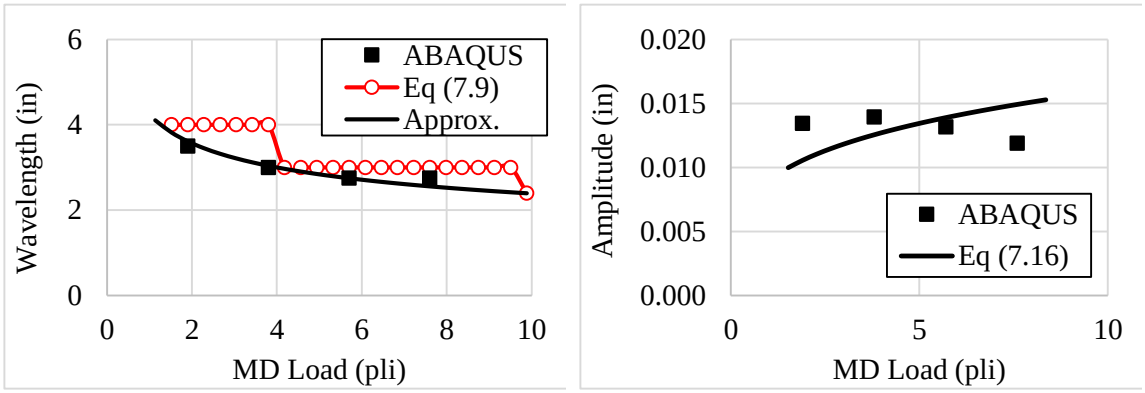

(a) Critical CMD Stress (b) Wavelength

Figure 7.16 – Wavelength and Amplitude of Troughs for a Two-layer Laminate with Clamped Edges

The half wave number from expression (7.7) increases with web MD tension, which results in a small wavelength of troughs. The exact wavelength from Equation (7.9) requires the integer value of half wave number n, and the approximate wavelength is determined by the real number of

n. In the simulation, the wavelength and amplitude of troughs are determined by the web out-of-plane deformations as plotted in Figure 7.13. The approximate wavelength compares well with the simulation results in Figure 7.16(a) and Table 7.3. The boundary conditions and external loads of the model to develop equation (7.16) are not the same as the one in the simulation. For amplitude in Figure 7.16(b), the order of the magnitude is the same for expression and simulation.

The failure criterion for a laminated web to generate troughs (7.6) (7.8) was developed and validated by finite element simulations in Table 7.2. The expressions for the wavelength (7.9), and amplitude of troughs (7.16) provide reasonable values as compared with the simulation results in Table 7.3. The simulations contain a web span between two rollers, and all edges are clamped. Uniform MD tension applied at web two ends, and troughs formed in a laminate due to a CMD compression. In industry a web needs to pass over multi-rollers to form to a final product, tension and velocity are controlled by the winding roller, unwinding roller, nip roller, etc. The CMD compressive stress could be generated and controlled in a web line as the web passes over a misaligned roller. With the expression for the critical CMD load N'_{ycr} to induce troughs in a laminate we can now employ it for a case where the web is moving. The expression to predict the degree of misalignment of downstream roller at which troughs should form will be developed and explored with finite element analysis.

7.4 Troughs in an Orthotropic Laminated Web due to Roller Misalignment

Prior to trough formation a laminated web can be treated as a beam as shown in Figure 2.1. The sign convention of the loads and displacements was shown in Figure 2.2. The stiffness matrix in expression (7.18) relates the applied loads N and moments M on the web beam to the lateral deformations v and slopes θ in a web span between two rollers i and j.

$$\begin{Bmatrix} N_i \\ M_i \\ N_j \\ M_j \end{Bmatrix} = \begin{bmatrix} \frac{12E_xI}{L^3(1+\phi)}+\frac{6T}{5L} & \frac{6E_xI}{L^2(1+\phi)}+\frac{T}{10} & -\frac{12E_xI}{L^3(1+\phi)}-\frac{6T}{5L} & \frac{6E_xI}{L^2(1+\phi)}+\frac{T}{10} \\ \frac{6E_xI}{L^2(1+\phi)}+\frac{T}{10} & \frac{(4+\phi)E_xI}{L(1+\phi)}+\frac{2TL}{15} & -\frac{6E_xI}{L^2(1+\phi)}-\frac{T}{10} & \frac{(2-\phi)E_xI}{L(1+\phi)}-\frac{TL}{30} \\ -\frac{12E_xI}{L^3(1+\phi)}-\frac{6T}{5L} & -\frac{6E_xI}{L^2(1+\phi)}-\frac{T}{10} & \frac{12E_xI}{L^3(1+\phi)}+\frac{6T}{5L} & -\frac{6E_xI}{L^2(1+\phi)}-\frac{T}{10} \\ \frac{6E_xI}{L^2(1+\phi)}+\frac{T}{10} & \frac{(2-\phi)E_xI}{L(1+\phi)}-\frac{TL}{30} & -\frac{6E_xI}{L^2(1+\phi)}-\frac{T}{10} & \frac{(4+\phi)E_xI}{a(1+\phi)}+\frac{2TL}{15} \end{bmatrix} \begin{Bmatrix} v_i \\ \theta_i \\ v_j \\ \theta_j \end{Bmatrix} \quad (7.18)$$

where the shear deformation parameter $\phi = \frac{12E_xI}{G_{xy}A_sL^2}$, area moment of inertia $I = \frac{tW^3}{12}$, the area of the cross section subject to shear $A_s = \frac{5tW}{6}$, and t is the total thickness of the laminate.

There are several boundary conditions based on assumptions. If the roller at x = 0 is the upstream roller i, the lateral deformation of the web entering the span v_i was assumed to be zero:

$$v_i = 0 \quad (7.19)$$

The web was assumed to exit the upstream roller with shearing deformation due to the downstream misaligned roller:

$$\theta_i = \frac{N_j}{G_{xy}A_s} \quad (7.20)$$

The angle of the misaligned roller θ_j was known and the elastic axis of the web at entry to the misaligned roller has that slope due to the normal entry. From the stiffness matrix in expression (7.18) we can now solve for the lateral deformation of the web v_j as it enters the downstream roller (x = L) and the force N_j that must be sustained by friction for the boundary conditions quoted to be valid.

$$N_j = \frac{A_sG_{xy}\left[240E_x^2I^2+3T^2L^4(1+\phi)+8E_xITL^2(13+3\phi)\right]}{240E_x^2I^2+TL^4\left(2A_sG_{xy}+T\right)(1+\phi)+8E_xIL^2\left(15A_sG_{xy}-T(2-3\phi)\right)}\,\theta_j \quad (7.21)$$

Expression (7.21) is valid until the downstream roller is misaligned to the extent that web edge slackness occurs at the upstream roller. This lateral force N_j induces an average shear line load in the web, $N_{shear,applied}$:

$$N_{shear,applied} = \frac{N_j}{W} = \frac{A_s G_{xy}\left[240E_x^2I^2+3T^2L^4(1+\phi)+8E_xITL^2(13+3\phi)\right]}{240E_x^2I^2+TL^4\left(2A_sG_{xy}+T\right)(1+\phi)+8E_xIL^2\left(15A_sG_{xy}-T(2-3\phi)\right)}\ \frac{\theta_j}{W} \quad (7.22)$$

The critical shear load associated the critical CMD load (7.8) to induce troughs can be calculated by using a Mohr's circle approximation:

$$N_{shear,critical} = \sqrt{\left(\frac{N'_x}{2}-N'_{ycr}\right)^2-\left(\frac{N'_x}{2}\right)^2} \quad (7.23)$$

By equating $N_{shear,applied}$ with $N_{shear,critical}$ and solve for the misalignment of the downstream roller that should induce troughs:

$$\theta_{LaminateTrough} = \frac{N_{shear,critical}W}{CON} \quad (7.24)$$

where $CON = \frac{A_s G_{xy}\left[240E_x^2I^2+3T^2L^4(1+\phi)+8E_xITL^2(13+3\phi)\right]}{240E_x^2I^2+TL^4\left(2A_sG_{xy}+T\right)(1+\phi)+8E_xIL^2\left(15A_sG_{xy}-T(2-3\phi)\right)}$. For the orthotropic laminated webs, the bending stiffness in the stiffness matrix (7.18) is replaced by an equivalent stiffness E_xI [69]:

$$E_xI = \sum_{k=1}^{N}(E_x)_k(I)_k \overset{N=2}{=} (E_x)_1(I)_1+(E_x)_2(I)_2 \quad (7.25)$$

where $(E_x)_k$ is the modulus in direction x of the k^{th} lamina, and $(I)_k$ is the area moment of inertia of the kth layer relative to the middle plane. The shear modulus G_{xy} and Young's modulus E_x in expression (7.24) are determined by expression (7.26) [70], only a laminate with two layers was considered.

$$E_x = (E_x)_1 V_1 + (E_x)_2 V_2$$
$$G_{xy} = \frac{(G_{xy})_1 (G_{xy})_2}{(G_{xy})_1 V_2 + (G_{xy})_2 V_1} \tag{7.26}$$

where $V_1 = \frac{t_1}{t_1+t_2}$, and $V_2 = \frac{t_2}{t_1+t_2}$. t_1 and t_2 are the thicknesses of the Lamina1 and Lamina2 as shown in Figure 7.1, respectively.

The critical misalignment of the downstream roller $\theta_{LaminateTrough}$ in expression (7.24) is based on the assumption that the web does not have slackness prior to trough formation. The slack edge will occur as the compressive bending stress that resulted from the misaligned roller exactly cancel the nominal tensile stress due to web tension. If the slack edge occurs prior to the buckling in the web span, the expression (7.24) to predict the critical misalignment may not accurate. The critical misaligned angle of the downstream roller needed to generate web slackness must be determined. For a web span with a downstream misaligned roller the bending strains are maximum as the web exits the upstream roller:

$$\varepsilon_{bending} = \frac{My}{E_x I} = \frac{\left(\frac{2E_x I\theta_j}{L}\right)\frac{W}{2}}{E_x I} = \frac{W}{L}\theta_j \tag{7.27}$$

The uniform strain in a two-layer laminated web due to web tension will be:

$$\varepsilon_{tension} = \frac{N'_x}{(E_x)_1 t_1 + (E_x)_2 t_2} \tag{7.28}$$

The web slackness will appear as the misalignment of the roller generate the bending strain larger than the uniform tensile strain. The misalignment at which the onset of a slack edge occurs can be found by equating the strains in expression (7.27) and (7.28):

$$\theta_{LaminateSlack} = \frac{L}{W}\left(\frac{N'_x}{(E_x)_1 t_1 + (E_x)_2 t_2}\right) \tag{7.29}$$

Both finite element simulations and tests will be employed to validate the accuracy of the expressions for the critical misaligned angle of the roller for troughs (7.24) and for slack edges (7.29). The High Speed Web Line (HSWL) in the Web Handling Research Center of Oklahoma State University will be used for verification. Web tension and web span length variables were explored to verify the expression for the critical roller misalignment (7.24) which will produce troughs prior to slack edge behavior on HSWL. The maximum tension that can be operated on HSWL is 90 lb, and the maximum test span length is 51 inches.

The laminated web material properties and thickness were presented in Table 7.1 and was chosen for the simulations and tests. This two-layer laminate has one paper layer and one polymer layer. This is a reasonably thick web with high modulus layers. The web was tested to withstand load larger than 100 lb without delamination or rupture on the Instron machine[10].

An angle difference variable θ_{Diff} (radian) was introduced to search for a realm of web tension T (lb) and span length L (in) that will produce troughs prior to slack edge behavior. θ_{Diff} is the critical angle for slack edge (7.29) minus the critical angle for troughs (7.24) :

$$\theta_{Diff} = \frac{L}{W}\left(\frac{N'_x}{(E_x)_1 t_1 + (E_x)_2 t_2}\right) - \frac{N_{shear,critical} W}{CON} \tag{7.30}$$

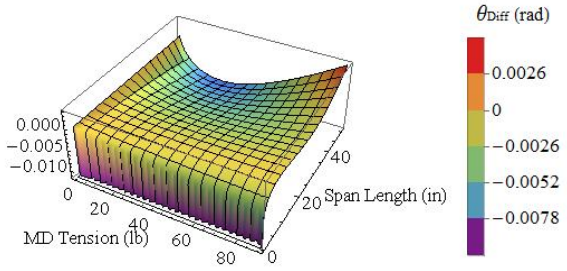

Figure 7.17 –Angle Difference for a Laminate

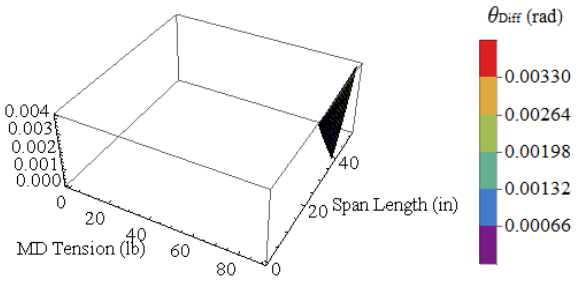

Figure 7.18 –Positive Angle Difference for a Laminate

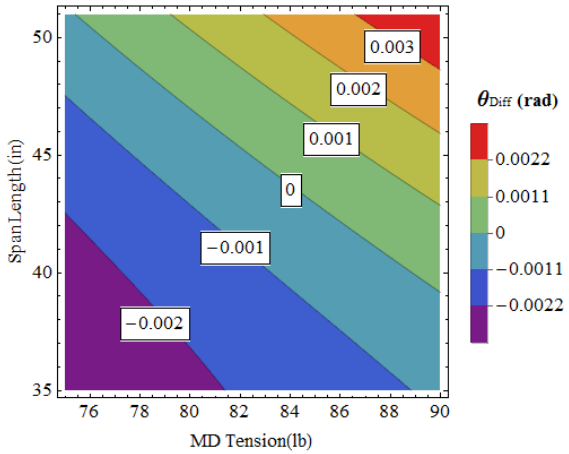

Figure 7.19 – Contour Chart of the Positive Angle Difference

The domains of web tension and span length where θ_{Diff} was positive were explored. Although there is no linear relation between the web tension and span length with θ_{Diff}, the plot in Figure 7.17 showed θ_{Diff} becomes largest for high web tension (~90 lb) and long span lengths (~51 in). The angle difference is 0.004 rad at this point. The positive θ_{Diff} in Figure 7.18 indicated the appropriate web tension and span length is limited. Better definition of the realm where θ_{Diff} is positive is provided contour chart in Figure 7.19. The positive region is a triangle. At a tension of 76 lb a span length of 51 in is needed. At a tension of 90 lb the span length could decrease to 39 inches. The web tension of 80 lb and a span length of 50 in were chosen for the following simulations and tests. According to expression (7.24) and (7.29), the critical angle for troughs is 0.025 rad, and the critical angle for slackness is 0.026 rad, θ_{Diff} = 0.026 – 0.025 = 0.001 rad. Note

the angle difference is small compared with the critical angles. The following sections will focus on two verification simulations with test setup: static and dynamic.

7.5 Static Analysis of Troughs in a Laminated Web due to a Lateral Deflection

Static simulations and tests will be used to validate the expression for troughs (7.24). The web was supplied by Avery Dennison[11] with material properties in Table 7.1. A coupon was used to simulate the laminated web span between an aligned roller and a misaligned roller. The simulation model has the left end (Figure 7.20) totally fixed where the web exits the aligned roller and the right end was subjected to 80 lb tension and a lateral deflection v_L. This CMD deflection could be induced by a misaligned roller but was an input as a displacement in these simulations. The web span before deformation was shown in Figure 7.20(b), and the undeformed web would bend to the deformed web Figure 7.20(a) due to a misaligned roller at the right side. The rollers were not considered in this model. The web was assumed to follow the normal entry rule without any slippage on the rollers. The right end can translate in MD and CMD directions with free rotation about y axis. Shell elements S4R were utilized to mesh the web. The converged mesh density was found to be 0.25”×0.25”.

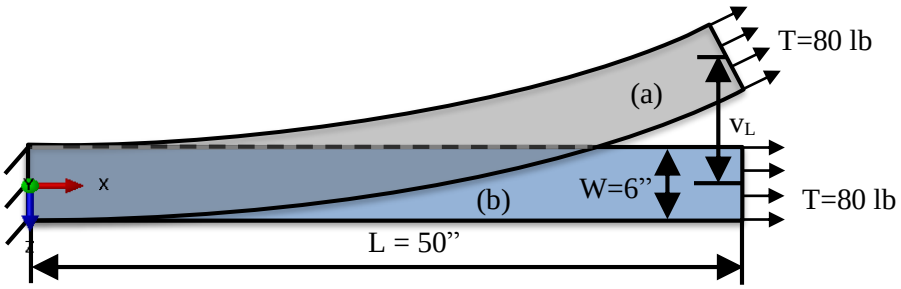

Figure 7.20 – FE Model of the Static Simulation

The relation between the roller misalignment and the lateral deflection at the entry to the misaligned roller was shown in expression (5.4) with x = L. If the web span has width W, length

L, MD tension T, the lateral deflection at x = L (i.e. v_L) is presented in expression (7.31) as the misaligned angle is θ.

$$v_L = \frac{L(\lambda \cosh \lambda - \sinh\lambda)}{\lambda(\cosh\lambda - 1)}\theta \tag{7.31}$$

where $\lambda = \sqrt{TL^2/E_xI}$, and E_xI was defined in expression (7.25) for a laminate.

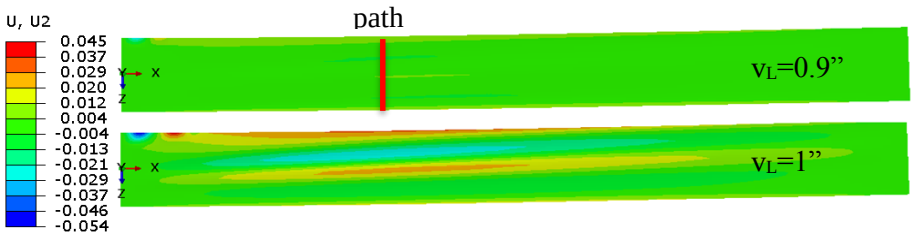

Figure 7.21 – Out-of-plane Deformations of a Laminate due to Lateral Deflections

Expressions (7.24) and (7.29) predicted the critical misalignment angle for troughs is 0.025 rad, and 0.026 rad for slack edges. According to expression (7.31), the corresponding v_L are 0.87 in and 0.9 in, respectively, for those angles. The out-of-plane deformations from simulations were shown for two different lateral deflections 0.9 in and 1 in in Figure 7.21. The web has clearly troughed as v_L approached 1 in, close to the expression result 0.87 in. Note the critical lateral deflection of troughs is 1 in from simulations which is larger than the expression value for the slackness 0.9 in.

The out-of-plane deformations across web width were plotted for various v_L (0.8”~1.2”) in Figure 7.22. The path was built at 1/3 web length as indicated by the red line in Figure 7.21. The amplitude of troughs would increase with the lateral deflection that was applied at the right end of the web span. The small deflections at web edge (z = -3”) as v_L are 0.8” and 0.9” indicated the web had a curled edge before troughs, and this curl increases with increased v_L.

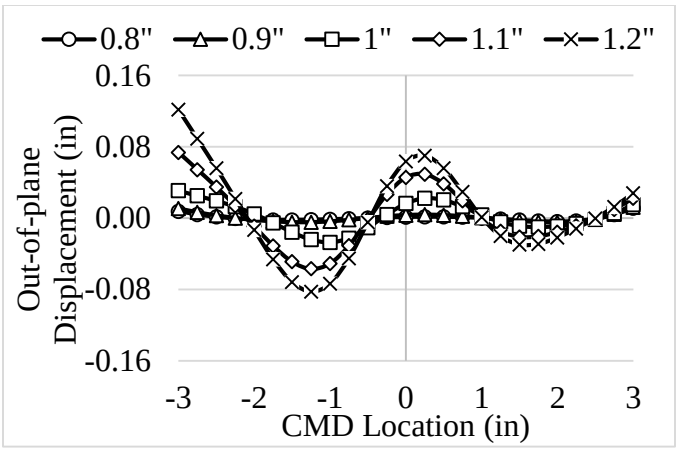

Figure 7.22 – Out-of-plane Deformations Across Web Width due to Lateral Deflections

The onset of slack edge is difficult to observe in tests, but it is easy to determine in simulations. For the laminated web, if all laminae have zero or negative MD membrane stresses at certain point, it means the laminate has slackness at this location. The laminated web used herein only has two layers – paper and polymer. In simulations, the lateral deflection was applied at the right end of the web span, the slack edge will occur at the left end of the web, where the moment is maximum. A range of v_L deformations were applied to the web in the simulations. As v_L approached 0.9 in the web span near zero MD membrane stress resulted in both laminae near the left end. Figure 7.23(a) displays the MD membrane stresses for the paper layer and the polymer layer when v_L is 0.9 in. The maximum moment at web left end is resulted from the uneven MD stresses, both maximum and minimum MD stresses appear at this left end of the web. The internal moment in the web decreased to the right side as the stresses tend to be uniform. The web in the red box was zoomed in Figure 7.23(b). The black contour indicated zero or negative MD stresses. The web has a slack edge as both laminae have zero/negative MD membrane stresses at the same location.

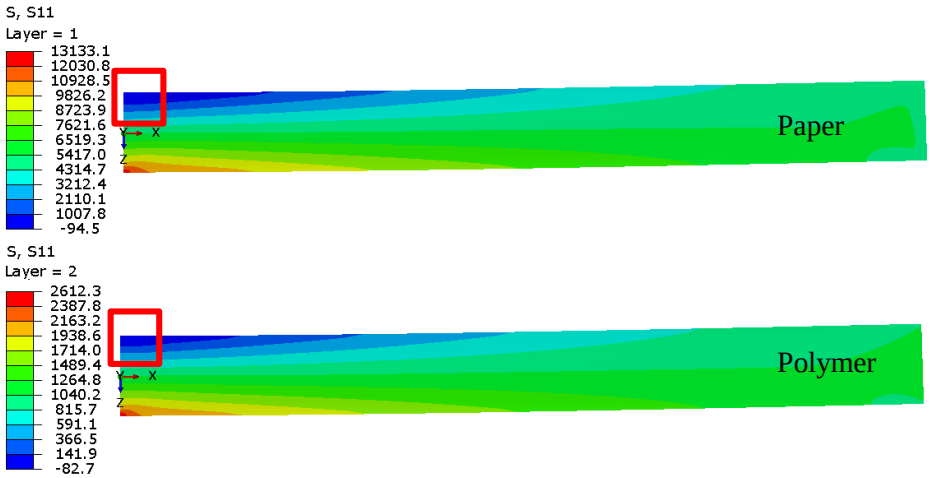

(a) Whole Web Span

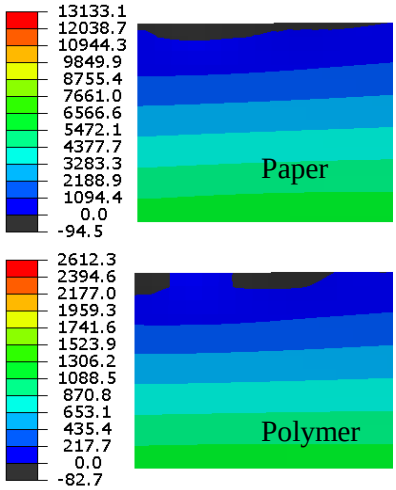

(b) Zoomed Web in Red Box

Figure 7.23 – MD Stresses of a Laminate due to a Lateral Deflection (v_L = 0.9 in)

In simulations, the slack edges appeared as the lateral deflection applied at the right end of the web approached to 0.9 in. To determine the onset of troughs in tests, a specimen with similar boundary conditions as the model in Figure 7.20 was created. Both simulations and tests used the same laminate. The test set up is shown in Figure 7.24, a laminate coupon 50 in long and 6 in wide was clamped at two ends. A dead weight of 80 lb was applied through a pin joint to the clamped web end to simulate web tension. The lateral deflection v_L was increased manually from zero by

pulling the rope attached to the web clamp until the troughs could be observed visually. A micrometer at the opposite side of the web measured the lateral deflection when web troughs first occurred. These measurements were repeated 3 times. The rope and micrometer exchanged sides and the tests were repeated and the results were averaged. The critical v_L for the onset of web troughs was 0.95 in as shown in Table 7.4, it is close to the expression result (i.e. 0.87 in), and the simulation result (i.e. 0.9 in).

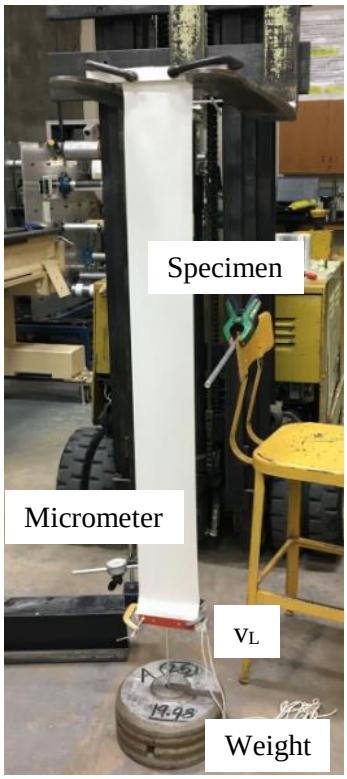

Figure 7.24 – Test Setup

Table 7.4 –Tests of Troughs in a Two-layer Laminate due a Lateral Deflection

	Lateral Deflection for Troughs (in)		
Micrometer at Left Side	1.0	1.03	0.95
	1.0		
	1.1		
Micrometer at Right Side	0.8	0.87	
	0.9		
	0.9		

Expression (7.24) predicted the web should generate troughs as the misalignment approached 0.025 rad, and expression (7.31) was used to provide the lateral deflection associated with this misalignment angle, i.e. 0.87 in. Both simulations and tests studied a web coupon without rollers, the interaction between the web and the roller was not considered. The lateral deflection v_L was directly measured in the simulation and test, and the corresponding angle was calculated by expression (7.31). A slack edge should occur after the troughs according to expression (7.29). However, slack edges appeared before troughs in the simulation. Note that the angle difference θ_{Diff} from expressions (7.30) is only 0.001 rad (0.026 - 0.025) thus it is not surprising that the slack edge was witnessed slightly prior to troughs. Table 7.5 showed the critical angles for troughs from the expressions, simulations and tests do not match exactly but the differences are small and provide one form of verification.

Table 7.5 –Static Trial for Troughs in a Two-layer Laminate due a Lateral Deflection

	v_L (in)	θ_{Trough} (rad)
Expression	0.87	0.025
Simulation	1.00	0.029
Test	0.95	0.027

The static simulations and tests indicated troughs formed in a web span with a lateral deflection imposed at the web end. This lateral deflection resulted from the roller misalignment that can be calculated from expression (7.31). The direct misaligned angle of a downstream roller will be explored in simulations and tests. The dynamics trial for the trough and slackness formation in a laminate is necessary to validate the accuracy of expressions (7.24) and (7.29).

7.6 Dynamic Analysis of Troughs in a Laminated Web due to a Misaligned Roller

The model for the dynamic simulation is shown in Figure 7.25. The web would move from the left to the right and the third roller R3 is the misaligned roller. Other rollers R1, R2 and R4 are

aligned and can only rotate about their axes. The model has the same tension and span length as used for the static simulations. The web tension 80 lb was applied at the upstream end and MD velocity was applied at the downstream end. The span length between R2 and R3 is 50 inches. The web is the same laminate used in static tests. The material properties and thickness of the laminae were shown in Table 7.1. Sufficient web length was modelled prior to R1 to allow 4 time constants of web to pass through the 50" span and over the misaligned roller and achieve a steady state lateral behavior. The shell element S4R was used for the web and all rollers are rigid body. The element size was found to be 0.25"×0.25" with converged results and efficiency. In order to prevent any slippage for the web on the roller, the friction coefficient between the rollers and the web was assumed to be 4. This section will explore if a laminate web will have troughs as a downstream roller misalignment angle approaches the predicted value from expression (7.24), as well as the slack edge formation as the misalignment reaches to the value predicted from expression (7.29).

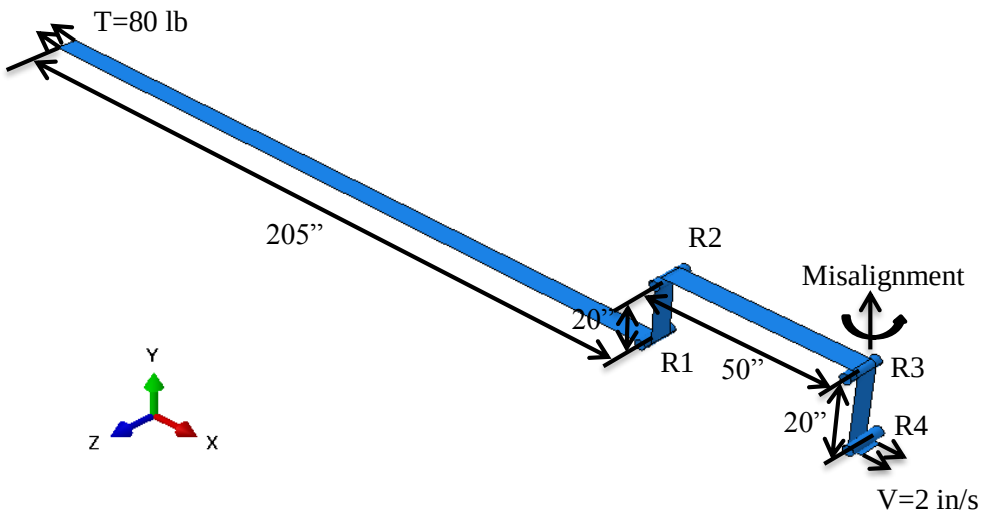

Figure 7.25 – FE Model of a Laminate Transiting a Misaligned Roller

The out-of-plane deformation of the laminate between R2 and R3 was shown in Figure 7.26. The misalignment angle of R3 is 0.03 rad in Figure 7.26(a) and 0.035 rad in Figure 7.26(b). The rollers were not shown. The deformation scale factor in y direction was increased to 20. The troughs were hardly seen for the misalignment angle of 0.03 rad. The critical angle to generate

troughs is 0.035 rad in simulations. Recall expression (7.24) predicted troughs would begin at 0.025 rad, and onset of slack edge at angle 0.026 rad by expression (7.29). These predicted angles are less than the critical angle for troughs found in simulation (i.e. 0.035 rad).

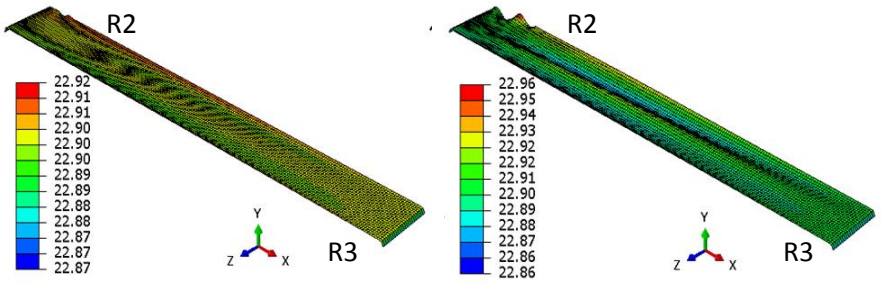

(a) 0.03 rad (b) 0.035 rad

Figure 7.26 – Out-of-plane Deformations Between R2 and R3

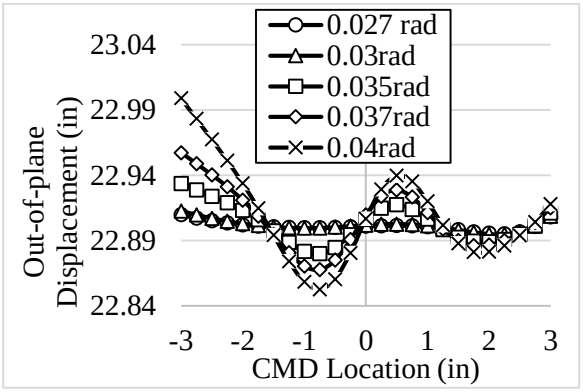

Figure 7.27– Out-of-plane Deformations Across Web Width

The out-of-plane displacements across web width were plotted for various misalignments of R3 in Figure 7.27. The path was built at 1/3 web length as indicated by the red line in Figure 7.21. The web has large out-of-plane deformations at web left side (z = -3 in) as a result of web slackness, especially when the misalignment larger than 0.03 rad.

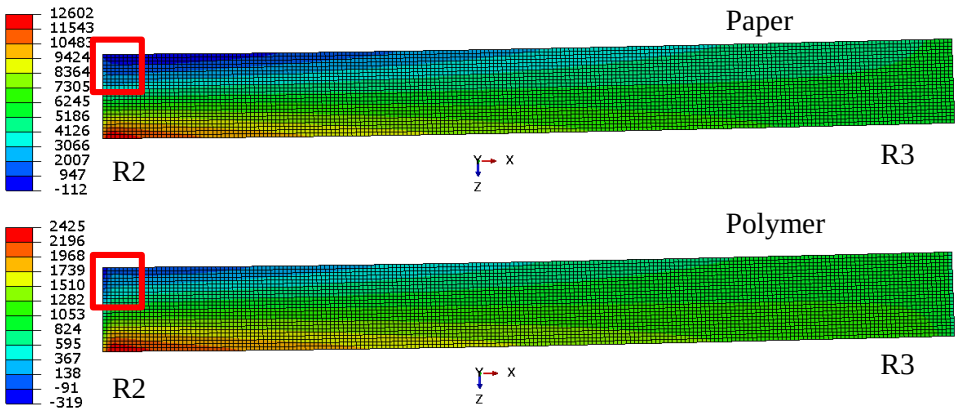

(a) Web Span Between R2 and R3

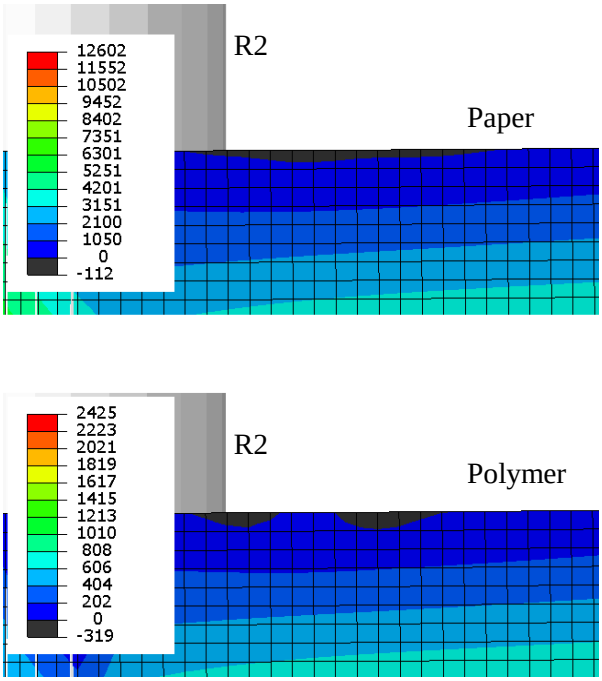

(b) Zoomed Web in Red Box

Figure 7.28 – MD Stresses of a Laminate Transiting a Misaligned Roller R3 ($\theta = 0.03$ rad)

The same procedure was used here as discussed for the static coupon to determine the onset of edge slackness in a simulation. A variety of misalignments were simulated for roller R3. When the misalignment angle reached to 0.03 rad the web span between R2 and R3 has zero/negative MD membrane stress in both laminae. Figure 7.28(a) showed the minimum MD membrane stress

appeared at the exit of R2 for both laminas, and the zoomed Figure 7.28(b) are the locations indicated by the red boxed in Figure 7.28(a). Zero MD membrane stresses appear at the same locations as indicated by the black area for both laminas. The laminated web has just achieved a slack edge at this misalignment. In the simulations, the slack edges (i.e. 0.03 rad). appear earlier than troughs (i.e. 0.035 rad). The misalignment for slackness matches well with the expression result (i.e. 0.26 rad).

A test was conducted on the high speed web line (HSWL) as the laminated web passes over a misaligned roller R3. A micrometer is used to misalign a yoke that supports Roller R3 in Figure 7.29. When a trough or slack edge was witnessed the micrometer reading was divided by the distance between the micrometer and the center of rotation of the yoke to infer the angle of misalignment. High friction tape[8] on rollers R2 and R3 was used to decrease the potential for moment transfer or slippage. The web tension was set to 80 lb and web span length is 50 inches identical to the static test and the static and dynamic simulations. The same laminate web was common to all tests and simulations in this chapter.

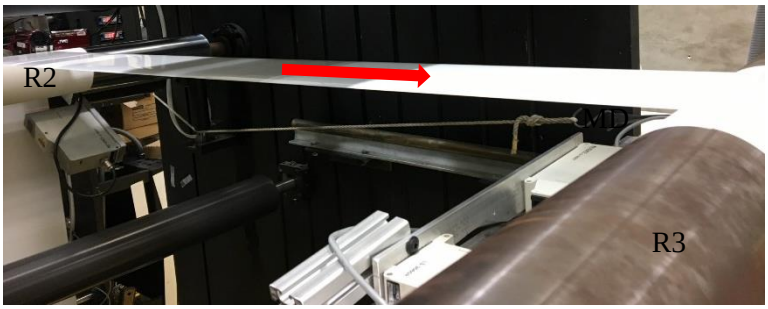

Figure 7.29 – Test on HSWL

R3 was misaligned clockwise and counterclockwise until a trough or slack edge is witnessed. The magnitudes of the misalignment were averaged to nullify the impact of web length nonuniformity in the CMD. Large troughs and slack edges can be visually observed, but determining the misalignment for their onset is difficult in tests, especially for a slack edge.

The onset of troughs can be observed in Figure 7.30 (a) from the deformed reflection of the cylinder above the web. The web in Figure 7.30(b) has a clear slack edge, the misalignment of R3 was beyond the onset to allow this to be visible.

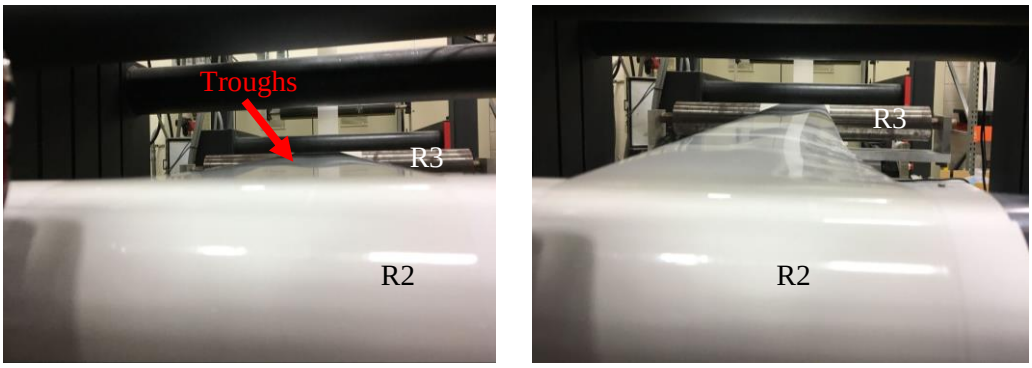

(a) Trough (b) Slack Edge

Figure 7.30 – Troughs and Slack Edges on HSWL

On the HSWL, the tram error (in) was measured using the micrometer to induce a trough or slack edge. The corresponding misalignment angle is this tram error divided by the distance between the center of rotation of the yoke supporting R3 and the micrometer (15 in). In tests, the average critical angle for the laminate to induce troughs was 0.032 rad, and the angle for the onset of a slack edge was 0.030 rad. The slack edges appear before the troughs, which was the same behavior witnessed in simulations. Table 7.6 displayed the test results from HSWL.

Table 7.6 –Critical Angles from HSWL

Test	Critical Angles (rad)									
	Trough					Slack Edge				
	Left	Right	Average	Standard Deviation	Final	Left	Right	Average	Standard Deviation	Final
No.1	0.0350	0.0339	0.034	0.001	0.032 ± 0.002	0.0300	0.0300	0.030	0.000	0.030 ± 0.001
No.2	0.0333	0.0300	0.032	0.002		0.0300	0.0283	0.029	0.001	

The critical angles for the two-layer laminate to have troughs and slack edges were shown in Table 7.7. Both static and dynamics simulations and tests were compared with the expression results. The grey background in the cells indicates the results inside were directly calculated from the expressions or measured in the test/simulations, and other numbers were harvested based on expression (7.31). All the critical angles from simulations and tests for the laminate to generate troughs and slackness are close to the expression results. The expressions predicted the web would have troughs prior slack edges, while both simulations and tests showed the troughs would appear after slack edges as web tension is 80 lb, and web span length is 51 in. Note the angle difference from the expression (7.30) is 0.001 rad, only 4.0% of the critical angle for troughs (i.e. 0.025 rad) from expression (2.24) and 3.8% of the critical angle for slack edges (i.e. 0.026 rad) from expression (2.29). The angle difference from the simulations and the tests is between 0.002 ~ 0.005 rad which is also a small percentage of the critical angles. The wavelength and amplitude of troughs from simulations compared well with the expression results in Table 7.8.

Table 7.7–Critical Angles and Lateral Deflections for Troughs and Slack Edges

	Trough		Slack Edges	
	Critical Angle (rad)	Lateral Deflection v_L (in)	Critical Angle (rad)	Lateral Deflection v_L (in)
Expressions (7.24)(7.29)	0.025	0.866"	0.026	0.901"
Dynamic Test-HSWL	0.032	1.052"	0.030	1.039”
Static Test-coupon	0.027	0.950"	None	
Dynamic Simulation-4rollers	0.035	1.280"	0.030	1.090"
Static Simulation-coupon	0.029	1.000"	0.026	0.900"

Table 7.8–Wavelength and Amplitude of Troughs in a Laminate

	Wavelength (in)	Amplitude (in)
Expressions (7.9)(7.16)	2.9	0.023
Static Simulation	3.4	0.025
Dynamic Simulation	3.4	0.019

The expression for troughs (7.24) does not account for a slack edge occurring in the derivation. Likewise, the expression for slack edge (7.29) does not account for troughs occurring first. In both cases the stresses are affected and the expressions cannot be expected to be accurate with both behaviors (slack edge & trough) being present. The differences in Table 7.7 are not bad, however, any disagreement is due to the presence of multiple behaviors.

Note the angle difference for the web to have slackness and troughs predicted by expressions is quite small 0.026 - 0.025 = 0.001 rad. Higher tension and longer span length should result in a larger angle difference, and web should have less effect from the slackness. However, larger tension will induce more slack edges before buckling, which may affect the result for troughs.

7.7 Conclusions

The trough failure criterion for the orthotropic laminated webs has been developed for a web coupon with uniform tension in the MD and compression in the CMD. Beam theory has been used to develop the expressions for critical CMD load (7.6) and (7.8) to induce troughs, the associated half wave number (7.7), and wavelength of troughs (7.9). Cerda's inextensibility claim has been used for developing the expression of trough amplitude (7.16). All laminas in a laminate are orthotropic and have the principal axes aligned with MD, CMD and out-of-plane directions.

The orthotropic laminate web span with simply supported edges and uniform MD tension and CMD compression has been simulated. A two-layer laminated web was chosen for simulations and tests. The material and thickness of the laminas are different: one layer is paper, and another one is polymer. Varied MD tensions were applied on the laminate, and the simulations provided the desired MD stress distribution in each lamina. The critical CMD loads, the wavelength, and amplitude of troughs harvested from simulation were close to the expression results as shown in Table 7.2 and Table 7.3.

The critical misaligned angles of the downstream roller for troughs (7.24) and for slackness (7.29) were developed based on the failure criterion (7.8). The high web tension (i.e. 80 lb) and long web span (i.e. 50 in) were determined for simulations and tests, troughs were expected to occur prior slack edges to satisfy the assumption for developing expression (7.24). Both static and dynamic simulations/tests were used to validate the accuracy of expressions (7.24) and (7.29). The static simulations and tests employed a lateral deflection which result from roller misalignment to generate troughs. The lateral deflections for troughs from static simulations and tests were close to the expression results in Table 7.5. The dynamic simulations and tests require the laminated web transiting four rollers. The third roller rotated until troughs or slack edges appear in the web span prior to this misaligned roller. The troughs were expected to occur before slack edge under high tension and long web span, while not accomplished in the simulations or tests. However, reasonable but not exact agreement was found with finite element simulations with expressions and tests in Table 7.7.

CHAPTER VIII

SUMMARY, CONCLUSIONS AND FUTURE WORK

8.1 Summary

The research objectives of this thesis were concerned with web instability and lateral registration error of webs transiting over rollers in process machinery. Implicit and explicit finite element simulations were used to explore registration and stability behaviors. In some cases, this exploration resulted in new findings and in others closed form solutions that can be used as predictive tools. All cases were validated by testing.

8.2 Conclusions

1. Cylindrical idler rollers were found to induce tensile spreading stresses in webs which enhance web stability. These spreading stresses were found to stem from anticlastic plate bending behavior. This spreading effect was previously unknown and has resulted in a publication [71].
2. A new curvature boundary condition (5.3D) was established for a web approaching a misaligned roller. This boundary condition was used to produce a closed form solution for the lateral deformation and registration error for a web approaching a misaligned roller (5.4). The boundary condition and the closed form solution were published [29,72].

3. A new curvature boundary condition (5.8) was established for a web approaching a roller with a linear taper in radius across its width. This boundary condition was used to produce a closed form solution for the lateral deformation and registration error for a web approaching a tapered roller (5.9). The boundary condition and the closed form solution were published [29,72].
4. Simulations of cambered webs approaching aligned cylindrical rollers established that closed form solutions for the lateral deformation and registration error do not exist. The closed form solutions cannot exist because of slippage that was observed as the web exits the upstream roller and as the web enters the downstream roller. Simulations have the capability to predict this slippage and the effect on lateral deformation and registration error. Studies of web steering due to web camber have been ongoing and fruitless for many years. These findings explain why a closed form solution for the lateral deformation and registration cannot be posed and has been published [29,72].
5. Trough web stability (7.6-7.9) and edge slackness criterion (7.27,7.28) have been established for laminated webs. These criteria were used to establish the first closed form expressions which predict troughs (7.24) and slack edges (7.29) in laminate webs as a result of downstream roller misalignment. The criteria, the closed form expressions and their validation will be the subject of a future publication.

8.3 Future Work

1. A cambered web span bounded by aligned rollers has been simulated and the results agree with test data. The simulations proved the fourth boundary condition (i.e. the deformed radius of curvature in the web entering the downstream roller) for solving the equation (5.1) requires laboratory tests or dynamic simulations. Webs must encounter many rollers in a web process line. Future research should focus on cambered webs transiting multiple rollers. It is expected that moment transfer due to slippage will occur over all rollers when

the friction between the web and rollers is low. No steady state solution is expected when the friction coefficient is large.

2. In this work both laminas in laminate simulations joined together without any tension or strain at the initial state. The laminated web has the same deformation in each layer due to the MD tension and CMD compression. In real lamination two or more webs are joined. Often MD strain matching is done in an attempt to minimize MD curl of the laminate. However, CMD strains will not match due to different material properties. Further exploration may improve the simulation model which considering lamination process for a laminate.
3. Trough formation in a laminated web span has predicted by a closed form expression and validated by simulations and tests. Wrinkles can follow the troughs when the condition gets more severe. The wrinkle criterion for single layer web has been developed. The prediction of wrinkles as a laminated web on a roller would be useful.

REFERENCES

[1]. Good, J. K., Kedl, D. M., and Shelton, J. J., "Shear Wrinkling in Isolated Spans", Proceedings of the Fourth International Conference on Web Handling, Oklahoma State University, June 1997.

[2]. Puckhaber, C. F., "Print-registration Control in a Rotogravure Printing Press Combined with Extrusion-coating or Lamination Processes", TAPPI Journal, Vol. 78, No. 3, March 1995.

[3]. Lee, C., Lee, J., Kang, H., and S, K., "A Study on the Tension Estimator by Using Register Error in a Printing Section of Roll to Roll E-printing Systems", Journal of Mechanical Science and Technology, Vol. 23, No. 1, January 2009.

[4]. Seshadri, A., Pagilla, P. R., and Lynch, J. E., "Modeling Print Registration in Roll-to-roll Printing Presses", Journal of Dynamic Systems, Measurement and Control, Transactions of the ASME, Vol. 135, No. 3, May 2013.

[5]. Noh, J., Yeom, D., etc., "Scalability of Roll-to-roll Gravure-printed Electrodes on Plastic Foils", IEEE Transactions on Electronics Packaging Manufacturing, Vol. 33, No. 4, August 2010.

[6]. Good, J. K., and Beisel, J. A., "Buckling of Orthotropic Webs in Process Machinery", Proceedings of the Seventh International Conference on Web Handling, Oklahoma State University, June 2003.

[7]. Good, J. K., and Beisel, J. A., "Calculations Relating to Web Buckling Resulting from Roller Misalignment", TAPPI Journal, Vol. 5, No. 12, December 2006.

[8]. Timoshenko, S. P., and Goodier, J. N., "Theory of Elastic Stability", 3rd Ed, McGraw-Hill, New York, 1970.

[9]. Timoshenko, S. P., and Woinowsky-Krieger, S., "Theory of Plates and Shells", McGraw-Hill, New York, 1959.

[10]. Przemieniecki, J. S., "Theory of Matrix Structural Analysis", McGraw-Hill, New York, 1968.

[11]. Eriksson, L. G., "Measurement and Control of the Web in a Newspaper Printing Press", Proceedings of the First International Conference on Web Handling, Oklahoma State University, May 1991.

[12]. Paukku, J, and Parola, M., "Measurement Method and Analysis of Dynamic Dimensional Stability of Paper Web", TAGA, 1998.

[13]. Parent, F, and Hamel, J, "Evaluating the Impact of Non-uniform Paper Properties on Web Lateral Instability on Printing Presses", Proceedings of the Twelfth International Conference on Web Handling, Oklahoma State University, June 2013.

[14]. Shelton, J. J., "Lateral Dynamics of a Moving Web", Ph.D. Dissertation, Oklahoma State University, July 1968.

[15]. Fu, B., Reddy, A., etc., "Boundary Conditions that Govern the Lateral Mechanics of Flexible Webs in Roll to Roll Process Machines", ASME Journal of Computational and Nonlinear Dynamics, Vol. 9, No. 1, January 2014.

[16]. Swift, H. W., "Cambers for Belt Pulleys", Processing Institute of Mechanical Engineers, June 1932.

[17]. Shelton, J. J., "A Simplified Model for Lateral Behavior of Short Web Spans", Proceedings of the Sixth International Conference on Web Handling, Oklahoma State University, June 2001.

[18]. Yurtcu, H. Y, Beisel, J. A, and Good, J. K., "The Effect of Roller Taper on Webs", TAPPI Journal, Vol. 11, No.11, November 2012.

[19]. Swanson, R. P., "Mechanics of Non-uniform Webs", Proceedings of the Fifth International Conference on Web Handling, Oklahoma State University, June 1999.

[20]. Shelton, J. J., "Effects of Web Camber on Handling", Proceedings of the Fourth International Conference on Web Handling, Oklahoma State University, June 1997.

[21]. Swanson, R. P., "Lateral Dynamics of Non-uniform Webs", Proceedings of the Tenth International Conference on Web Handling, Oklahoma State University, June 2009.

[22]. Swanson, R. P., "Air Support Conveyance of Uniform and Non-uniform Webs", Proceedings of the Second International Conference on Web Handling, Oklahoma State University, June 1993.

[23]. Olsen, J. E., "Lateral Mechanics of an Imperfect Web", Proceedings of the Sixth International Conference on Web Handling, Oklahoma State University, June 2001.

[24]. Olsen, J. E., "Lateral Mechanics of an Imperfect Web", Journal of Pulp and Paper Science, Vol. 28, No.9, September 2002.

[25]. Olsen, J. E., "Shear Effect and Lateral Dynamics of Imperfect Webs", Proceedings of the Seventh International Conference on Web Handling, Oklahoma State University, June 2003.

[26]. Jones, D. P., "Web Sag and the Effect of Camber on Steering", Proceedings of the Ninth International Conference on Web Handling, Oklahoma State University, June 2007.

[27]. Brown, J. L., "Effects of Concave Rollers, Curved-Axis Rollers and Web Camber on the Deformation and Translation of a Moving Web", Proceedings of the Eighth International Conference on Web Handling, June 2005.

[28]. Fu, B., and Good, J. K., "Explicit Simulations of Cambered Web Steering", Proceedings of the Thirteenth International Conference on Web Handling, June 2015.

[29]. Good, J. K., Ren, Y. and Shi, J., "Boundary Conditions for Lateral Deformation of Webs Transiting Rollers in Roll-to-roll Process Machines", Proceedings of the Fourteenth International Conference on Web Handling, Oklahoma State University, June 2017.

[30]. Gehlbach, L. S., Kedl, D. M., and J. K. Good, "Predicting Shear Wrinkles in Web Spans", TAPPI Journal, Vol. 72, No. 8, August 1989.

[31]. Dobbs, J. N., and Dedl, D. M., "Wrinkle Dependence on Web Roller Slip", Proceedings of the Third International Conference on Web Handling, Oklahoma State University, June 1995.

[32]. Good, J. K., "Shear in Multispan Web Systems", Proceedings of the Fourth International Conference on Web Handling, Oklahoma State University, June 1997.

[33]. Shelton, J. J., "Interaction Between Two Web Spans Because of a Misaligned Downstream Roller", Proceedings of the Eighth International Conference on Web Handling, Oklahoma State University, June 2005.

[34]. Fu, B, "Explicit Finite Element Simulations of Web Transport through Process Machines", Ph.D. Dissertation, Oklahoma State University, May 2013.

[35]. Beisel, J. A., and Good, J. K., "Analysis of Trough Formation and Lateral Steering of a Web Due to a Tapered Downstream Roller", Proceedings of the Eighth International Conference on Web Handling, Oklahoma State University, June 2005.

[36]. Morgant, E. J., Seide, P., and Weingarten, V. I., "Elastic Stability of Thin-walled Cylindrical and Conical Shells Under Combined Internal Pressure and Axial Compression", AIAA Journal, Vol. 3, No. 6, June 1965.

[37]. Knox, K. L., and Sweeney, T.L., "Fluid Effects Associated with Web Handling", Industrial Engineering Chemical Process Design Development, Vol. 10, No.2, 1971.

[38]. Shelton, J. J., "Buckling of Webs from Lateral Compressive Forces", Proceedings of the Second International Conference on Web Handling, Oklahoma State University, June 1993.

[39]. Webb, D. K., "Prediction of Web Wrinkles Due to Misalignment of a Downstream roller in a Web Span", M.S. Thesis, Oklahoma State University, December 2004.

[40]. Good, J. K, Beisel, J. A., and Yurtcu, H. "Predicting Web Wrinkles on Rollers", Proceedings of the Tenth International Conference on Web Handling, Oklahoma State University, June 2009.

[41]. Good, J. K., and Straughan, P., "Wrinkling of Webs Due to Twist", Proceedings of the Fifth International Conference on Web Handling, Oklahoma State University, June 1999.

[42]. Beisel, J. A., and Good, J. K., "The Instability of Webs in Transport", Journal of Applied Mechanics, Vol. 78, No. 1, January 2011.

[43]. Gopal, H., and Kedl, D. M., "Using Finite Element Model to Define How Wrinkles Form in a Single Web Span Without Moment Transfer", Proceedings of the First International Conference on Web Handling, Oklahoma State University, June 1991.

[44]. Jones, D. P., McCann, M. J., Bishop, C. A., etc., "Wrinkle Initiation and Development in Heated Webs on Drums", Proceedings of the Twelfth International Conference on Web Handling, Oklahoma State University, June 2013.

[45]. Baipa, S. G., "Wrinkling Analysis on Webs with Circular Non-uniform Regions Using Finite Elements", M. S. Thesis, Oklahoma State University, May 2012.

[46]. Sandesh, M., "Investigation of the Effect of Voids on the Stability of Webs", M. S. Thesis, Oklahoma State University, May 2007.

[47]. Yurtcu, H, H., "Development of Nonlinear Finite Element Codes for Stability Studies of Web Material with Strain State Dependent Properties", Ph.D. Dissertation, Oklahoma State University, Stillwater OK, December 2011.

[48]. Beisel, J. A., "Single Span Web Buckling Due to Roller Imperfections in Web Process Machinery", Ph.D. Dissertation, Oklahoma State University, Stillwater OK, October 2006.

[49]. Vaijapurkar, S., and Beisel, J. A., "The Behavior of Webs Transiting Crowned Rollers", Proceedings of the Twelfth International Conference on Web Handling, Oklahoma State University, June 2013.

[50]. Fu, B., and Good, J. K., "Web Wrinkling Resulting from Moment Transfer", Proceedings of the Twelfth International Conference on Web Handling, Oklahoma State University, June 2013.

[51]. ABAQUS Documentation 6.14, 2014.

[52]. Hilber, H. M., Hughes, T. J. R., and Taylor, R. L. "Improved Numerical Dissipation for Time Integration Algorithms in Structural Dynamics", Earthquake Engineering and Structural Dynamics, Vol. 5, No. 3, July 1977.

[53]. Higham, N. J., "Accuracy and Stability of Numerical Algorithms", 2nd Ed, SIAM, Philadelphia, 2002.

[54]. Ashwell, D. G., "The Anticlastic Curvature of Rectangular Beams and Plates", Journal of the Royal Aeronautical Society, Vol. 54, No. 479, November 1950.

[55]. Rivello, R. M., "Theory and Analysis of Flight Structures", 1st ed, McGraw hill, 1969.

[56]. Shelton, J. J., and Reid, K. N., "Lateral Dynamics of an Idealized Moving Web", ASME J. Dyn. Syst., Meas., Control, Vol. 93, No. 3, September 1971.

[57]. Shelton, J. J., and Reid, K. N., "Lateral Dynamics of a Real Moving Web", ASME J. Dyn. Syst., Meas., Control, Vol. 93, No. 3, September 1971.

[58]. Lorig, E. T., AISE (Association of Iron and Steel Engineers) Annual Convention, Cleveland, Ohio, 1950.

[59]. Olsen, J. E., "Lateral Mechanics of Baggy Webs at Low Tensions", Proceedings of the Eighth International Conference on Web Handling, Oklahoma State University, June 2005.

[60]. Benson, R. P., "The Influence of Web Warpage on Lateral Dynamics of Webs", Proceedings of the Fifth International Conference on Web Handling, Oklahoma State University, June 1999.

[61]. Benson, R. C., "Lateral Dynamics of a Moving Web with Geometrical Imperfection", Journal of Dynamic Systems, Measurement, and Control, Vol. 124, No. 1, March 2002.

[62]. Shimizu, S., and Yoshida, S., "Buckling of Plates with a Hole under Tension", Thin-Walled Structures, Vol. 12, No.1, 1991.

[63]. Shelton, J. J., "Machine Direction Troughs in Web Spans and Corrugations in Wound Rolls", Internal Report Web Handling Research Center, WHRC Project 9000-1, August, 1991.

[64]. Cerda, E., Ravi-Chandar, K., and Mahadevan, L., "Wrinkling of an Elastic Sheet under Tension", Nature, Vol. 419, October 2002.

[65]. Cerda, E., and Mahadevan, L., "Geometry and Physics of Wrinkling", Physical Review Letters, Vol. 90, No. 7, February 2003.

[66]. Nukala, V., "Buckling of Isotropic and Orthotropic Webs", M. S. Thesis, Oklahoma State University, July 2016.

[67]. Kollár, László P., "Mechanics of Composite Structures", Cambridge University Press, 2003.

[68]. Szilard, R., "Theory and Analysis of Plates", Prentice Hall, 1974.

[69]. Hibbeler, R. C., "Mechanics of Materials", 8th ED, Pearson Prentice Hall, 2011.Le.

[70]. Jones, R. M., "Mechanics of Composite Materials", 2nd Ed, Taylor & Francis, England, 1998.

[71]. Shi, J., Markum, R. E., and Good, J. K., "Impact of Large Deformations of Webs Transiting Rollers", Proceedings of the Fourteenth International Conference on Web Handling, Oklahoma State University, June 2017.

[72]. Ren, Y., Shi, J., and Good, J. K., "Lateral Deformation of Webs Transiting Spans in roll-to-roll Process Machines", ASME J. Dyn. Syst., Meas., Control, accepted.

VITA

Jinxin Shi

Candidate for the Degree of

Doctor of Philosophy

Dissertation: THE INTERACTION BETWEEN WEBS AND ROLLERS IN ROLL-TO-ROLL MANUFACTURING PROCESS MACHINES

Major Field: Mechanical and Aerospace Engineering

Biographical:

Education:

Completed the requirements for the Doctor of Philosophy in Mechanical and Aerospace Engineering at Oklahoma State University, Stillwater, Oklahoma in May, 2019.

Completed the requirements for the Master of Science in Machinery in Chemical Industry Process at Beijing University of Chemical Technology, Beijing, China in 2013.

Completed the requirements for the Bachelor of Science in Process Equipment and Control Engineering at Beijing University of Chemical Technology, Beijing, China in 2010.

Experience:

Employed by Oklahoma State University, School of Mechanical and Aerospace Engineering as a graduate research assistant from August, 2013 to May, 2019.

Employed by Beijing University of Chemical Technology, College of Mechanical Engineering as a graduate research assistant from September, 2010 to July, 2013.